USING LIDAR DERIVATIVES TO ESTIMATE SEDIMENT GRAIN SIZE ON BEACHES IN FALSE BAY

JAMES BURNS (BSC HONS GEO-INFORMATICS)

Thesis presented in partial fulfilment of the requirements for the degree of Master of Science (Geoinformatics) in the Faculty of Science at Stellenbosch University

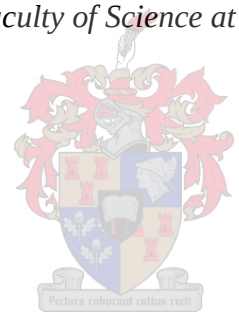

SUPERVISOR: DR M LüCK-VOGEL

December 2019

DEPARTMENT OF GEOGRAPHY AND ENVIRONMENTAL STUDIES

DECLARATION

By submitting this report electronically, I declare that the entirety of the work contained therein is my own, original work, that I am the sole author thereof (save to the extent explicitly otherwise stated), that reproduction and publication thereof by Stellenbosch University will not infringe any third party rights and that I have not previously in its entirety or in part submitted it for obtaining any qualification.

Signature: James Burns

Date: December 2019

ABSTRACT

The coastal zone is a dynamic environment that is regulated and influenced by natural ocean processes and anthropogenic phenomena. Beaches are important elements within the coastal zone and are highly valued for the ecosystem services that they provide, such as buffering against wave erosion and their recreational value. Characteristics of beaches, such as slope and grain size, need to be monitored for protection and management purposes. These continuously changing variables can indicate vulnerability to erosion, for example. South Africa's False Bay includes a number of beaches that vary in terms of such vulnerability.

Active remote sensing technologies are increasingly used as monitoring tools that allow for precise measurements of the status and changes in coastal environments. These technologies include LiDAR systems which have the capacity to record intensities which relate to surface characteristics.

The aim of this study is to establish whether LiDAR derived intensity and slope of beaches can be correlated with, or serve as proxies for, sediment grain size. There are two supporting objectives. The first is to analyse airborne LiDAR data of False Bay to derive information on key physical characteristics of selected beaches and to relate these to the sand grain size of these beaches. The second objective is to conduct controlled laboratory-based analysis of sediment samples using a terrestrial LiDAR scanner, and to establish the correlations between different categories of grain size and measured LiDAR intensities.

The results of the laboratory-based study reveal a strong correlation between LiDAR intensity and sediment grain size, for the individual size fractions. As grain size increases, the LiDAR intensity decreases linearly. For the natural mixed samples, a slight correlation was also detected between LiDAR intensity and average grain size; i.e. samples with a coarser average grain size generally presented lower measured intensities.

Although the analysis of the airborne LiDAR data produced plausible beach slope information, the data does not reflect the expected correlation between recorded intensity and slope to describe grain size. Temporal decorrelation could be an explanation for this, since the airborne data was acquired approximately two years prior to sample collection. Interestingly, the correlations between the airborne LiDAR derived intensity and slope data contradict the widely acknowledged relationship that exists between these two variables: finer grained sediments are generally associated with flatter-sloped beaches, while coarser grained sediments are associated

with steeper-sloped beaches. Analysis of the airborne LiDAR data shows that intensity increases steadily with steeper slopes. This is unexpected as controlled laboratory-based measurements show that higher intensities are indicative of finer-grained sediments which are associated with flatter beaches.

This study concludes that LiDAR has the potential for monitoring key physical characteristics of beaches. However, if airborne LiDAR data are to be used for such monitoring, further investigation is needed with the aim of establishing data capture and processing requirements in order to produce reliable intensity measurements. Although individual grain size fractions has been proven to strongly correlated with LiDAR intensity in a controlled environment, characterising natural beach sediments of mixed grain size fractions, using airborne LiDAR, is more difficult to accomplish.

KEYWORDS

Coastal zone, beaches, False Bay, grain-size, LiDAR, intensity

OPSOMMING

Die kussone is 'n dinamiese omgewing wat gereguleer en beïnvloed word deur natuurlike oseaanprosesse en menslike verskynsels. Strande is belangrike elemente binne die kussone en word hoog aangeskryf vir die ekosisteemdienste wat hulle bied, soos die beskerming teen erosie van die golwe asook die ontspanningswaarde wat strande bied. Die verskillende eienskappe van strande, soos helling en sedimentkorrelgrootte, moet gemonitor word vir beskerming en bestuursdoeleindes. Hierdie veranderlikes kan byvoorbeeld die kwesbaarheid van die strand vir erosie aandui. Suid Afrika se Valsbaai sluit 'n aantal strande in wat wissel van sulke kwesbaarheid.

Aktiewe afstandswaarneming tegnologie word toenemend gebruik as moniterings gereedskap vir akkurate waarnemings van die status en veranderinge in kusomgewings. Hierdie tegnologie sluit LiDAR-stelsels in wat die vermoë het om intensiteite wat verband hou met die oppervlakkenmerke op te teken.

Die doel van hierdie studie is om vas te stel of LiDAR-afgeleide intensiteit en helling van 'n strand gekorreleer kan word, of sedimentkorrelgrootte kan verteenwoordig. Daar is twee ondersteunende doelwitte. Die eerste is om LiDAR-data van Valsbaai wat vanuit die lug geneem is te analiseer om inligting oor belangrike fisiese eienskappe van sekere strande te ontleed en om dit dan met die sedimentkorrelgrootte van hierdie strande te vergelyk. Die tweede doelwit is om gekontroleerde laboratoriumgebaseerde analise van sedimentmonsters te maak deur 'n terrestriële LiDAR-skandeerder te gebruik om die korrelasies tussen verskillende kategorieë van sedimentkorrelgrootte met die ooreenkomstige LiDAR-intensiteite te bepaal.

Die resultate van die laboratoriumgebaseerde studie toon 'n sterk verband tussen LiDAR intensiteit en sedimentkorrelgrootte vir die verskillende grootte klasse. Namate korrelgrootte toeneem, neem die LiDAR intensiteit lineêr af. Vir die natuurlik gemengde monsters is 'n ligte korrelasie ook tussen die LiDAR intensiteit en gemiddelde korrelgrootte opgespoor; byvoorbeeld, monsters met 'n growwe gemiddelde korrelgrootte het gewoonlik laer intensiteite getoon.

Alhoewel die analise van die LiDAR-data vanuit die lug aanvaarbare helling informasie voorsien het, was daar nie 'n sterk verband tussen die aangeduide intensiteit en helling om

sedimentkorrelgrootte te beskryf. Temporale verfraaiing kan wel 'n verduideliking hiervan wees aangesien daar ongeveer twee jaar tussen die versameling van die data vanuit die lug en die versameling van die monsters vir hierdie studie verloop het. Interessant egter is dat die korrelasies tussen die LiDAR-afgeleide intensiteit en hellingdata in teenstelling is met die algemene erkenning wat tussen hierdie twee veranderlikes bestaan: naamlik dat fynkorrelige sedimente in die algemeen geassosieer word met strande met ‘n kleiner, of platter, helling, terwyl grootkorrelige sedimente geassosieer word met strande met steiler hellings. Ontleding van die LiDAR-data uit die lug toon dat intensiteit geleidelik toeneem met steiler hellings. Dit is onverwags, aangesien beheerde laboratoriumgebaseerde metings toon dat hoër intensiteite op fynkorrelige sedimente dui, wat met platter strande geassosieer word.

Hierdie studie het tot die gevolgtrekking gekom dat LiDAR wel die potensiaal het om die fisiese eienskappe van strande te monitor. As LiDAR-data vanuit die lug egter gebruik word vir sodanige monitering, is verdere ondersoek nodig om data-opname en verwerkingsvereistes vas te stel ten einde betroubare intensiteitsmetings te lewer. Alhoewel dit bewys is dat individuele korrelgrootte sterk gekorreleer is met LiDAR-intensiteit in 'n beheerde omgewing, is dit moeiliker om natuurlike strand-sedimente van gemengde korrelgroottes te karakteriseer.

TREFWOORDE

Kussone, strand, Valsbaai, korrelgrootte, LiDAR, intensiteit

ACKNOWLEDGEMENTS

I sincerely thank:

- My supervisor Dr Melanie Lück-Vogel for support and guidance
- My family for financial and moral support
- Fellow post-graduate students, Michael Johnson for inspiration and assistance with transport and fieldwork, Herman Luyt for helping with lab work, and others for general encouragement and motivation (Shelley, Leighton, Andre, Cikizwa, Kirstyn and Kirodh)
- The Department of Environmental Affairs (DEA) for permission to obtain samples during fieldwork
- The City of Cape Town (CoCT) for LiDAR data and granting access to beaches, including Kogel Bay camp site, for sample collection
- Kishan Tulsi for assistance with operating the RIEGL LiDAR scanner
- Theo Pauw and Divan Vermeulen at the Centre for Geographic Analysis (CGA) in Stellenbosch for technical assistance and advice
- Mareli Grobbelaar from the Geology Department (Stellenbosch University) for assistance with the mechanical sieve equipment and lab facilities
- Ashley Davids (CSIR) for assisting with use of the laboratory facilities
- The DST-CSIR interbursary program for funding my second year of Master's research
- Most thanks to my Father in heaven for undeserved yet abounding grace

CONTENTS

TABLES

FIGURES

ACRONYMS AND ABBREVIATIONS

ALS	Airborne LiDAR system / Airborne Laser Scanning
ASPRS	American Society for Photogrammetry and Remote Sensing
ATM	Airborne Topographic Mapper
CGA	Centre for Geographic Analysis
CoCT	City of Cape Town
CSIR	Council for Scientific and Industrial Research
CTA	Cumulative Threat Assessment
CZMIL	Coastal Zone Mapping and Imaging LiDAR
DEA	Department of Environmental Affairs
DEM	Digital Elevation Model
DGPS	Differential GPS
DIM	Digital Intensity Model
(n)DSM	(normalized) Digital Surface Model
DTM	Digital Terrain Model
EIA	Environmental Impact Assesment
GDP	Gross Domestic Product
GNSS	Global Navigation Satellite System
GPS	Global Positioning System
IMU	Inertial Measurement Unit
INS	Inertial Navigation System
IPCC	Intergovernmental Panel on Climate Change
LiDAR	Light Detection and Ranging
NIR	Near-Infrared
SAR	Synthetic Aperture Radar
SLR	Sea-level Rise
SU	Stellenbosch University
TLS	Terrestrial Laser Scanning
x, y, z	point coordinates (longitude, latitude, elevation)

CHAPTER 1 INTRODUCTION

Coastlines define the margins of land masses and entire continents and, despite their narrow physical definition, they determine the location of what is commonly referred to as the coastal zone, so named for its width, depth and length dimensions (Sheeja & Gokul 2016). It is in this zone that sea, land and atmosphere meet and interact to create, and continuously influence, a variety of different environments. These include dunes which are often covered or partially covered by characteristic dune vegetation, beaches which can be described as shores of unconsolidated material alternately exposed or covered by tides or waves and thus free of vegetation (Badenhorst 1988; Carter 1988), and near- and offshore environments which comprise a number of marine and submarine features and ecosystems. In addition to being largely defined on the basis of bio-physical features, the coastal zone can also be defined by administrative or management boundaries.

Of the different types of coastal systems, sandy beaches are of particular interest as the basis for this study. One of the reasons for focussed research into sandy beaches is that, because they are mostly free of vegetation, they are not commonly recognised as ecosystems and are thus often not managed or conserved effectively (Harris et al. 2015), particularly when they are not of interest for coastal protection or tourism. Often overlooked, the biota existing in numerous sandy beach habitats include a variety of vertebrates, micro-, meio- and macro-fauna which rely on specific physical beach characteristics and coastal processes (McLachlan & Dorvlo 2005; Harris et al. 2015). Outlined in a cumulative threat assessment (CTA), Harris identifies and addresses many of the threats that sandy beaches are exposed to including predicted sea level rise, coastal development, mineral and sand mining, piers and breakwater construction, pollution, over-fishing and harvesting. There are, to a large extent, no structured boundaries protecting the coast from threats such as oil or chemical spills, for example, which emphasises the critical importance of coastal conservation and management.

Another reason for studying coasts is that a significant percentage of the current human population resides within the confines of the coastal zone (Duxbury & Dickinson 2007). This is explained mainly by the ecosystem services that the coastal zone provides for humans. It provides access to fisheries, suitably sheltered water-bodies in which ports can be constructed for the import and export of resources and products, its recreation and general aesthetic value,

etc. (Jackson et al. 1984). Counter-balancing the value of its ecosystem services is the vulnerability of the coastal zone to environmental influences, including extreme events that can compromise human safety and well-being. Over millennia, humans have been exposed to natural hazards such as storms and flooding of low-lying coastal areas; however, anthropogenic factors, particularly relating to global warming and climate change due to the combustion of fossil fuels and rapid population growth in coastal areas, have magnified these risks, with serious potential consequences for human well-being (McGranahan, Balk & Anderson 2007).

A term commonly used to describe the degree to which a coastal system is impacted by various factors is *vulnerability*. Coastal vulnerability can be described by both the likelihood that an event with harmful effects will occur as well as the consequences of these threats, for example, to the human polulation (Rumson, Hallett & Brewer 2017). One of the major factors leading to the increasing likelihood of harmful phenomena are anthropogenic activities which, as previously mentioned, may result in climate change causing sea-level rise (SLR) of between 0.52 and 0.98 meters by 2100 as predicted by the Intergovernmental Panel on Climate Change (IPCC 2013). Climate scenarios for Southern Africa also forecast an increase in the number and severity of storm events (Davidson-Arnott 2016). Amongst others, these will materialise in the form of major storms which, in the coastal zone, may result in the landward surging of high energy waves beyond recently experienced limits. Whilst extreme natural events have always been a feature of the coastal zone, in future, they are likely to occur more frequently and with greater levels of intensity than previously recorded (Cartwright 2008). The consequences of these extreme events and changes can manifest in the form of storm wave-related flooding, shoreline erosion, destruction of built infrastructure and other hazards compromising the safety of the human populations established within the coastal zone.

The ability to adapt to threats affecting the coastal zone is crucial for sustainable management and development (Rumson, Hallett & Brewer 2017). Means of conserving coastal habitats as well as managing risk to coastal developments and infrastructure need to be taken into consideration. For this to be achieved, it is essential that there are established methods of predicting the likelihood and consequences of extreme events such as storms and increased SLR. Linked to this, it is essential that physical and other responses that occur within the

coastal zone as a result of these conditions can be measured and tracked in terms of trends, applying especially to particularly vulnerable shorelines such as sandy beaches.

Recognising the importance of adaptation to coastal changes, it is essential that careful and frequent monitoring of coastal environments be undertaken (Rumson, Hallett & Brewer 2017). In the case of beaches, the observed physical characteristics can be used as indicators of vulnerability. The physical characteristics of sandy beaches include, among others, slope, sediment grain size and composition, orientation or exposure to waves and wind. These characteristics are to a large extent correlated and sound assessment of certain parameters allows for the approximation of those less obvious.

1.1 PROBLEM FORMULATION

As is evident from the above section, the monitoring of coastal beach systems is vital for the effective management and conservation of these environments. Although there are currently numerous techniques for coastal monitoring, one of the most common being ground surveys, these are often time consuming, expensive and unsustainable as well as intrusive and damaging to the environment (Eitel et al. 2016). In addition, many beaches are at remote locations or can be otherwise inaccessible for ground surveying in terms of terrain and equipment capability. There is thus the need for a method of quickly and accurately surveying larger areas in a more cost-effective manner than the more traditional practices (Amatya et al. 2013).

Knowledge of the average grain size for beaches helps to characterise the beach ecosystems and indicates the vulnerability of the coastal environment to oil spills, chemical pollution and also potential erosion caused by wave energy (Jackson et al. 1984; Harris et al. 2005). Therefore, information about beach grain size will allow for better planning with regards to coastal protection and engineering, once again highlighting the importance of effective monitoring.

An effective solution to this problem has been remote sensing. For a number of decades, remote sensing technology has been used to implement large scale studies of the coastal zone, including the surveying of beaches. Probably the most widely utilised and understood technologies for monitoring are optical sensors, both air- and space-borne. Images of coastal environments are readily available and can be used in a variety of applications. The

multispectral nature of these sensors makes identification of features easier but applications are for the most part limited by the spatial resolution of the images. For a single optical image, the amount of information that can be derived is limited to the received spectral reflectance. Other useful information, such as elevation and slope, can only be obtained by capturing additional images to perform stereographic analysis. This is not always possible and, especially in beach environments with brightly reflecting sand and low contrast, orthophoto applications for deriving surface models may produce low accuracies.

Active remote sensing technologies such as light detection and ranging (LiDAR), have overcome many of the limitations associated with the more traditional passive optical sensors and can be used to accurately and precisely measure surface attributes such as elevation (Yan & Shaker 2014; Bloetscher & Wood 2016; Eitel et al. 2016). The extent to which active sensors can describe surface characteristics still needs to be determined and this research aims to explore the effectiveness of using LiDAR in this capacity.

As with any remote sensing technology, however, the problem of temporal decorrelation is a significant contributor to uncertainty when interpreting results. The validation of remotely sensed data is only possible if physical ground observations are made in the area of interest near or at the time of acquisition. To address this issue, laboratory-based approaches are used to test the capabilities of remote sensing technology with known high levels of accuracy and precision.

1.2 ASSUMPTIONS AND HYPOTHESIS

The first assumption in this study is that there is a strong relationship between beach slope and sediment grain size, with steeper foreshore slopes equating to a larger grain diameter, as suggested in the literature (Reis & Gama 2010). Having accurate slope information for beaches may thus, in future, be used to estimate grain size.

Another assumption is that sediment grain size will affect the reflected energy signal recorded by the active sensing technology (intensity) to such a degree that different grain sizes will be distinguishable, which leads to the hypothesis that this study will be investigating. This study hypothesizes that active LiDAR technology can be used to determine accurate beach slope, and grain size can be approximated using LiDAR intensity.

1.3 RESEARCH AIM AND OBJECTIVES

The aim of this research is to establish whether sediment grain size can be approximated using LiDAR derivatives such as slope and intensity. To address this aim, the following objectives have been constructed to guide this study:

The primary objective is to use airborne LiDAR data to derive products such as elevation and intensity to assess whether they can be used to describe beaches in terms of slope and grain size.

A secondary objective is to systematically assess the relationship between beach sand grain size and LiDAR intensity.

To support these objectives, the following research steps were set:

1. Review available literature to determine the context and relevance of this study and identify the potential contribution which this research will make to current knowledge in this field.
2. Collect and consolidate necessary data, including the airborne LiDAR data.
3. Process the LiDAR data for False Bay (produce slope and intensity derivatives).
4. Select study areas representative of different beach types (slope and grain size).
5. Determine for the selected beaches the correlation between slope and intensity.
6. Obtain beach profile measurements and sand samples in the field.
7. Conduct laboratory tests to further investigate the effect of grain size and slope on intensity under controlled conditions.
8. Synthesise results and present significant findings graphically as well as in a structured report.

1.4 STUDY AREA

Situated south of Cape Town in the Western Cape Province of South Africa, False Bay is an example of a typical bay and is also the largest true bay in South Africa (see Figure 1.1 below). The bay is about 1 000 square kilometres in size and can be described as approximately square (30 x 30 km in east-west, north-south direction). The bay is bounded on

the west by the Cape Peninsula with the Table Mountain Range. The northern shore is largely sandy and flat and forms the southern border of the Cape Flats, much of which is only a few tens of meters above sea-level. The Hottentots-Holland range of mountains forms the eastern side of the bay. The south facing opening of the bay is defined by Cape Point to the west and Cape Hangklip on the east.

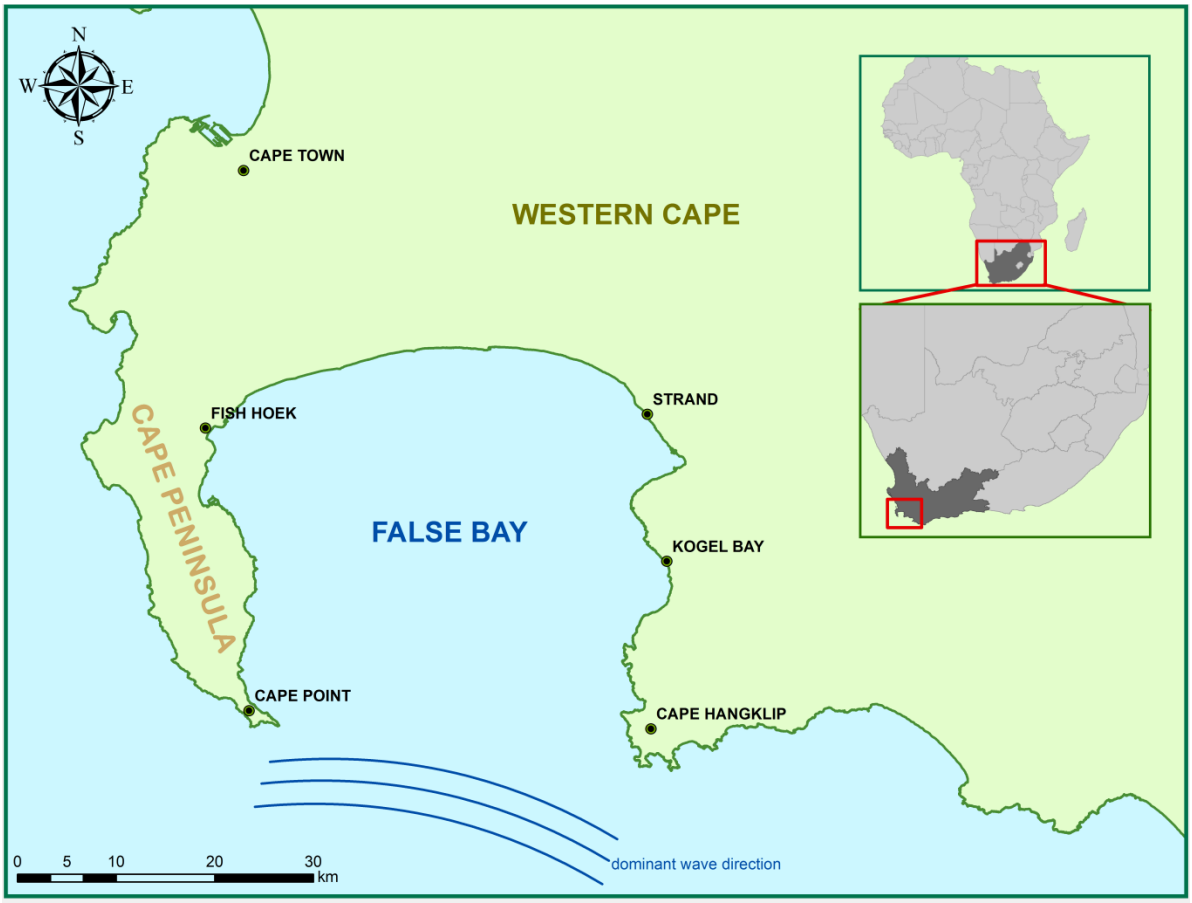

Figure 1.1 Study area map, False Bay in South Africa

False Bay offers a large variety of coastal environments which makes it ideal for the purposes of this study. The shore running from Fish Hoek at the north western corner of the bay (see Figure 1.1) to Strand in the north eastern corner is comprised of mostly sandy beaches bordered by low, vegetated dunes. In contrast, the western and eastern margins consist predominantly of rocky shores. The coast from Fish Hoek to Cape Point has more sheltered stretches with the occasional sandy or boulder beach while the shore from Strand to Cape Hangklip is characterised by steep cliffs exposed to larger waves, with a small number of high-energy beaches.

In addition to the diverse range of coastal environments, there are a number of reasons for choosing False Bay for this study. Airborne LiDAR campaigns surveying the False Bay coast were commissioned by the City of Cape Town (CoCT), and these provided much of the data used in this study. Additional benefits include its close proximity for conducting fieldwork, thus making more frequent site observations and access for sample collection.Three beaches were selected as representative of the various combinations of physical characteristics (slope, orientation, wave energy). These beaches are Fish Hoek, Strand and Kogel Bay (A, B and C respectively in Figure 1.2 below). Apart from being representative of different beach types, these sites were accessible and in reasonable proximity for fieldwork.

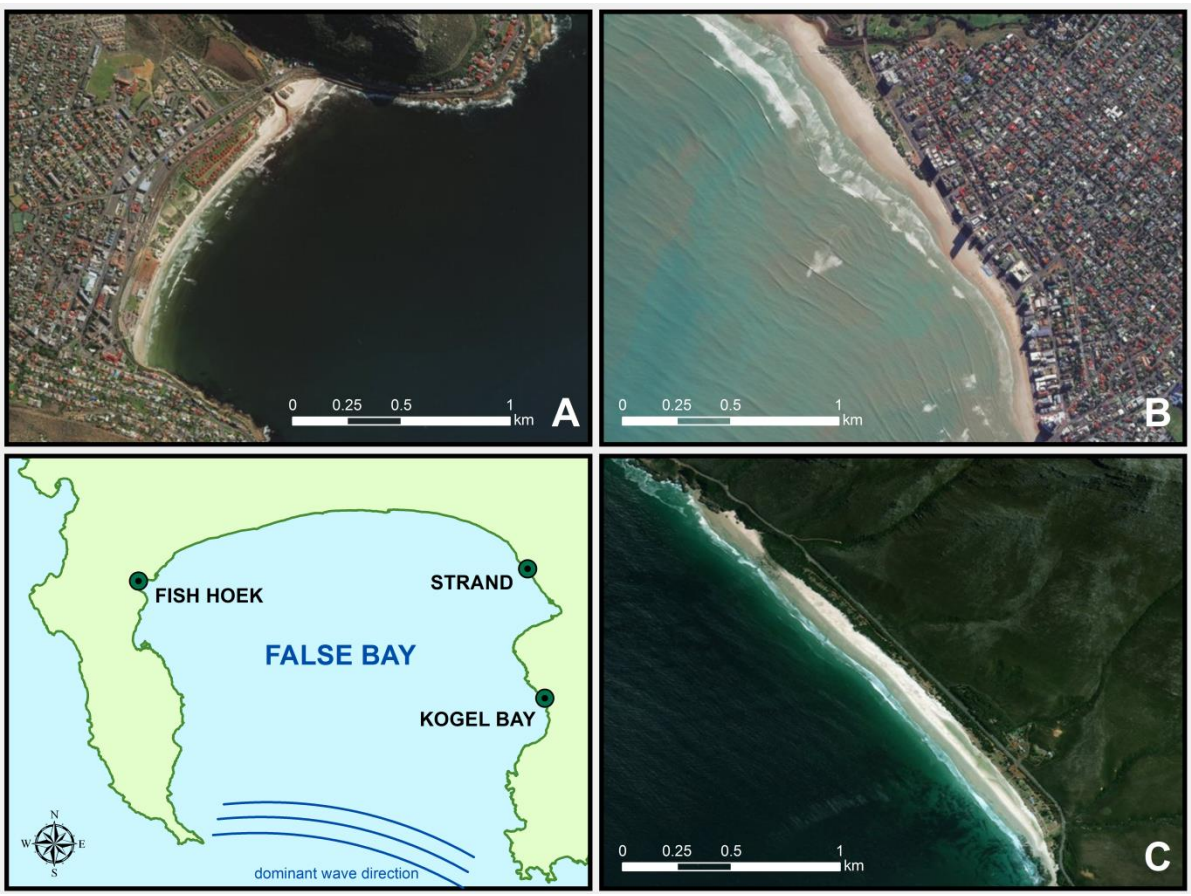

Figure 1.2 Study sites in False Bay: a) Fish Hoek; b) Strand; and c) Kogel Bay (with DigitalGlobe satellite basemaps)

Fish Hoek is a coastal town on the Western side of False Bay and is part of the CoCT municipality. It is a popular residential area for many commuters and pensioners but is also a much frequented destination for holidaymakers and tourists. Small-scale commercial and recreational net-fishing and angling occur alongside activities such as surfing, sailing and

bathing. Fish Hoek is located at the south eastern end of a broad valley that cuts through the Cape Peninsula to Kommetjie on the Atlantic side. Historically, this valley was submerged during a period where higher sea-levels formed a sea passage separating the Cape Peninsula from the mainland. The valley is sandy on Cape granite bedrock. Fish Hoek has a mild mediterranean climate with winter rainfall and hot, dry summers. Due to its orientation and location in the Bay, Fish Hoek is very sheltered from the majority of ocean waves entering False Bay from the south-west direction, in particular during storms. The beach, approximately 1.3 km long, is flat and relatively wide during low tide. The low slope and resulting low elevation above sea level mean that, even at low tide, large portions of the beach lie close to the water table and remain saturated with water.

Strand is a coastal town on the north-eastern edge of False Bay, about 50 km east-southeast of Cape Town. Its coastline is characterised by a 5 km stretch of white sandy beach of varying width and composed of weathered quartzite and sandstone from the Malmesbury group (Adelana, Xu & Vrbka 2010). Strand is a very popular destination for both tourists and locals, and the climate provides good conditions for swimming and surfing. However, especially in summer, strong south-easterly winds often occur on this beach and, at many times, the blowing sand and blustery conditions make beach activities unpleasant. A shallow offshore submerged reef disperses most of incoming wave energy in the eastern part of Strand and the beach is thus exposed to less wave action than would be expected under the mainly south-westerly direction of incoming waves. Despite this, the beachfront infrastructure is at constant risk from the ocean during spring high tides and periods of extreme storminess. This threat is all the more pronounced in Strand as the first rows of houses and building were constructed on the upper beach and are thus located in a zone which is naturally part of the active coastal environment.

The Kogel Bay resort is located on the eastern margin of False Bay. It consists of a campsite and just less than 2 km of narrow beach. In terms of geology, Kogel Bay falls under the Tygerberg formation of the Malmesbury Group (Kisters 2016). This is a very popular surfing destination and, due to dangerous conditions and strong currents, there are tidal pools for swimming adjacent to the often frequented campsites. As a result of wave refraction around the Cape Peninsula, Kogel Bay is directly affected by large, incoming waves from the west

and south-west (see Figure 1.2C). The beach is quite steep and relatively narrow with a coarse grain size.

1.5 RESEARCH OUTLINE AND THESIS STRUCTURE

The diagram below (Figure 1.3) outlines the research steps undertaken in this study. Also indicated are the respective chapters addressing each of the steps in more detail.

The second chapter of this document (Chapter 2) discusses, with the aid of relevant literature, various underlying topics which form an essential part of this research. Chapter 3 describes in detail the methodology followed in this study, from data acquisition to analysis. The results will be presented and discussed in Chapter 4 followed by the concluding chapter (Chapter 5) in which the aim and objectives are revisited and significant findings are highlighted.

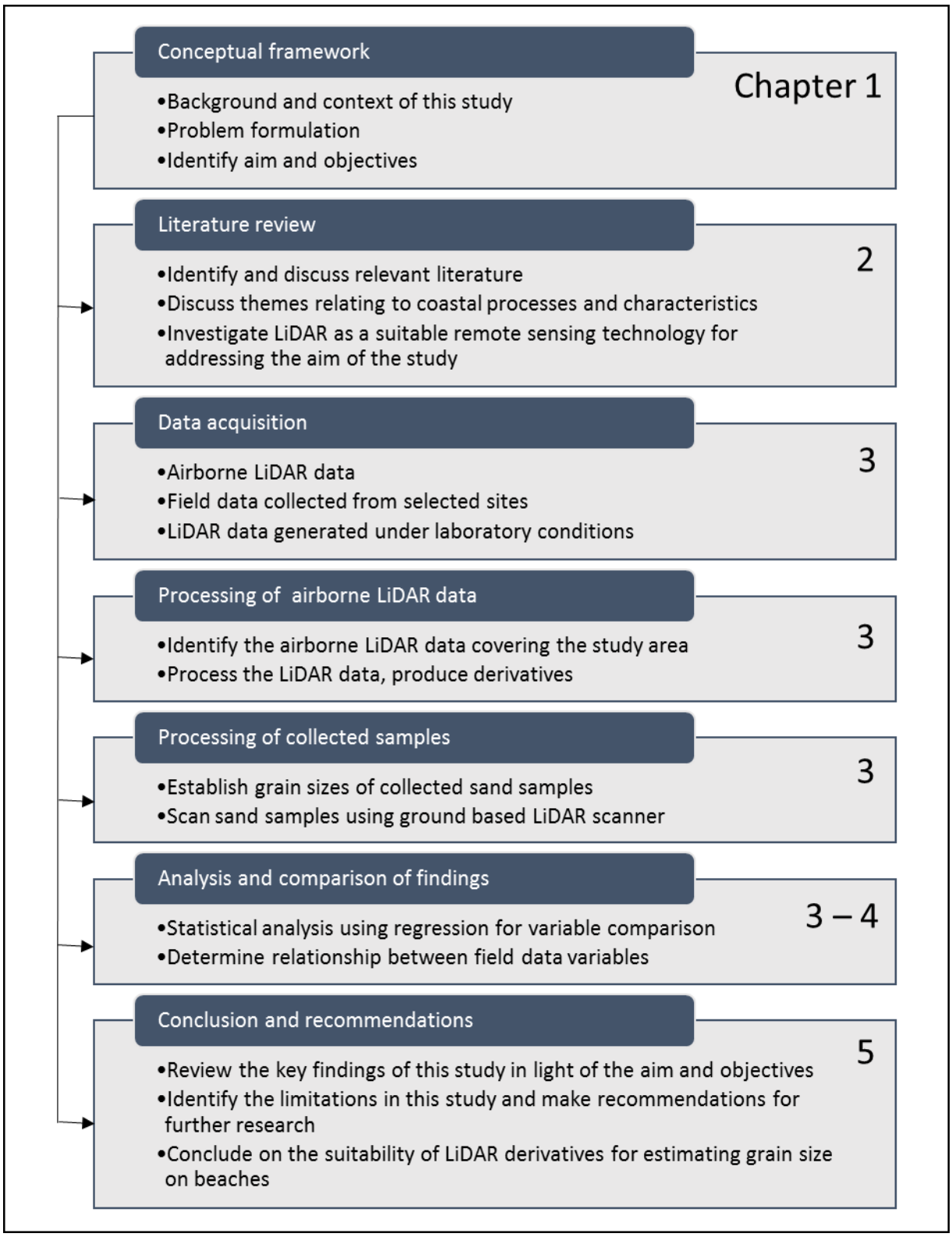

Figure 1.3 Research design overview

CHAPTER 2 THEORY AND APPLICATIONS

This chapter provides a review of selected literature as it relates to topics relevant to the research that is presented in this paper. The chapter begins with a brief discussion of certain values attributed to the coastal zone and some significant threats to which these values are currently exposed. The discussion provides a contextual basis for the research aims and objectives that are presented in the previous chapter as well as the methods, results and conclusions in subsequent chapters. Following this, the chapter is divided into two main sections. The first deals with a numbert of physical coastal processes that either directly or indirectly determine the sedimentary characteristics and dynamics of sandy beaches, which are the main focal areas of this study; the second covers some of the important elements of remote sensing technology, mainly relating to LiDAR, and the elevation and intensity-based applications in which it has been deployed globally in the coastal environment.

2.1 THE COASTAL ENVIRONMENT: VALUES AND THREATS

2.1.1 Economic values of the Coastal Environment

The coastal environment is a national asset providing a multitude of social and economic opportunities for the country. South Africa has a very extensive coastline (approximately 3 900 km) and consequently claims jurisdiction over an Exclusive Economic Zone (EEZ) of around 1.5 million square kilometres (Operation Phakisa 2014). Within this zone economic growth and job creation are promoted through a variety of initiatives, including marine transport and manufacturing, offshore oil and gas exploration, aquaculture and other services. The contribution of these ocean economy elements to South Africa's gross domestic product (GDP) is expected to be more than R20 billion by 2019 (SAnews 2015).

Direct economic benefits of coastal resources are estimated to be around 35% of the annual GDP for South Africa, with fishing, for example, contributing 0.5% and supporting the livelihoods of over 100 000 people (WWF-SA 2016). There are also indirect benefits to the economy which are offered by natural coastal features such as beaches, dunes, coastal vegetation and other bio-physical features, which are enablers, for example, of tourism, recreation and residential development. Saadat et al. (2016) investigated the various touristic

attractions of countries and found that the natural environment has a big impact on a destination's image. The authors conclude that coastal environmental aspects are among the highest ranked features, with a clear correlation evident between numbers of tourists and coastal areas, including beaches, with a high level of aesthetic appeal. Valuable infrastructure along the coast such as roads and other built structures, including residential areas, are protected by natural coastal features such as beaches, dunes and rocky shorelines, against potentially damaging effects of storm waves, flooding and wind. These indirect benefits of the coastal environment account for approximately 28% of the country's GDP (DEA 2015).

South Africa's commercial ports, which can be explained in terms of their location and breakwater designs to physical coastal features that afford protection (inter alia) from waves, tidal influences and littoral sediment dynamics, are also extremely important for the country's economy and that of the African sub-continent. By way of illustration in this regard, South Africa's ports that have container handling capacities enabled the import and export of over 48 million containers in 2014 (WWF-SA 2016). Large scale importing and exporting of goods via ports and harbours make up around 95% of South Africa's trade volume (80% by value). Total imports and exports contribute 60% to the country's GDP (WWF-SA 2016).

2.1.2 Threats to the coastal environment

2.1.2.1 Anthropogenic activities

There are millions of people living in the coastal zone (D'Alessandro & Tomasicchio 2016; Doig & Ware 2016), with approximately two thirds of the world population resident within 100 km of the coast (Sheeja & Gokul 2016). With an increase in population, pressures on the coastal environment are also increasing. To support coastal human populations, intensive industrial and extensive residential development is occurring (Sheeja & Gokul 2016). Prominent amongst the threats to the coastal environment and the important economic and social services that it provides is the development encroachment into the littoral active zone, comprising, for example, beaches and dune systems.

2.1.2.2 Natural hazards and disasters

Coastal environments, specifically sandy beaches and dunes, are 'soft systems' that naturally respond dynamically to high energy controlling influences, including waves, wind and

flooding (D'Alessandro & Tomasicchio 2016; Kron 2013). These environmental forcing variables only become hazardous when they intercept with human activities and development established within the littoral active zone. Intense storms and wave fronts present a threat to coastal development and can result in damage and destruction of property and infrastructure (Palaseanu-Lovejoy et al. 2016) and the endangerment of the lives and livelihoods of people living within the coastal zone (Poelhekke et al. 2016; Tõnisson et al. 2016). In the case of sandy coastlines, human developments on beaches and dunes often results in situations where these natural features are compromised in terms of their ability to buffer the effects of storms and other extreme events (Yates et al. 2009). Beaches, which have a capacity to absorb a large portion of the energy from incoming waves (McLachlan & Dorvlo 2005), are particularly compromised in this regard (Tõnisson et al. 2016). Flooding of coastal areas and destruction of infrastructure is increasingly materialising where natural barriers to storms and other physical threats, such as beaches and dunes, are removed or degraded through development – or have lost their natural defensive capacity in the face of emergent environmental phenomena, for example, attributable to climate change. This can have disastrous consequences for human populations resident in low-lying areas in the immediate hinterland.

Coastal erosion is a phenomenon that occurs largely in response to natural forces such as wind, waves, tides and currents (Fourie et al. 2015; Prasad & Kumar 2014). It entails the wearing away and redistributing of solid elements as well as sediments along the shoreline (Figure 2.1). Erosion is often marked by the recession of the shoreline and is defined as 'the encroachment of land by the sea' (Prasad & Kumar 2014). This leads to the loss of not only economically but also ecologically valuable land. Accretion, which is often the consequence of erosion elsewhere, occurs as a result of excessive sediment supply to the coastline, often with negative consequences. Coastal erosion is often countered with beach nourishment, which involves artificially replenishing the beach with sand to enhance shoreline resilience and to restore its utility value (De Schipper et al. 2016).

Figure 2.1 Coastal erosion at Monwabisi (False Bay)

2.1.2.3 Climate change and Sea Level Rise (SLR)

Although they are ultimately attributable to anthropogenic causes, greenhouse gasses are causing an increase in ocean and air temperatures (Crain et al. 2009). In this regard, the IPCC predicts an increase in ocean temperature of between 0.3 – 2.0°C by the end of the 21st century (IPCC 2013). In addition to having many direct marine and other biological impacts, rising temperatures cause water to expand and accelerate the melting of ice caps. This drives a phenomenon known as sea-level rise (SLR) which has been reported to manifest as an increase of 3.7 mm/year (IPCC 2013). SLR rates have however been observed as reaching up to 10 mm/year in certain places. Around 10% of the current global population lives in low-lying coastal regions, which are between 0 and 10 m above sea-level (Patrizio et al. 2016), which implies that there will be severe consequences of SLR, for example, due to shoreline erosion, damage to infrastructure through storm wave effects and flooding.

A second important aspect of climate change is the effect it will have on weather patterns, which may be associated with increased storm frequency and intensity affecting the coastal zone (Theron et al. 2010). As a manifestation of climate change, high energy waves have already been shown to aggravate coastal erosion, posing threats to coastal infrastructure and human well-being (Fang, Yin & Wu 2016).

Adaptation to climate change will require physical interventions in order to safeguard the coastal environment. These could include the imposition of development set-back limits or the construction of sea-walls, which will need to account for a range of physical coastal elements and processes, including the relationships between sandy beach characteristics and

wave regimes (Theron & Schoonees 2007). Monitoring of coastal dynamics will be key in this regard.

2.2 COASTAL PROCESSES INFLUENCING SANDY BEACH DYNAMICS

This section describes how different types of coastline are formed and the various physical processes that influence and shape them. Coastal geomorphology focusses on the morphology of the coastal zone and the processes, including waves, tides and currents, that shape its diverse features, which range from rocky and cliffed shorelines to sandy beaches with associated dune systems (Davidson-Arnott 2010).

Often used synonymously in referring to the coast, Wiegel (1964) describes the shore as being the strip of ground bordering any body of water, which is alternately covered and exposed by changing tides and wave conditions. Woodroffe (2003), on the other hand, describes the coast as being the interface between the land and the sea, with the shoreline being the actual margin. The latter author includes in a description of the coastal zone, all marine environments influenced by terrestrial environments as well as all terrestrial environments influenced by ocean wind and salt spray, waves, tides, and water salinity. In many instances, the constant changing of a shore creates a state of dynamic equilibrium with regular seasonal and other temporal fluctuations in coastal conditions (Wiegel 1964). In the face of some of the threats to the coastal zone, discussed above, many previous dynamic equilibrium states are now in a state of flux.

2.2.1 Evolution of coasts

Coastal environments include a wide variety of land and water surface types, topographies and geological and biological settings. These features combine to create some of the more common coastal environments, which include beaches, dunes, reefs, rocky shores and estuaries (Gardner 1977).

Existing coastlines have been established during the recent era, and reflect a quite different situation than what prevailed, for example, during the Pleistocene, ending a little more than 10 000 years ago. As has happened in the past, the future will almost certainly introduce considerable changes to coastal environments (Davis 1994). These changes will be controlled by a combination of factors including, for example, plate tectonics, climate change and,

associated with this, new wind, wave and tidal regimes that will influence and shape the coast in integrated ways (Sheeja & Gokul 2016).

The morphology of the South African coastal zone reflects in many ways the result of the break-up of the Gondwana supercontinent. The country's west and east coasts are generally straight, with narrow continental shelves that have formed as a direct result of the shearing of the crust during the active break-up of Gondwana (Rust 1991). The irregular shape of the Cape south coast, is defined by numerous bays with their points of extremity created by outcrops of hard Table Mountain quartzite. The irregular coastline of the Cape Peninsula is mostly controlled by joints and faults in the bedrock (Rust 1991) also with contributions made by Table Mountain sandstone, which is highly resistant to erosion.

Coasts are characterised not only by the macro unweathered geological features of the type outlined above, but also by the type of sediment that contributes to the shoreline morphology (Inman & Nordstrom 1971).

2.2.2 Sources of sediment

Many of the physical dynamics of the coast are associated with sediment movement (Yates et al. 2009). Only occasionally can coastal sediments be linked to one particular source; more commonly, they originate from a variety of sources and delivered at different times. Coastal sediments are reworked, incorporated into and released from dynamic depositional features, such as beaches and dunes, continuously (Figure 2.2). The longer the period of mixing, the more difficult it becomes to identify the original source of coastal sediments (Carter 1988).

Primary sources of coastal sediment include erosion of cliffs, platforms and submarine outcrops by wave action. Although the rate of sediment production in this manner is inevitably low, substantial amounts may accumulate over an extended period of time (Prasad & Kumar 2014).

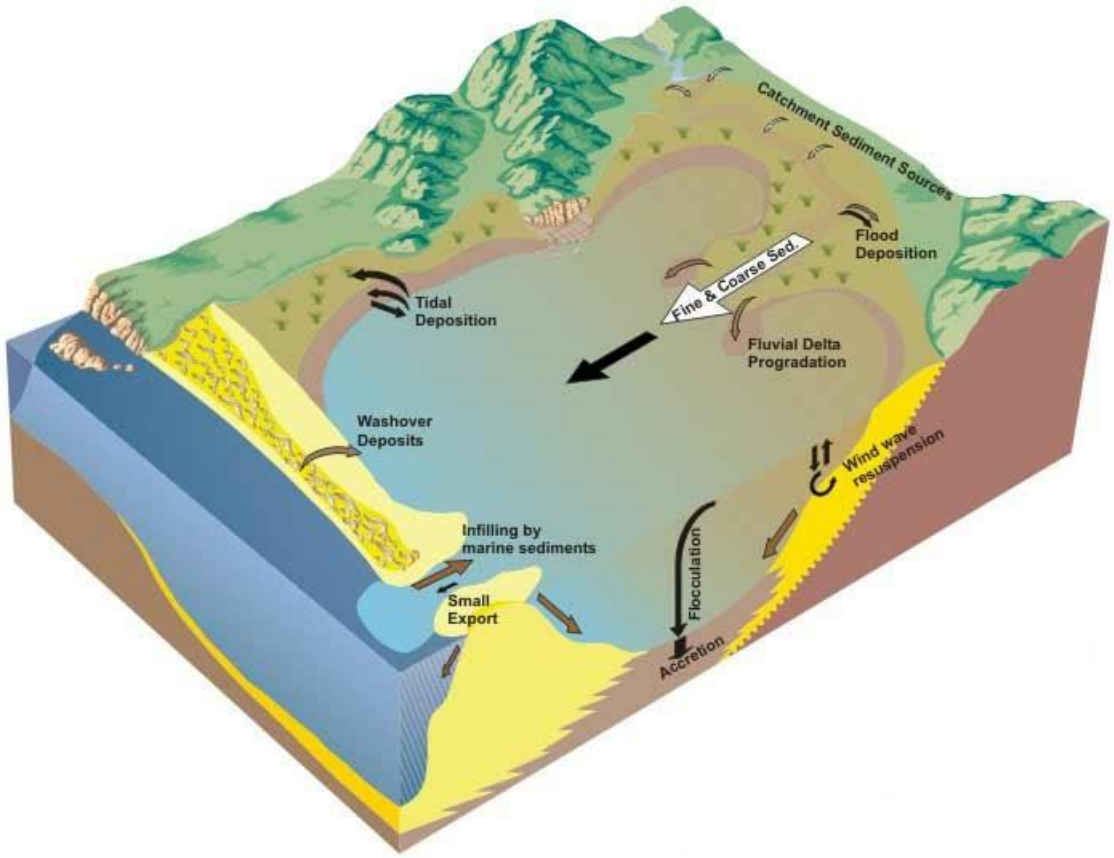

Source: Ozcoasts (2015)

Figure 2.2 Sources of sediment

Biogenic sources of sediment also make important contributions, for example, to the composition of beach deposits. Marine organisms such as corals, molluscs and crustaceans all contribute significant quantities of calcic biological material to coastal sediment reservoirs.

The dominant secondary sources of sediment are rivers. Sediment, originating from eroding inland geological structures is carried by rivers to their points of discharge to sea from where it is either widely distributed by physical coastal processes or deposited locally to create or replenish beaches and associated dune systems (Prasad & Kumar 2014). In South Africa, rivers are important sources of sediment and are responsible for nourishing many of the country's beaches. The type of sediment encountered along the shore therefore closely reflects the geological source and fluvial origin. Aeolian, or wind-blown, sediment is another example of a secondary source, with fine grained material often transported over considerable distances before settling (O'Keeffe et al. 2016).

Sediment from secondary sources has usually been through some form of initial sorting process (only fine, lighter sand can be transported by wind, for example) before entering the coastal environment and is supplied at irregular intervals along the coast.

2.2.3 Beaches

As defined by Wiegel (1964), a beach is "a shore of unconsolidated material", which refers to the nature of the accumulated sediment. Although all beaches are unique and dependent on the environmental conditions at specific locations, there are certain characteristics that are common for most beaches. Figure 2.3 below provides an illustration of a typical beach with its main contributing components. As illustrated, primary dunes are often backed by a series of secondary dunes. Secondary dunes are older and typically more consolidated through processes assisted, for example, by colonizing vegetation. Vegetation can play an important role in trapping and retaining wind-blown sediment and fortifying dunes as buffers against wave impacts, for example. This is a crucial function, or ecosystem service, particularly in areas where there are adjacent human settlements and infrastructure.

Where naturally dynamic dune systems have been artificially stabilised, often with alien invasive species, they lose their capacity to release sediment into the littoral active zone, often aggravating shoreline erosion.

The upper beach, which is often bounded at its seaward extreme by a berm, is largely unaffected by the effects of wave run-up (Soltau 2009) and sediment dynamics are principally maintained by wind, as opposed to wave effects. Found mostly on coarse sediment beaches, berms are formed by the deposition of sediment through low-energy waves (Short 1987; Short 2006). Berms notably mark a change in slope towards the upper beach. The landward aspect of a berm is often flatter than the seaward aspect, which is generally steeper as a result of wave action.

The beach face, including the inter-tidal zone, is the part of the beach that is most influenced by the dynamics of tides and wave action.

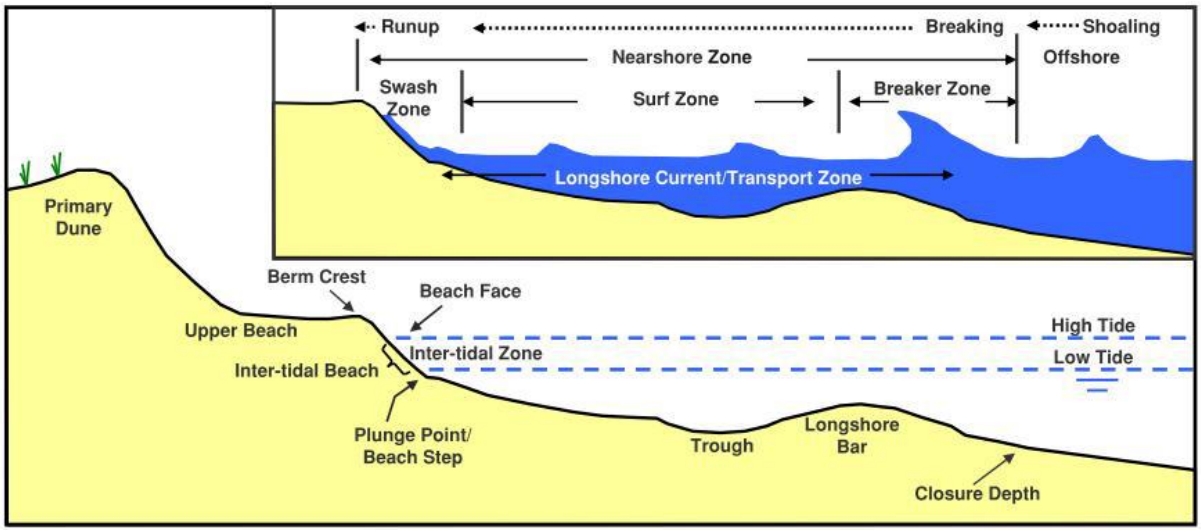

Source: Soltau (2009)

Figure 2.3 Illustration of a beach profile

Beaches can be classified differently: on the basis of how they formed, by a description of the physical beach depositional characteristics or by a combination of factors. The physical processes at play along the shoreline are the main factors that affect the morphology and state of a beach, with wave and tide action having the most obvious impact.

Wave dominated beaches (where shape is determined by wave action) can be categorised as reflective, intermediate or dissipative. Reflective beaches have the steepest slopes and are composed of coarse grain sediments (Abuodha 2003). They are associated with surging waves in the intertidal zone, and the surf zone is relatively narrow (see Figure 2.3). The coarseness of the sediments provides resistance to entrainment by wave backwash, thus allowing for more material to be deposited in the swash zone. Dissipative beaches, on the other hand, are mostly flat with finer sediment (Rust 1991). Here, spilling waves in the breaker zone tend to dissipate much of their energy before reaching the intertidal zone.

Tides can exert considerable influence on the shape of beaches, with tide-modified and tide-dominated beaches forming where there is a high tidal range associated with low wave energy regimes (Short 2006). Sediment movement is thus governed by tides rather than wave energy. Rip currents and long shore currents, originating from oblique angles of wave incidence, contribute significantly to the on-offshore and alongshore transport of sediment and the dynamics of beaches.

Beaches are not only defined in terms of wave climate and tidal regime, as discussed above, but also by sediment grain size characteristics. Grain size is determined by a number of physical processes as well as the geological composition of the material (McLean & Kirk 1969). A variety of sand types are produced through erosion of different rock types, both from cliffs within the coastal zone and from inland. Physical forces that influence and determine sediment grain size include wave, tide and current processes, proximity to the source, the nature of the source material and topography or beach slope (Abuodha 2003).

Many authors have investigated the relationship between slope and grain size (Bascom 1951; Wiegel 1964; McLean & Kirk 1969; MacLachlan & Dorvlo 2005; Reis 2009; Reis & Gama 2010) and confirm the tendency of steeper slopes to indicate a coarser grain size. Figure 2.4 shows how a decrease in slope correlates to a decrease in grain size.

Knowledge of beach grain size presents a valuable contribution to the understanding of the dynamics, monitoring and management of beaches. Sediment grain size, measured as particle diameter, is commonly classified according to a specific scale. One of the most frequently utilised of these is the Wentworth size classification.

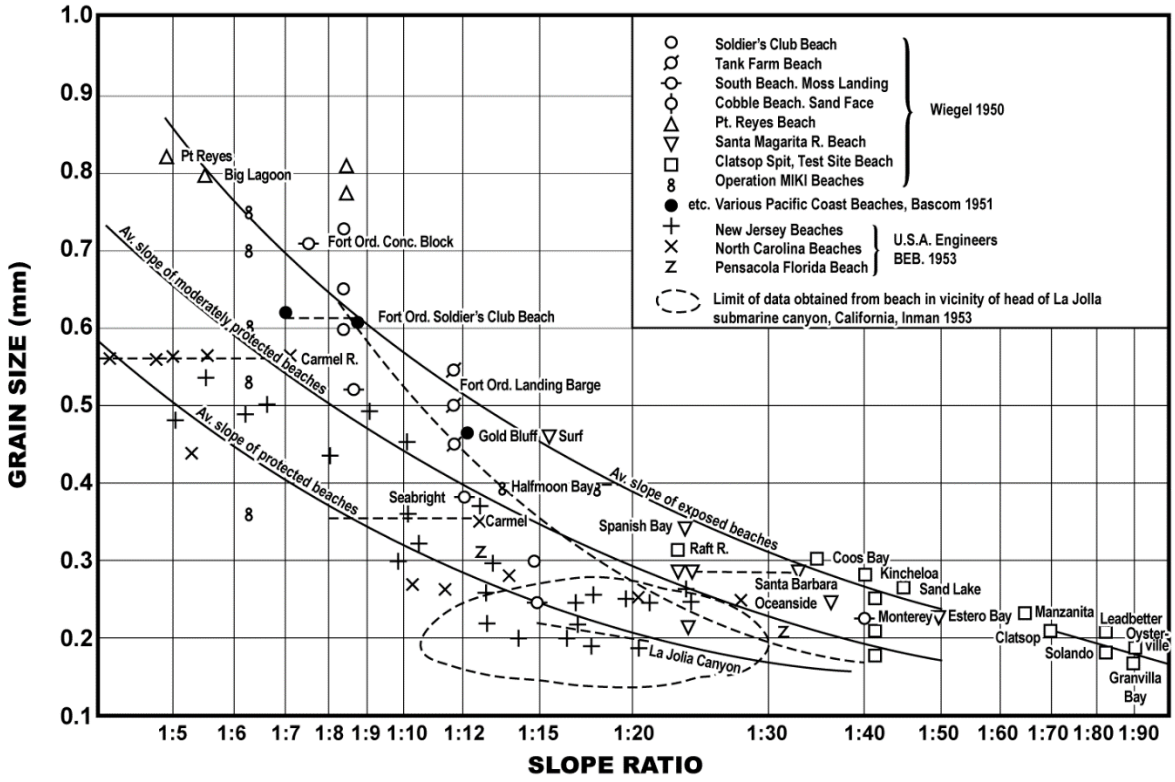

Source: Wiegel (1984)

Figure 2.4 Relationship between slope and grain size

2.3 REMOTE SENSING FOR COASTAL APPLICATIONS

As discussed above, the marine and coastal environment is an important asset to any coastal country. It is therefore essential that the coast is preserved and measures are taken to guard against the threats identified in the previous section. Effective means of coastal monitoring must be developed and regular surveys need to be implemented to identify any threats or changes to this dynamic environment (Amatya et al. 2013).

Historically, ground observations and surveys were used to obtain monitoring information pertaining to a given site (Chust et al. 2008). This approach is becoming increasingly costly and is also time-consuming (Sharma, Rout & Garg 2010). Additionally, ground surveys can only be conducted in accessible areas. More recently, remote sensing technologies have been developed and are one of the most common and effective ways of surveying extensive areas such as the coast (Prasad & Kumar 2014). Remote sensors can be divided into two categories; passive and active.

2.3.1 Passive and Active sensors

Passive sensors are reliant on receiving energy from the target or surface being observed. Most optical sensors record reflected solar energy in multiple wavelengths, thus allowing for the creation of multispectral datasets. There are very many applications for these types of datasets. For example, a study by Mbolambi (2016) shows how multispectral imagery can be used to identify degraded vegetation in coastal areas; another study by Klaar et al. (2014) uses satellite imagery to document changes in vegetation type and catchment sediment availability in Alaska. The limitations associated with these passive sensors are mostly related to atmospheric conditions and dependence on sunlight. Amongst other factors, cloud cover, shadow and darkness place limitatioins on the use of these sensors.

Active sensing technologies often complement applications incorporating passive remote sensing. The basis of active sensing technology is the emission of energy pulses and recording of the energy that is reflected back to the sensor. There are many different types of active sensors such as sonar and laser. Radar, including synthetic aperture radar (SAR), is another type of sensor used, for example, by Kemp & Burns (2016) to monitor the structure and change of vegetation in an agricultural setting. Active systems overcome many of the limitations associated with passive sensors, in that they are capable of acquiring data in adverse weather and atmospheric conditions and at night (Eitel et al. 2016). Some limitations to their use include the large power requirement for operation and the complex data processing that is required. Also, the resolution of data acquired by active sensors can be quite low, depending on flying altitude or platform range. LiDAR systems, a radar based technology, overcomes the latter limitation and can produce data with high resolution and accuracy.

2.3.2 Components of a LiDAR system

This section presents a summary of the generic components of a LiDAR system; however, many systems do not require all of the decribed components to operate. For example, the components recording motion and orientation will only be applicable to mobile and airborne platforms; on stationary platforms, such as tripods, the navigation system is obsolete. The components that are essential to all LiDAR systems are the scanning unit and computer.

2.3.2.1 Laser scanning unit

As illustrated in Figure 2.5, the laser scanning unit consists of a pulsed laser transmitter, a rotating mirror to direct the pulse, an optical telescope receiver and a photomultiplier tube to convert the returning light energy into electrical impulses (Schwarz 2010).

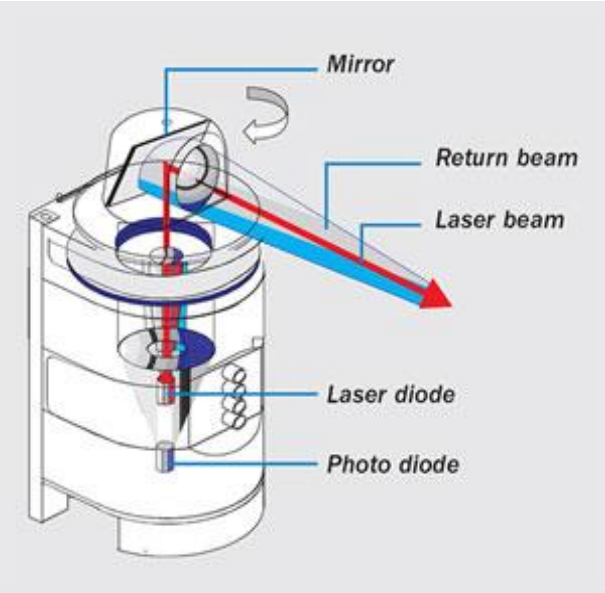

Source: Anandan (2015)

Figure 2.5 Diagram of a laser scanning unit

By directing the laser pulse onto the spinning mirror, the system effectively creates a 'fan' of laser light in a predetermined viewing angle of between 70 and 360 degrees around the sensor axis (Schwarz 2010). As soon as each pulse reaches a target, it is immediately reflected back to the mirror and to the receiver, which is the photo diode indicated in Figure 2.5.

2.3.2.2 Global Positioning System (GPS)

The ability to measure accurate location attributes is essential for a wide range of applications. The operation of GPS positioning entails space, ground and user segments (Breuer et al. 2002). The space and control segment consist of the orbiting satellites and master control and tracking stations respectively. The third segment constitutes the GPS receiver, which can be stationary or mobile. Accurate positioning is derived through communication between the three segments.

2.3.2.3 Inertial Navigation System (INS)

This component is used to correct for sensor orientation and speed (Saye et al. 2005). This is accomplished by combining the GPS receiver with an inertial measurement unit (IMU). An IMU is made up of three accelerometers and gyroscopes (Saye et al. 2005) that measure the gravitational, acceleration and angular rate vectors at a sample frequency of around 200Hz. Post-processing is then done to integrate GPS and IMU measurements to accurately determine the orientation of the platform carrying the scanner.

2.3.2.4 Computer

The final component necessary for the functioning of a LiDAR system is a computer and dedicated software. This is a key component as it is responsible for controlling the complex system and storing the data that is captured. LiDAR systems are known for producing very large datasets and it is thus essential that the computer has sufficient storage capabilities (Viles 2016).

2.3.3 Different LiDAR Platforms

It is necessary to mount a LiDAR sensor onto a platform before it can be operationally used in most applications. These platforms can be mobile or stationary as well as ground based or airborne (Pe'eri & Long 2011). There are certain advantages and disadvantages to using different platforms for acquiring LiDAR data. The sections below describe some of the platforms and highlight some of the advantages and disadvantages associated with each.

2.3.3.1 Ground-based platforms

Terrestrial LiDAR systems mounted on ground-based platforms are often used for close-range and high-accuracy applications (Carrea et al. 2016). Their use, for example, in crime scene analysis and in monitoring bridge and dam structures illustrates the diverse range of possible applications (Harrap & Lato 2010). One of their fundamental attributes is the potential for extremely high levels of sensing accuracy.

Ground-based platforms for terrestrial laser scanning (TLS) can be either stationary, employing tripods or masts, or mobile, employing, for example, mobile vehicles including

boats (De Moreas et al. 2016). For static implementation, LiDAR components such as the GPS and INS may not be necessary, for example, where a tripod or mast (onto which the LiDAR system is mounted) is set up over a known point (Harrap & Lato 2010). This situation allows for relative positioning of a returning signal to be determined on the basis of an established georefenced location; also, reference points can be surveyed in the field of view of the scanner to accurately georeference the captured data. Some of the most common applications of tripod based scanning systems are in the mining sector. Open pit mines, or quarries, are scanned using highly accurate laser systems, allowing for the creation of dense 3D point clouds that are used, for example, to detect structural weaknesses and potential rock-fall hazards (Harrap & Lato 2010).

Mobile, or dynamic, ground-based LiDAR systems are similar to airborne systems in that they utilise GPS and INS for accurate positioning (Harrap & Lato 2010). This would apply, for example, where the laser scanner is fixed to the roof of an automobile in order to capture data as the vehicle travels along a route. An example of such system application is described by Göhring et al. (2011) who developed an algorithm enabling cars to autonomously follow other vehicles using highly sensitive LiDAR sensors. Another, is described by De Moreas et al. (2016) who used a laser scanning system installed on a boat to monitor riverbank erosion in hydroelectric reservoirs in Brazil. See Figures 2.6a and 2.6b below for examples of mobile LiDAR platforms:

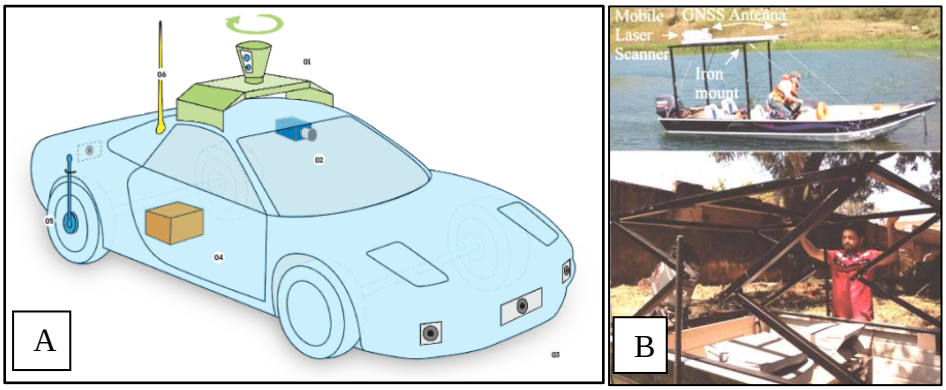

Figure 2.6 Mobile LiDAR platforms: A: car; B: boat.

There are a number of advantages to using ground-based platforms as opposed to airborne, and stationary as opposed to mobile. Ground-based systems are generally capable of achieving much higher point densities than airborne systems due to closer proximity to targets (Wenger 2016). The accuracy and resolution of the captured data makes ground-based

platforms ideal for applications requiring a high resolution particularly where the target of the scan contains very small objects, such as sediment grains. The close proximity of terrestrial scanning systems also minimises any atmospheric interference that may affect the data (Song et al. 2012).

Some examples of limitations of ground-based systems include reduced coverage of the captured data, terrain inaccessibility for equipment deployment and the time consuming and labour intensity of survey operations (Harrap & Lato 2010).

2.3.3.2 Airborne platforms

The most widely used platforms for LiDAR systems are airborne, which is largely explained by the high demand for survey data pertaining to extensive geographic areas. Airborne LiDAR systems (ALS, also airborne laser scanners) are used for a broad range of applications including mapping and characterisation of urban and other landscapes, including the coastal zone, for example, in order to detect shoreline and other patterns of change (Flood 2001; Carrea et al. 2016). The advantages of airborne platforms are that they are capable of covering large areas in a relatively short period of time, also permitting synoptic views of inaccessible terrain and remote regions (Viles 2016). The majority of Airborne LiDAR system applications relate to the acquisition of topographic data (Höfle & Pfeifer 2007).

Although ALS platforms include helicopters, balloons, unmanned aerial vehicles and others (Viles 2016), the main system elements applicable to a standard fixed wing aircraft, which is discussed here for illustration purposes, also apply to other airborne platforms.

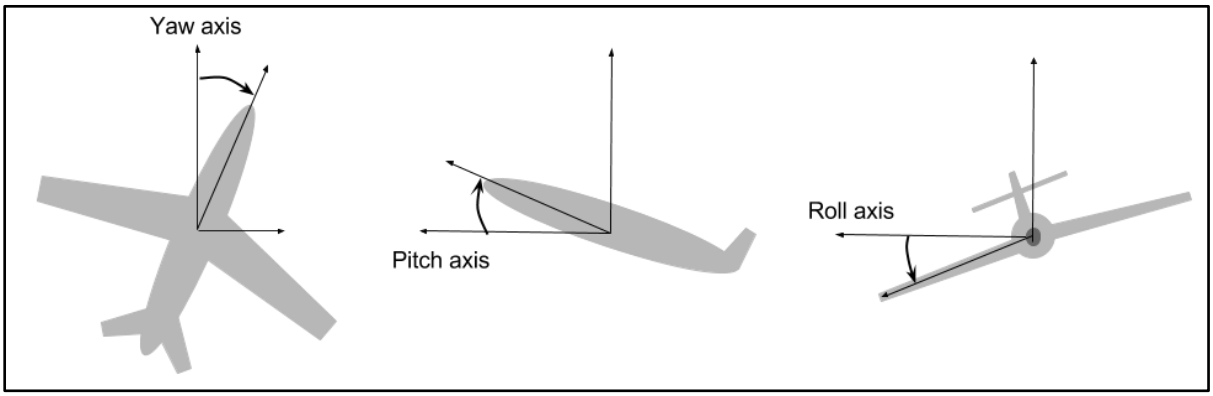

Source: Viles (2016)

Figure 2.7 Orientation of airborne platforms

In addition to the actual laser scanning technology and GPS, the onboard INS is critical in order to account for the aircraft's yaw, pitch and roll. As illustrated in the following Figure 2.8; (a) shows the yaw or bearing as being rotation around the z-axis; (b) shows the pitch, or rotation around the y-axis and; (c) shows roll which is rotation around the x-axis. To ensure the precision of LiDAR data capture, these movements are corrected through system processing of INS data (Vain et al. 2009).

Other factors that influence scanning precision are flying speed and altitude. Although the ideal might be to maintain a survey aircraft's constant speed and altitude, conditions very rarely allow this. Environmental factors such as wind, turbulence and natural terrain features will inevitably influence the flight path, altitude and attitude of an aircraft (Metcalf-Lindenburger 2016). Aviation laws and regulations also impose limitations in this regard (Wenger 2016).

A significant disadvantage to using an ALS is that the optical footprint of the laser is quite large, depending on the flying altitude, resulting in a lower point density (Wenger 2016). Because of the increased spacing between points, an ALS is not able to acquire data for small-scale features. Vain et al. (2009) also describe how received power decreases with an increase in flying height. Although LiDAR is a popular survey technology, its use is limited in high-relief terrain and built up areas that present shadow zones where laser pulses cannot reach (Xharde, Long & Forbes 2006).

2.3.4 Laser scanning

There are two main classes of LiDAR scanning systems, namely topographic systems, which acquire data over land, and bathymetric systems that detect bathymetry in shallow water. The ability of LiDAR to operate in these different environments results from the different wavelengths of the emitted laser pulses.

Topographic LiDAR systems operate within the near-infrared (NIR) wavelength of the electromagnetic spectrum (Schwarz 2010). These light pulses are absorbed by water (Wang & Philpot 2007), which is better penetrated using bathymetric LiDAR operating in a different range of the electromagnetic spectrum. In order to achieve water column penetration,

bathymetric LiDAR systems operate in the shorter green wavelength ranges of the electromagnetic spectrum (Wang & Philpot 2007; Guenther et al. 2000).

The Scanning Hydrographic Operational Airborne Lidar Survey (SHOALS) is an example of an operational airborne LiDAR bathometer developed for the US Army Corps of Engineers (Irish & Lillycrop 1999). More recent has been the development of the Coastal Zone Mapping and Imaging LiDAR (CZMIL), which is designed to produce high resolution 3D imagery of beaches and shallow water seabeds, to characterise water columns and to inform benthic classifications (Tuell, Barbor & Wozencraft 2010).

The principle behind a LiDAR system is the sending and receiving of laser pulses. The system emits the laser pulses at certain wavelengths and then receives the reflected signal. The time taken for the pulse to travel to and from the target is measured and recorded precisely. Using the standard mathematical formula for distance, the range to the target can be determined as shown in equations 1a and 1b below (Chandler & Buckley 2016). The speed of the laser pulse is *c*, the speed of light (300 000 km/s). The recorded time is halved, taking into account the two-way nature of the propagation (Baltsavias 1999).

$$distance = \frac{speed}{time} \qquad \text{. . . . . Equation 1a}$$

$$R = c\frac{t}{2} \qquad \text{. . . . . Equation 1b}$$

Due to the high frequency at which the laser pulses are emitted, up to 10 000 pulses per second with terrestrial LiDAR (Pe'eri & Long 2011), the resulting information is measured and stored in the form of an exceedingly dense point cloud. Each point within the cloud has an x, y and z coordinate, calculated using trigonometric algorithms (Vain et al. 2009). In the final 3D product, the values represented by x and y denote latitude and longitude respectively, while the z value represents the vertical distance, or elevation, above a predetermined ellipsoid (Froese & Mei 2008).

The high density of the collected point data is characteristic of LiDAR systems. Point density can be described as the number of points per square meter on the ground (Schwarz 2010).

There are many factors affecting point density. Higher density, achieved through lower flight altitudes at which the data is captured, is often preferable for accurately identifying smaller features, but comes at the cost of a smaller coverage and higher volumes of data to be stored and processed.

In addition to its x, y and z coordinates, each point has a number of other attributes associated with it. The return number of the pulse is one of these attributes. The number of returns characterising each pulse is determined by the surface material it interacts with (Mallet & Bretar 2009). Surface features are often permeable or semi-permeable and thus allow for the laser pulses to propagate through the gaps and reflect off structures beneath. For example, a smooth concrete surface would present only one return because the pulses interacting with the surface are unable to penetrate beneath the surface. In contrast, vegetation canopies usually consist of many layers of foliage that can reflect the laser pulses at different heights. In this case, the fraction of light reflected off the top of the foliage canopy will be recorded as the first return, that reflected off the next, sub-canopy, layer will be the second return, and so on. Figure 2.9 below illustrates the multiple returns created through the interaction of the laser scanning with vegetation.

According to Carter (2012), up to five returns can be recorded for each pulse by most discrete return systems, although full waveform scanners have been developed that record more returns. For topographic mapping and many other applications, three returns are regarded as sufficient (Mpe 2015).

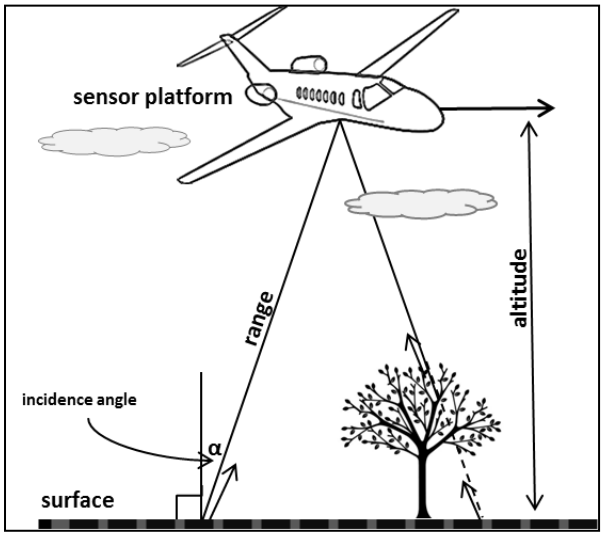

Figure 2.8 Illustration of LiDAR operation

In an airborne system, by integrating the information from the aircraft GPS and INS with the known parameters of the LiDAR scanner, such as range and incidence angle, each point in the cloud can be georeferenced. This enables the construction of a 3D view of the earth surface (Li et al. 2011). The ability of LiDAR to create multiple returns allows for complex 3D reconstructions of certain terrestrial surfaces (Webster et al. 2016; Saylam, Hupp & Averett 2017). This would have limited application, for example, in the case of beaches devoid of vegetation, where the first and last returns would tend to be in the same range.

Another characteristic attribute of each point in a LiDAR point cloud is intensity (Wang & Glenn 2009). The intensity value represents the strength, or amount of energy, of each returned pulse (Yan & Shaker 2014; Kashani et al. 2015; Carrea et al. 2016; Eitel et al. 2016). This term is synonymous with 'reflectance' in optical remote sensing. The factors influencing the return intensity of the laser pulses can be broadly divided into three categories; factors relating to the sensor, factors relating to the scanned surface, and those relating to the atmospheric conditions during scanning (Carrea et al. 2016). Parameters such as laser beam wavelength, emission power and internal calibration are specific to each LiDAR scanner, whereas factors relating to the scanned surface include range, incidence angle, surface composition and moisture content (Carrea et al. 2016). Atmospheric conditions may also alter the path of the laser beam and reduce the intensity of the backscattered signal. The strength of each individual return decreases as the number of returns per pulse increases (Carrea et al. 2016).

Due to the number of factors affecting intensity, which are not related to surface characteristics, intensity values tend to be corrected before they are used in most applications (Ding et al. 2013). Many studies have been made relating to methods of correcting intensity, both radiometrically and statistically (Höfle & Pfeifer 2007; Vain et al. 2009; Ding et al. 2013; Yan & Shaker 2014; Carrea et al. 2016); however, research into intensity correction is still relatively undeveloped, and there is currently no agreed upon method for optimal correction.

2.3.5 Products and derivatives

After acquisition by the LiDAR system, data are usually stored in the LAS file format, which combines the GPS, IMU metadata and the laser scanning measurements. LAS is a binary format and maintains information specific to the LiDAR in a relatively simple format.

Among the most common products generated from LiDAR data are digital surface and elevation models (Eitel et al. 2016). A digital elevation model (DEM) is a continuous surface in the form of a raster or grid where each cell (x, y coordinates) has an associated elevation relative to a reference height (Amatya et al. 2013). The reference height is often mean sea level (Ma 2005). There are different types of elevation models that allow representations of different surfaces, with varying precision. One, is the digital terrain model (DTM), which can be used to represent, for example, the ground, free of protruding features (Froese & Mei 2008). It is created through interpolation of ground points (i.e. the last returns), without accounting for earlier returns triggered by vegetation layers or other structures. Another model is the digital surface model (DSM), which complements the DTM by representing various surface features. With LiDAR, DSMs are created by interpolating first return data.

The highly accurate elevation models produced using LiDAR allow for slope and aspect surfaces to be derived based on recorded changes in elevation between cells in the grid. It is also possible to create a raster surface from recorded intensity values. This latter derivative is known as a digital intensity model (DIM), essentially representing the strength, including related patterns, of the returning signal (Yan, Shaker & El-Ashmawy 2015).

2.3.6 Applications of LiDAR

LiDAR technology is used in many applications. Examples that are relevant to the research presented in this dissertation, include those relating to both the general characterisation of the coastal zone (e.g. mapping the spatial distribution of coastal vegetation types and physical features such as beaches and dunes) and monitoring and quantification, for example, of the dynamics of shoreline positions, beaches and dunes. Also relevant, are the LiDAR deployment platforms, including the airborne and terrestrial alternatives that are used in these applications, and the captured data that is commonly of two main types: altimetry or elevation-based and intensity-based (see earlier discussion). In this context, a review of the

literature indicates that a significant proportion of contemporary research involves the use of airborne LiDAR platforms and the capture and interpretation of altimetry based data involving the creation of DEMs for various uses. In contrast, a much smaller proportion of published research involves applications of LiDAR that is deployed through terrestrial platforms and the capture and interpretation of intensity data for specified purposes within the coastal zone. The following literature review, which differentiates between elevation- and intensity-based examples of applications reflects the relative prevalence of the former compared to the latter.

2.3.6.1 LiDAR elevation-based applications

The use of LiDAR in the coastal environment is of particular interest due to its ability to capture small changes with a high level of precision. In a study by Revell, Komar & Sallenger (2002), a LiDAR system mounted on a small aircraft was used to document beach changes and shoreline erosion. The aim was to determine shoreline dynamics in response to increased mean sea-level and wave intensity during an El Niño event. The LiDAR data proved extremely useful in quantifying erosion, and also for providing a better understanding of erosion processes. The authors also showed how LiDAR can very accurately resolve elevation changes of beaches both alongshore and across beach profiles.

Sallenger et al. (2003) conducted another study to quantify beach changes using airborne topographic LiDAR along a stretch of open, un-vegetated beach in North Carolina. By conducting repeated surveys with NASA's airborne topographic mapper (ATM) and comparing the results to other ground based surveys, the authors were able to assess the accuracy of the ATM system. This study was aligned with a similar one, focused on the Assateague coastline, that was undertaken by Krabill et al. (2000). Making reference to extensive supporting surface observations, the latter authors used an ATM to effectively map the topography of a section of the coast using an airborne LiDAR system.

Richter et al. (2011) used a time series of airborne LiDAR data to monitor dune cliff erosion and beach width dynamics, on an intra- and inter-annual basis, along a coastal sand spit in Germany. Verification of the LiDAR data showed that the technology was effective and very accurate for the application in which it was deployed. The results showed, for example, seasonal patterns in dune erosion in response to storm surges, while beach width dynamics

tended to be aseasonal due to the persistency of the processes, including wave energy regime, that primarily determine shoreline position. The LiDAR data showed a close correlation between a decrease in beach width and the onset of dune erosion, while dune erosion and the release of accumulated sediment into the littoral zone was found to trigger an increase in beach width. Based on the LiDAR results, the study indicated that dune erosion could best be mitigated through beach nourishment intervention. In a similar application, Gares, Wang & White (2006) used time series LiDAR data to monitor the effectiveness of a beach nourishment project implemented in North Carolina, USA. The study detected, with precision, the volumetric changes to the beach and adjoining dune system following hurricane storm erosion. Different to the response detected by Richter et al. (2011), where beach nourishment proved an effective intervention against storm effects, interpretation of the LiDAR data by Gares, Wang & White (2006) showed that artificial beach nourishment was ineffective in the long term due to the rapid offshore loss of the imported material.

Casella et al. (2016) describe the use of drone technology and LiDAR to produce a series of DEMs of a stretch of beach in Itlay's Liguria Region. The focus of the survey was on precision mapping of the beach, repeated over several months, in order to quantify the effects of storms and human intervention in response to observed beach erosion. High energy storm waves were shown to account for beach sediment losses that were experienced, while sediment nourishment schemes implemented by beach management agencies accounted for the sediment volume gains that were quantified. The authors conclude that drones provide a practical airborne platform for LiDAR surveys undertaken within the coastal zone.

Obu et al. (2016) also use time series LiDAR elevation data, recorded using a traditional fixed wing aircraft platform, to monitor the coupled processes of coastline erosion and progradation along the Canadian Beaufort Sea. The results showed that low-lying sections of coastline are more prone to erosion than coastlines with higher backshore elevations. In some ways similar to the conclusions of Richter et al. (2001), interpretation of the LiDAR data shows that incidences of shoreline progradation are triggered by the release of slumped backshore material into the littoral zone, where it remains temporarily until erosion processes effect its removal and dispersion. The study concludes that these relatively short term shoreline dynamics may not be detected through more conventional methods of shoreline

monitoring of longer return period, indicating the potential of frequent airborne LiDAR surveys to eliminate this deficiency.

A comparison done by Sanders (2007) of different elevation models for depicting flood and inundation scenarios showed how LiDAR derived models proved to be the most accurate when compared to other high resolution alternatives. In this regard, Gesch (2009) describes how the high resolution of LiDAR derived elevation models allows for detailed delineation of potential inundation zones, showing with more certainty which areas are most vulnerable to sea level rise.

Smeeckaert et al. (2013) describe the use of airborne laser scanning in applications relating to coastal zone hazard identification, including flood risk. The authors use the technology and the DTMs that are created to differentiate between LiDAR point clouds associated with land topographic features and water surfaces respectively. Through a semi-automated analytical process described by the authors, this allows for rapid definition of shoreline positions, over extensive areas, for risk management purposes. In a similar application, Stockdon et al. (2009) used LiDAR topographic surveys of coastal dunes, focusing on crest elevations, to establish land vulnerability to inundation during hurricanes. Through cross-sectional analysis of the beach and dune profile continuum, vulnerability prediction was based on the proximity to the beach of the most seaward dune crests and the implication of this topographical variable for water inundation in the event of hurricanes. An algorithm, which was developed to perform the analysis, revealed that water levels likely to occur during hurricanes would overtop the LiDAR-determined dune crest elevations along most of the shoreline that was investigated.

In contrast to the airborne platforms used by Stockdon et al. (2009) and Smeeckaart et al. (2013), a terrestrial laser scanning platform was used by Schubert et al. (2015) to produce a series of high precision DTMs to monitor the dynamics of an anthropogenic beach berm used to manage flooding in southern California. The results proved effective in providing an accurate prediction of the onset and risks of flooding due to overtopping of the monitored berm.

Mitasova et al. (2009) used time series LiDAR data, sourced over more than a decade from several different airborne deployment platforms, to detect elevation and volumetric changes

in beach and dune elevations for a barrier island off North Carolina, USA. To confirm the precision of the sets of vertical differences that were measured, the authors highlight the need to use fixed reference points, such as a road, to correct the DEM model series to ensure the integrity of the analytical results. As for similar applications outlined above, the authors conclude that the technology is extremely effective as a tool for informing beach management interventions.

Xhardé, Long & Forbes (2006) used airborne LiDAR to map a section of the coast in Canada, which was done in parallel with ground surveys, using theodolites, to measure beach profiles for the validation of the LiDAR results. Also focusing on survey accuracy in the context of deployment platform options, Samsung-Lim et al. (2013) compared a vehicle-mounted mobile terrestrial LiDAR platform to that of a tripod based system that was used for calibration purposes, to measure extremely fine scale physical features along a coastal transect at Padre Island National Seashore, USA. The authors found the mobile technology to be appropriate for capturing elevation data of complex shoreline features, such as dunes, and found that the system was comparable in terms of accuracy relative to the robust tripod mounted system. Contributing to this positive result was the high density of the point cloud that the system could produce. It was concluded that the mobile terrestrial system has useful applications, for example, monitoring beach berm dynamics in advance of potential flood overtopping situations.

Saye et al. (2005) document a study done in England and Wales using LiDAR to characterise beach morphological relationships and to identify erosion and accretion instances. Concluding that this type of survey has potential as an early warning-indicator of erosion, the authors noted the critical importance of having ground truth data to validate results from a LiDAR survey. Boak & Turner (2005) also review various approaches to detecting and defining shorelines, for example using DEMs, and are critical of certain qualitative elements of visual interpretation that may be used. Objective approaches, such as using a reference to fixed features evident on remotely sensed imagery, are described by the authors as techniques that can overcome this deficiency. However, they also describe the use of algorithm-determined proxy indicators that can eliminate the need to incorporate fixed reference features in producing DEMs. Such an approach is described by Moore et al. (2006) who used contemporaneous aerial photography and airborne LiDAR topographic data to interrogate the

usefulness of traditional approaches to plotting the high and mean high water lines of a high energy, steeply sloping beach. Through comparison of the different water line positions that were determined, which were shown to vary considerably in terms of horizontal distance and vertical elevation, the authors derived what they term a proxy-datum offset. This permitted a consistent approach to plotting a high water line that could be used in monitoring shoreline dynamics over time. It was concluded that this offset introduced greater sensitivity and consistency in detecting shoreline changes than alternative approaches provide for.

2.3.6.2 LiDAR intensity-based applications

In a study that demonstrates the potential for intensity to be used to characterize the physical characteristics of beach sediments, Krooks et al. (2013) report on laboratory investigations of LiDAR data, sourced using terrestrial laser scanning platforms, to derive intensity corrections with the aim of enhancing the accuracy of field applications. The authors focus on a number of key variables, including incidence angle, scanning distance and surface topographic characteristics, and conclude that laboratory derived correction functions can introduce a high degree of integrity to field sourced intensity data. Of relevance to the research, the authors found that where topographic variations attributable to sediment grain size are smaller than the laser spot on the surface, this does not influence incidence angle effects.

With similar aims of enhancing the accuracy of LiDAR applications, Garestier et al. (2015) describe the production of LiDAR intensity maps, including an example of a sandy beach. The focus of investigation of these authors is on anisotropic and texture amplitude effects of scanned surfaces, where signal to noise ratios present challenges to mapping processes. These are described as relating mainly to spatial and temporal variations in sediment physical properties, including moisture content. They describe methodologies through which surface characterisations are produced that are more accurate than approaches based on textural data alone.

Kaasalainen et al. (2008) use radiometric calibration of LiDAR intensity data in order to enhance its practical utility value. In laboratory experiments, the authors measure the backscatter properties of sand and gravel samples, with measured physical properties, in order to produce reflectance calibration values for application to field measurements. The

incorporation of these calibration values into data sets derived from airborne laser field trials proved the repeatability of the results that were achieved.

Mpe (2015) found that intensity could be used to aid in identifying areas where strip-mining occurred along the west coast of South Africa. Focusing on a somewhat similar application, Burton et al. (2011) point to the limited number of lithology mapping and related studies where LiDAR intensity data are used in combination with the technology's capacity to register surface geological spectral data. The authors found that LiDAR's near infra-red wavelength can be used to differentiate, for example, between quartz rich sandstones and clay rich mudstones. They found that intensity data can also provide this differentiation, but that the precision of lithological mapping is reduced as the degree of surface weathering and moisture content increase.

Opportunities to use LiDAR intensity in different applications, independently of multispectral data, are also discussed by Song et al. (2012) who conclude that the separability of intensity between some land cover classes (e.g. asphalt road, roofs, grass- and tree-cover) is sufficient to warrant its use for basic land-cover classification. The authors also conclude that intensity data tend to contain considerable noise, which requires various approaches to filter the data. Similar approaches are described by Palaseanu-Lovejoy et al. (2009) who evaluate LiDAR intensity for predicting vegetation presence or absence, while Donoghue et al. (2007), using LiDAR data in combination with derived canopy height, show the technology's capacity for species differentiation in the vegetation types that the authors studied.

Potentially offering the greatest utility value, LiDAR has been used in combination with optical and other data to produce integrated datasets that have been shown to improve accuracies in land cover and vegetation classifications (Lück-Vogel et al. 2016). In this regard, Chust et al. (2008) describe how LiDAR intensity data are used, in combination with multispectral data, to support a range of physical surface mapping, terrestrial habitat characterisation and land-cover classification initiatives.

CHAPTER 3 METHODS AND MATERIALS

3.1 INTRODUCTION

The primary aim of this study is to determine whether the LiDAR intensity derivative can be used to approximate beach sediment grain sizes. A secondary aim of the study is to correlate elevation data, captured through an airborne LiDAR platform, with ground-based measurements of beach slope. LiDAR technology has proven to produce very accurate and high resolution digital elevation models, allowing slope surfaces to be calculated relatively easily. Potential limitations regarding the latter are recognised due to the interval elapsed between the airborne data capture and ground-based observations during sample collection.

As described earlier, there is a general correlation between wave energy, beach slope and sediment grain size. High levels of wave energy tend to produce steeper-sloped beaches with relatively coarse-grain sediments. The converse is true for beaches exposed to relatively low wave energy. Fundamental to the research methodology applied in this study is the selection of coastline sectors and beaches covering a range of exposure to different wave energy with related slope and sediment grain size characteristics. Advancing from this foundation of site selection, a methodology framework is used to guide the achievement of the stated research aims. The framework and contributing research methods are described in the following sections.

3.2 METHODOLOGY FRAMEWORK

The framework used to organise the research methodology for this study and to guide its implementation comprises two main streams of research. These encompass the analysis of terrestrial and airborne LiDAR data, respectively.

A break-down of the methodological stages and contributing steps is depicted graphically in Figure 3.1. For the terrestrial LiDAR analysis these include the selection of beach sites for sediment sampling and elevation measurements and the steps taken to obtain sorted sediment samples for LiDAR scanning, as a precursor to intensity analyses that are undertaken. The figure depicts the relatively fewer steps comprising the airborne LiDAR analysis, which include selection of LiDAR tiles covering the areo of interest and the elevation and intensity

analyses that are performed using rasterized aerial LiDAR data sets. The concluding methodological steps, which are aimed at establishing key correlations, are fundamental for addressing the stated research aims.

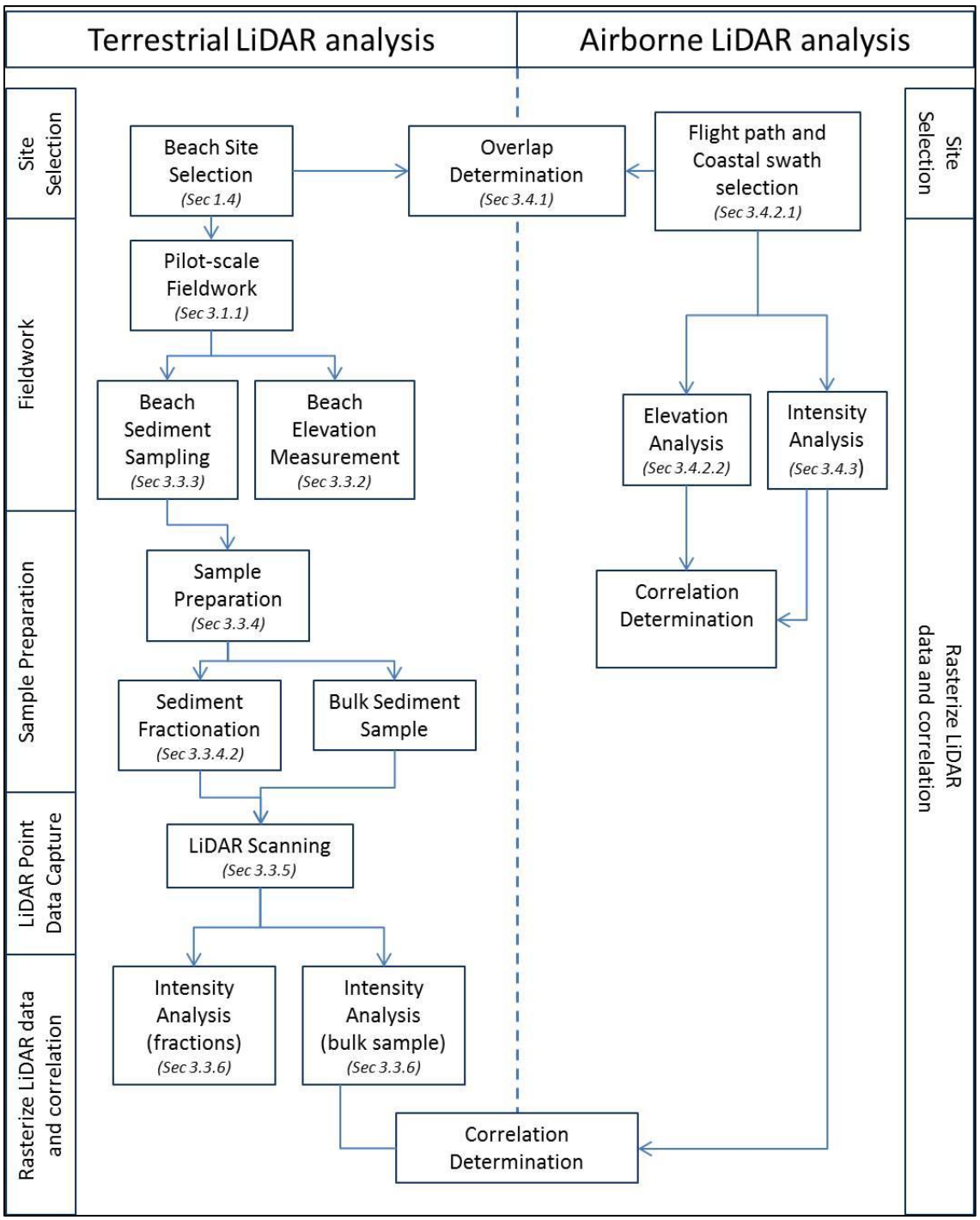

Note: The numbering of the steps depicted in the framework align with the section numbers used in the text below, which elaborates on the research methodology. This allows for the individual methodology descriptions to be considered in the context of an overall framework.

Figure 3.1 Methodology framework

3.3 EXPERIMENT 1: TERRESTRIAL LiDAR ANALYSIS

3.3.1 Fieldwork and sampling

A pilot fieldtrip to the Strand beach was conducted in order to establish a suitable method for field measurements and sediment sample collection. The aim was also to achieve familiarisation with the field equipment used.

Strand was chosen as the test location due to proximity and ease of access. A total of four samples was collected while the transects measured for elevation and slope are displayed in Figure 3.2 below. The sediment sample collection procedure proved suitable for use in the main fieldwork operations that were planned; however, procedural changes were made regarding the transect measurements. The intensive measurement of DGPS points along the transects proved unnecessarily time-consuming for the purposes of slope characterisation and a decision was taken to record fewer measurements along transects planned for the main field survey operations.

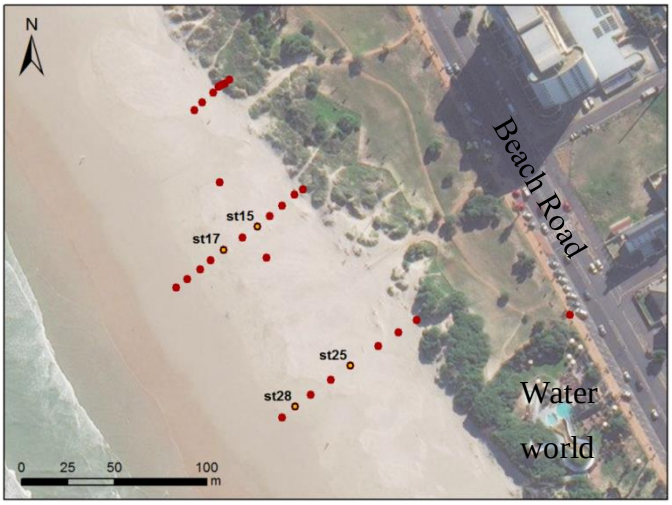

Figure 3.2 Pilot field site at the northern section of Strand beach in the vicinity of the Water world play park, 4 samples collected at hollow, labelled points. At all points, DGPS measurements were made.

Following the above exercise, field trips to the three main study sites in False Bay were conducted (Figure 1.2). This was done with the purpose of collecting beach slope data and sampling of sediment for subsequent scanning using a terrestrial LiDAR system.

3.3.2 Point measurement using differential GPS

A differential GPS (DGPS) was used to collect precise x, y and z coordinates at sample points along a number of representative transects at each of the main study sites. A DGPS uses a network of ground-based reference stations in combination with the GPS satellite network to determine the position of a receiver, with millimetre accuracy.

In this study, a TrimbleR4 DGPS was used to measure positions at the study sites (see Appendix 1 for the technical data sheet for the device). The Global Navigation Satellite Systems (GNSS) receiver was mounted on a 2 m monopod with an attached operating interface. The surface area of the monopod base was increased to prevent it sinking into the beach sediment so as to record accurate surface elevations (see Figure 3.3). The DGPS's post-processing kinematic (PPK) mode was used, as the device was not calibrated for Real-Time Kinematic (RTK). RTK processing relies on a data link between the mobile unit and at least one other stationary GNSS receiver providing reference data.

Figure 3.3 DGPS measurement on Strand beach

At each of the sampling sites a series of transect profiles was measured perpendicular to the water line. The number and distribution of the transects were ensure proper representation of conditions at the study sites, covering small variations in slope resulting from dynamic wave and beach interactions. The transects extended from the seaward limit of the dune systems and extended into the inter-tidal zone. Measurements for slope determination were taken at intervals of between two and four metres. Refer to Figures 3.5 to 3.7.

Table 3.1 lists the start and end-point coordinates of the surveyed transects at the three study sites. This locational data will aid the repeatability of the surveys, should this be considered in future.

Table 3.1 Start and end-point coordinates for surveyed transects

		TRANSECT START		TRANSECT END		SIZE
		X	Y	X	Y	
Kogel Bay	1	18.8501	-34.2352	18.8495	-34.2355	82 m
	2	18.8502	-34.2352	18.8496	-34.2356	80 m
	3	18.8503	-34.2353	18.8497	-34.2357	81 m
	4	18.8512	-34.2364	18.8506	-34.2367	77 m
	5	18.8513	-34.2364	18.8507	-34.2368	84 m
	6	18.8514	-34.2365	18.8507	-34.2369	86 m
	7	18.8522	-34.2376	18.8516	-34.2379	71 m
	8	18.8523	-34.2377	18.8517	-34.2379	71 m
	9	18.8523	-34.2377	18.8517	-34.2380	78 m
Fish Hoek	1	18.4324	-34.1401	18.4330	-34.1402	71 m
	2	18.4325	-34.1400	18.4331	-34.1401	69 m
	3	18.4325	-34.1399	18.4331	-34.1400	67 m
	4	18.4334	-34.1380	18.4338	-34.1382	54 m
	5	18.4335	-34.1379	18.4339	-34.1381	56 m
	6	18.4335	-34.1378	18.4341	-34.1380	64 m
Strand	1	18.8220	-34.1135	18.8216	-34.1136	45 m
	2	18.8220	-34.1135	18.8217	-34.1136	36 m
	3	18.8220	-34.1136	18.8217	-34.1137	35 m
	4	18.8221	-34.1139	18.8217	-34.1140	47 m
	5	18.8221	-34.1139	18.8218	-34.1140	47 m
	6	18.8222	-34.1140	18.8218	-34.1141	42 m
	7	18.8221	-34.1141	18.8218	-34.1142	41 m

3.3.3 Sediment sample collection

At the locations indicated by the hollow points in Figures 3.5 to 3.7 (with ArcMap basemap satellite imagery as background), about one kilogram – the approximate carrying capacity of the sample bags – of beach sand was collected from the upper layer of beach sand, no deeper than 10 cm below the surface. Laser pulses from a LiDAR system are not able to penetrate the ground so LiDAR returns will only be affected by the top layer of sediment on the beach.

Labels indicating the DGPS point names, for identifying the sample location, was placed in the sample bag before sealing with cable ties for transport (Figure 3.4 below).

Figure 3.4 Sample collection equipment and sample from Kogel Bay

Permission for obtaining samples from the public beaches was obtained from the CoCT municipality and the Department of Environmental Affairs (DEA) (see Appendix 2). The amount of sediment removed from the beaches was not of a magnitude that required any specific permits.

Beach slope measurements and sediment sampling activities at Kogel Bay were scheduled for 6 June 2016, commencing at 10h00 (Figure 3.5). Predicted low tide for this location was at 10h11, which exposed the intertidal part of the beach throughout the sampling period. Nine sediment samples were collected, with x, y, z coordinates recorded using a DGPS along nine different transects.

Permission was acquired from the CoCT municipality to access the beach through the Kogel Bay resort camping grounds (see Appendix 3).

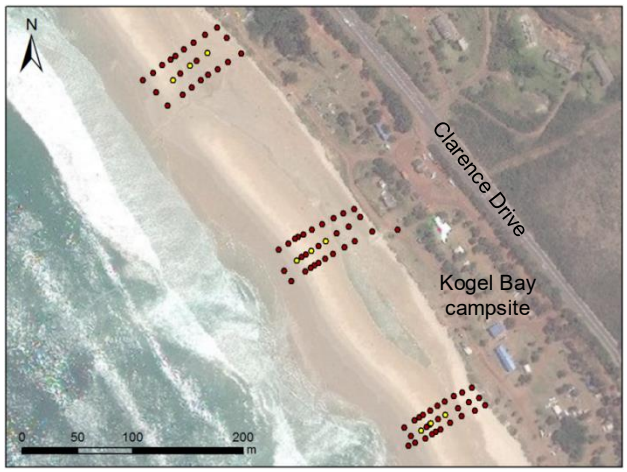

Figure 3.5 Sampling site at Kogel Bay, 9 samples collected at the hollow points. All points were measured using a DGPS.

Sampling at Fish Hoek was scheduled for 7 June 2016 (Figure 1.3A). Field activities were completed around low tide, which was predicted for the site at 10h55. Four sediment samples were collected and six transects were surveyed using DGPS. The sampling locations and transects are indicated in Figure 3.6.

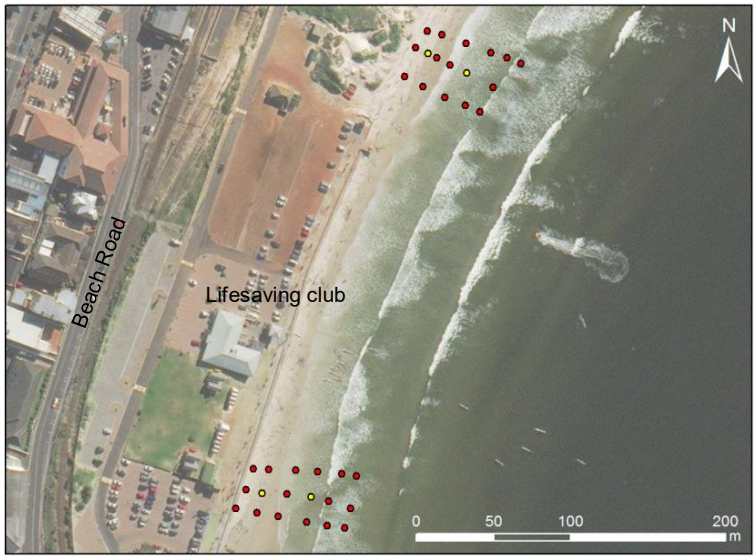

Figure 3.6 Sampling site at Fish Hoek. Four sediment samples were collected at the hollow points indicated in the figure. All points were measured using a DGPS.

At the conclusion of the initial set of field survey activities, a follow-up survey was repeated for the Strand beach sampling site. This was scheduled for 4 October 2016 and was completed at around 09h30 during the last stages of a falling tide, ahead of low tide predicted for 10h42. The repeat survey was conducted to ensure consistency with the systematic approach, gained through survey experience, adopted for the other sampling sites. Seven beach slope transects were surveyed and three sediment samples collected at the points indicated in Figure 3.7.

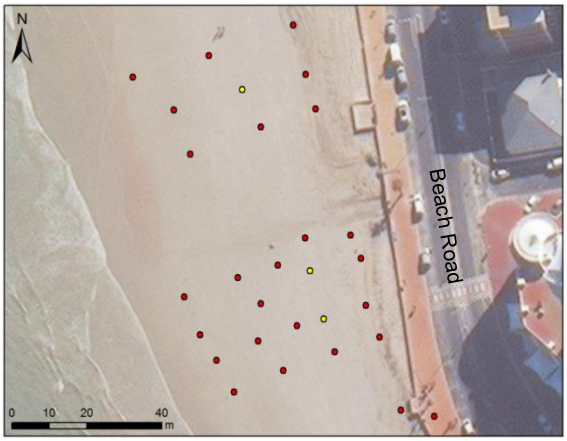

Figure 3.7 Second field trip to Strand, 3 samples collected at the hollow points. All points were measured using a DGPS.

3.3.4 Sample processing

The terrestrial LiDAR analysis was performed using the field-sourced sediment samples, with the aim of testing the hypothesis that sediment grain size is correlated with measured LiDAR intensity values. Conducting the analyses in a controlled laboratory environment aimed to eliminate potential distortions of captured LiDAR data caused by atmospheric conditions and other environmental factors.

3.3.4.1 Drying of sediment samples

For the majority of sediment samples, the collected material was wet and clumped, making it impossible to re-create the relatively smoothe beach surfaces from which the sediment originated. It was therefore necessary to dry the samples, which was achieved by opening the sample bags for air-dry over a period of up to a few weeks, depending on the degree of moisture incorporated into the various samples (Figure 3.8). On a regular basis during the drying process, the sediment was stirred to separate any clumps that formed.

Figure 3.8 Sample drying process

For the Fish Hoek beach samples, air-drying of the wet fine-grained sediment was too protracted and oven-drying was employed to speed up the process. Samples were heated to temperatures ranging between 50 and 100°C. No combustion of any of the sample material occurred.

3.3.4.2 Sieving of sediment samples

Leaving the bulk of the dried samples in their natural state, approximately 250 g of sediment was extracted from the samples and passed through a series of mechanical sieves in order to separate the different grain size fractions. The purpose of the sieving was to both characterise the natural samples in terms of proportions of contributing size fractions and to separate out the various homogenous fractions for separate laboratory-based laser scanning. The images below show an example of the setup of mechanical sieves at the Geology Department of Stellenbosch University (SU) where much of the work was performed for this study.

Figure 3.9 Mechanical sieve stack on the mechanical shaker at SU

The sieves were stacked with the largest mesh size on top, with progressively smaller meshed sieves placed beneathe (Figure 3.9). The entire stack was then placed onto a mechanical shaker and processed for between 5 and 10 minutes.

In order to complement the above results, a second round of sieving was performed at the Council for Scientific and Industrial Research (CSIR) laboratory which provides for a different range of sieve sizes. This second round of sieving used the already seperated fractions derived from the initial work performed at the university laboratory. Table 3.2 lists the sizes of the sieves in the two sieve stacks used in this study:

Table 3.2 Sieve sizes available at Stellenbosch University and CSIR

SU	CSIR
4.000 mm	
	2.000 mm
1.400 mm	1.400 mm
	1.000 mm
0.850 mm	
0.710 mm	0.710 mm
0.500 mm	0.500 mm
0.425 mm	
0.355 mm	0.355 mm
0.300 mm	
	0.250 mm
	0.212 mm
0.180 mm	0.180 mm
0.150 mm	0.150 mm
	0.120 mm
0.090 mm	0.090 mm
0.063 mm	0.063 mm

As indicated in the table above, the SU sieving facilities included sieves comprehensive in range from 0.3 to 0.85 mm. The additional sieve sizes provided by the CSIR laboratory, ranging from 0.1 to 0.3 mm, allowed for a more complete fraction characterisation of the study site beach sediments.

Following sieving of each sample, the weights of the resulting fractions were recorded (Figure 3.10). The sieve stack was then cleaned with acetone, compressed air and a brush before being rebuilt in order to process the other samples.

The recorded weights were entered into an Excel spreadsheet for analysis. Averages were calculated according to standard sediment analysis techniques, with assistance from an analyst at the CSIR.

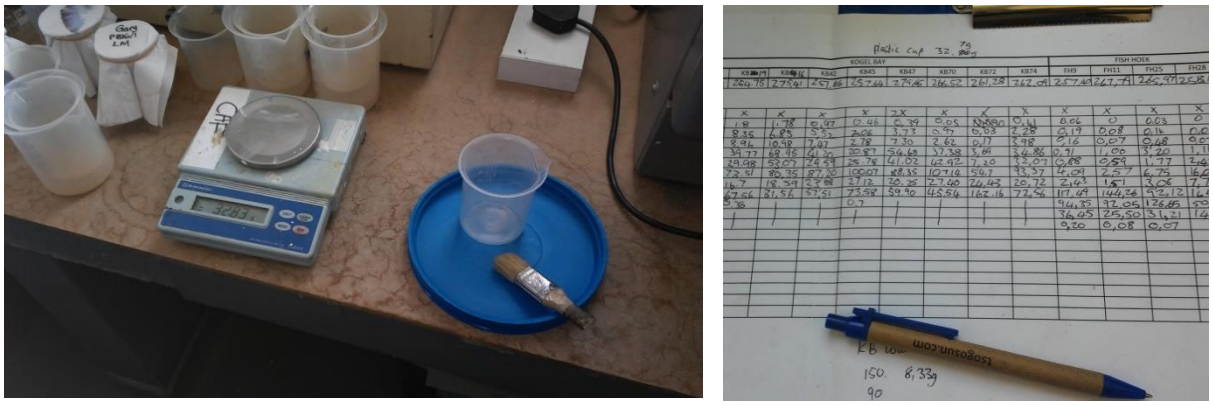

Figure 3.10 Weighing and recording weights of sediment fractions

3.3.5 LiDAR scanning of sediment samples

The dried bulked sediment samples and the sieved contributing fractions of each were prepared for LiDAR scanning. With the material placed into low-rimmed containers (paper plates), this was performed on a level surface that provided a clear exposure to the scanner that was used. The image below (Figure 3.11) schematically illustrates the arrangement of the sediment samples in a grid pattern, ready for scanning.

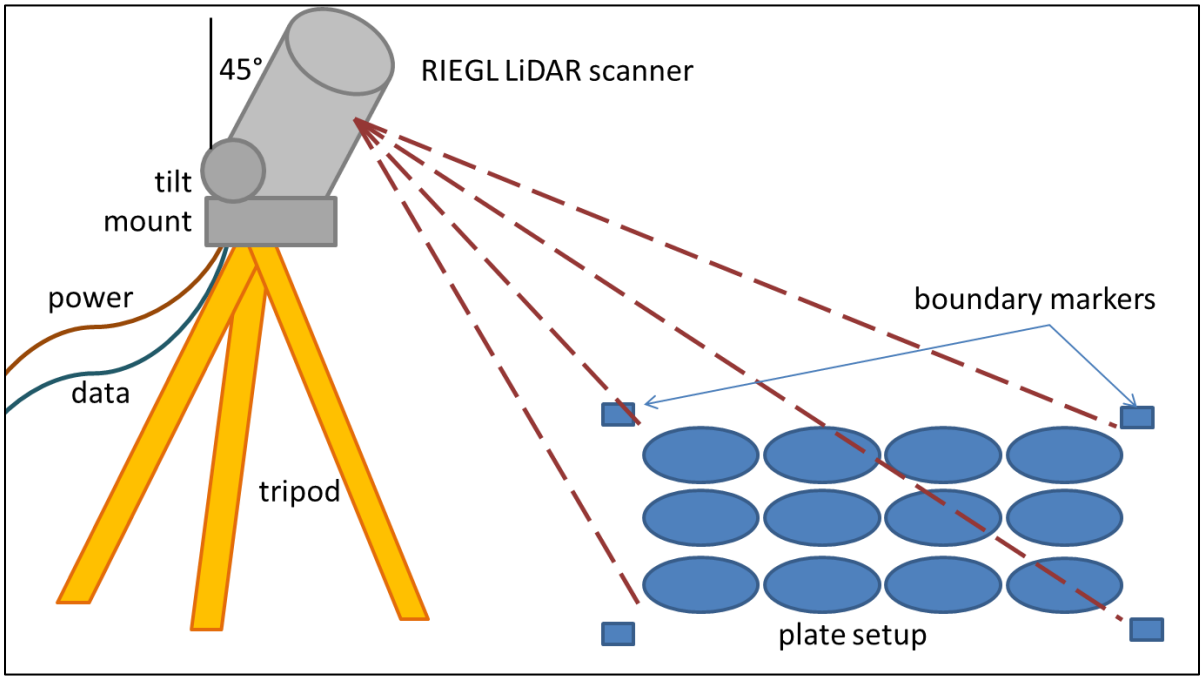

Figure 3.11 Schematic diagram of scanning setup with the RIEGL LiDAR scanning unit mounted on a tripod with the grid of samples arranged on a level surface

In order to relate grain size to LiDAR derivatives, this study made use of a stationary, ground-based LiDAR system with characteristic high resolution capabilities. It provides for a a much larger number of points per unit area than airborne systems due to proximity to the target being scanned. The scanning of the sediment samples was performed indoors, in a controlled environment, in order to avoid atmospheric, illumination and other environmental effects on the measured data.

The RIEGL VZ-400 LiDAR scanner provided by the CSIR was used. The scanning unit was mounted on a tripod with an adjustable tilt mount set to 45 degrees (Figure 3.11). An image of the scanner can be found in the appendices (Appendix 5).

GPS and INS measurements were not required as the scanning took place from a fixed position. All scanning steps were controlled using the RiSCAN Pro software on a dedicated laptop. The first step in the scanning process involved a quick overview scan of the 360 degree environment. The scanner does a complete rotation in approximately 8 seconds, sending out and receiving laser pulses to create a low resolution point cloud overview of its surroundings.

From this overview, a smaller area containing only the sample plates was selected and scanned at a much higher resolution. The resolution relates to point density and, for this study, a resolution of 1 mm was chosen as this provided a high number of measured points, or intensity values, per sample. This allowed for the recorded intensity to be effectively related to the surface characteristics of the sediment samples that were scanned. The scanning process took a couple of minutes per setup.

LiDAR scans were done using different arrangements of the samples comprising the natural mixed, or bulk, samples and others containing the sieved sediment fractions. Three arrangements of the samples were set up for scanning, as illustrated in the figures below. The letters ST, FH and KB abbreviate Strand, Fish Hoek and Kogel Bay respectively. The sieved sand from ST and FH was combined as neither beach individually produced sufficient quantities of each fraction to fill a plate.

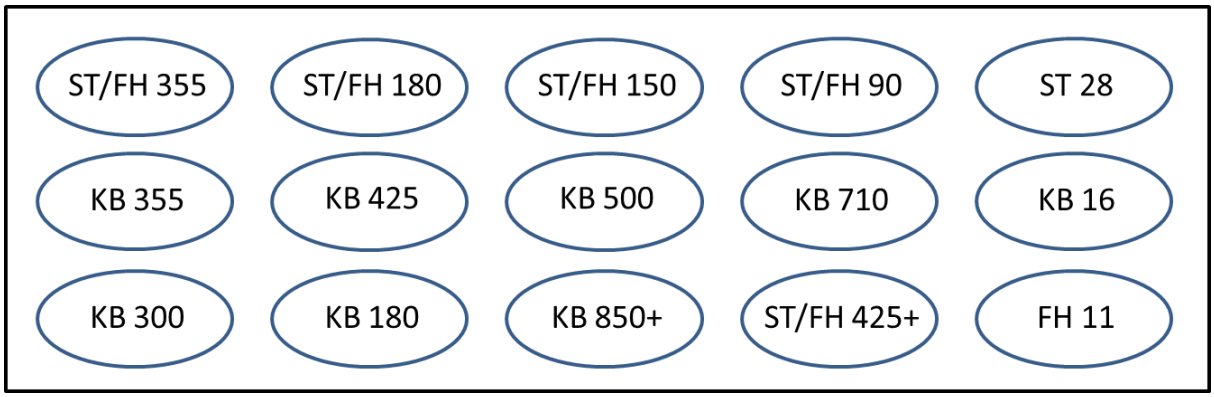

Figure 3.12 Plate setup 1 of scanning samples after the SU sieving

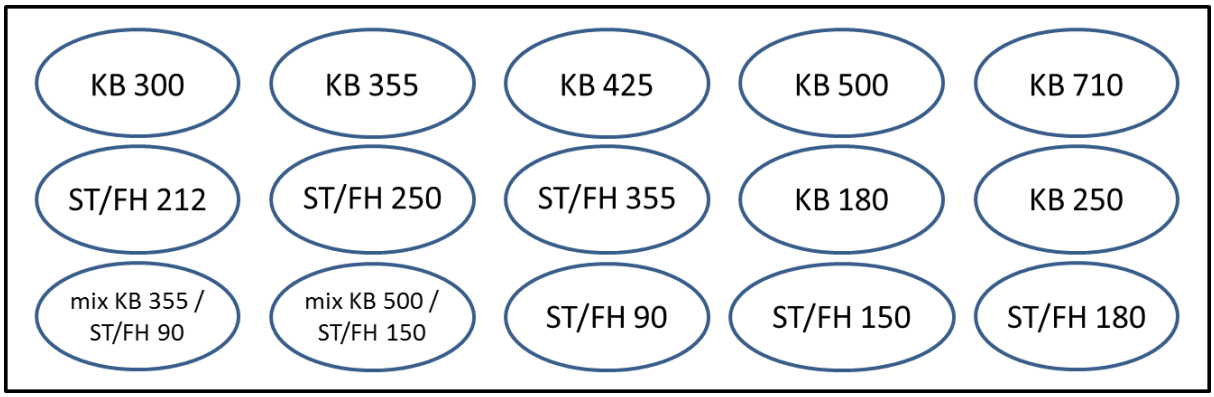

Figure 3.13 Plate setup 2 after the second round of sieving at the CSIR laboratories

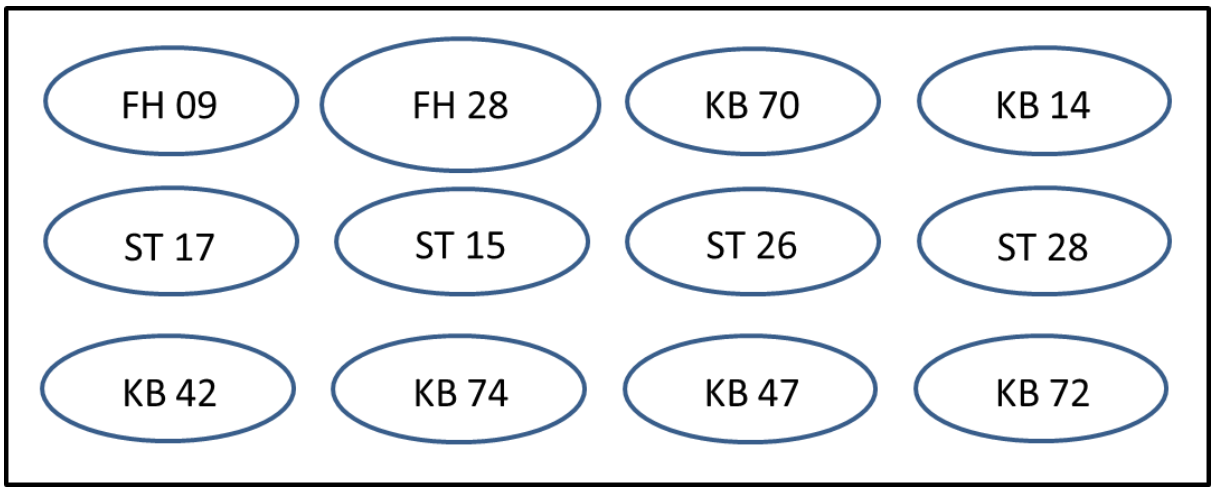

Figure 3.14 Plate setup 3 of some of the remaining natural mixed samples from the sampled beaches

The three digit numbers represent the grain size in microns (1 micron = 0.001 mm). Where the letters are followed by a two digit number, that plate contains the natural mixed sample from the location indicated by the label. After scanning, the sediment samples from each plate were stored in separate plastic bags with labels in the event that additional scans or further analyses should be required.

3.3.6 Processing of scanner data

The data were exported from the scanner's computer to LAS format using the RiSCAN Pro software package. LiDAR intensity was the only derivative required from the data in this approach.

The intensity values from the original pointcloud were rasterised in ArcMap to a continuous surface with a 2 mm resolution. Each cell contained at least one point. In the images below (Figure 3.15a) and b, those on the left show the point cloud, which is the output of the scanning. The image on the right shows the 2 mm resolution rasterised intensity values. The black, no data pixels in Figure 3.15b are likely caused by scanning angle-related shadows and these were excluded in further analysis.

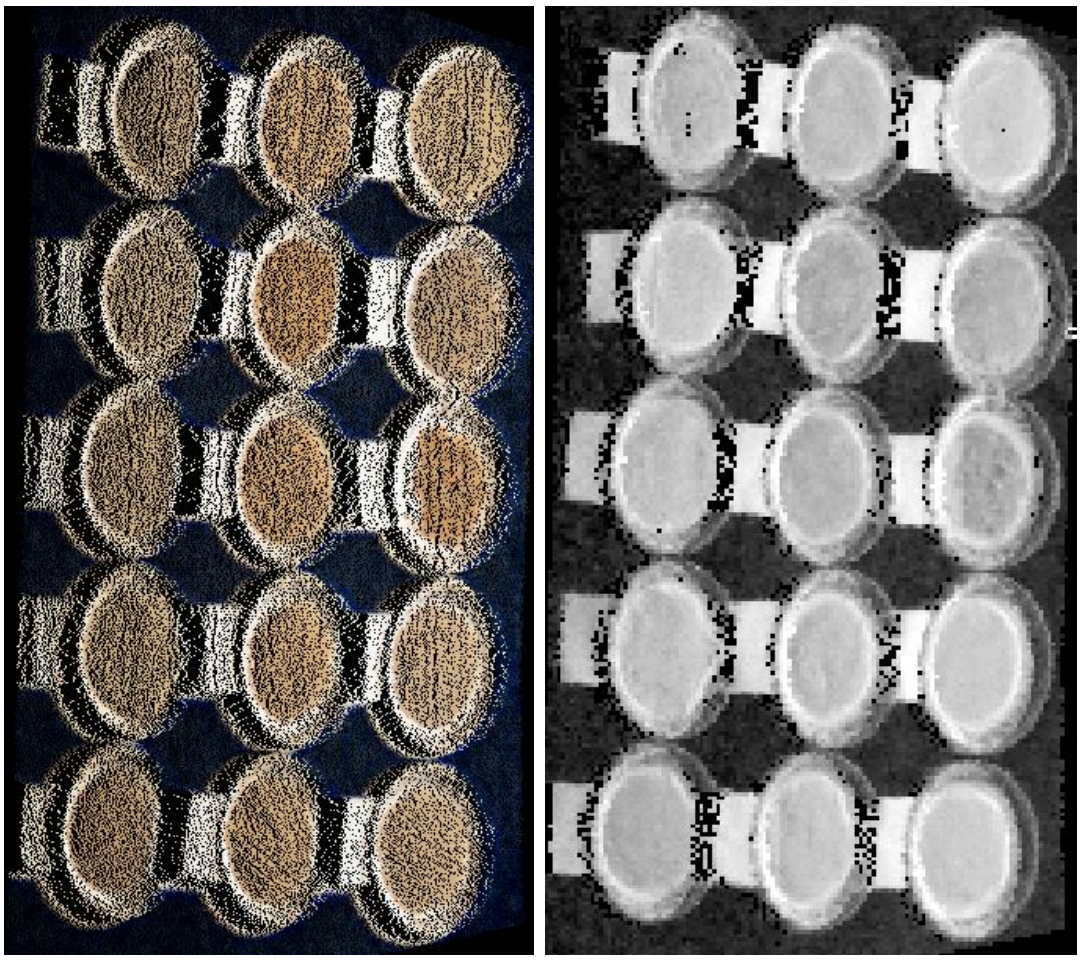

Figure 3.15 Example of scan: a) Raw elevation point cloud; and b) image of the rasterised intensity. The bright rectangles between the plates were sample tags.

Through further analysis, an average intensity value was extracted from each sample. This was done using zonal statistics in ArcMap 10. Polygons were drawn to include between 1 200 and 1 900 pixels of the sediment sample in each plate. Various statistics, including the average of all the intensity values, were calculated for each polygon and exported to a table format.

Using Microsoft Excel, grain size was plotted against corresponding intensity values and various regressions were calculated to establish statistical correlations.

3.4 EXPERIMENT 2: AIRBORNE LiDAR ANALYSIS

The second research stream comprising this study (Figure 3.1) made use of airborne LiDAR point data of the False Bay coast obtained by the CoCT municipality. The aim of the analysis of this data is to determine the extent to which airborne LiDAR derivatives can be used as

proxy for physical beach characteristics, for larger areas. The steps outlined in the following sections describe the processing and analysis of the LiDAR data using various software packages.

3.4.1 Collection of LiDAR data

LiDAR data were obtained from the CoCT through the Centre for Geographic Analysis (CGA) at Stellenbosch University. The CoCT had commissioned AOC, a surveying company, to conduct an airborne LiDAR campaign of traversing its coastline and immediate hinterland, including False Bay, which is the focus of the study described here. The data were provided in LAS format (see Section 2.2.5) by the CoCT to the CGA for research purposes. The resolution of the dataset was approximately 3 points per square metre. The following image was provided with the data showing the respective coverages and dates of each LiDAR survey.

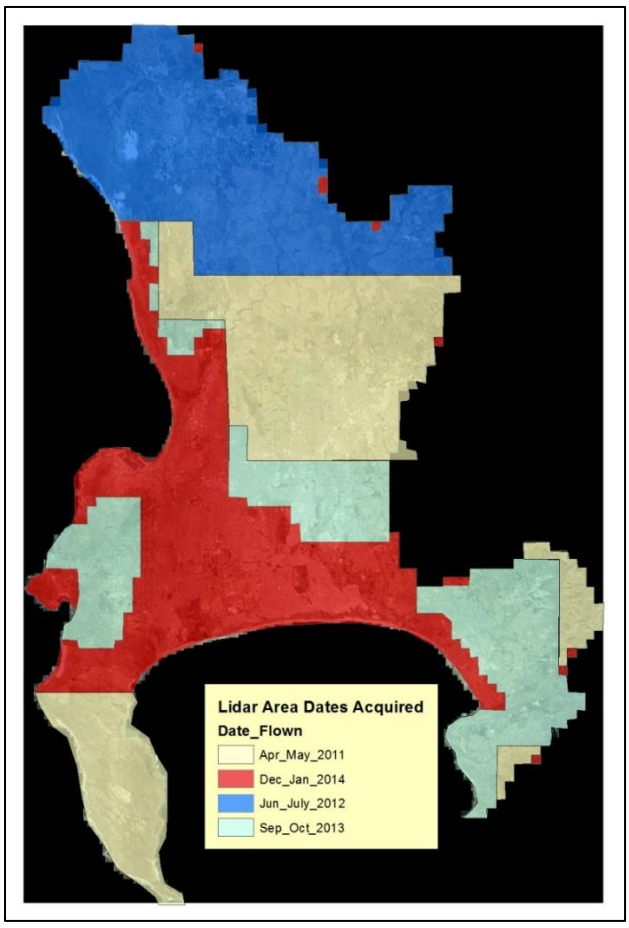

Figure 3.16 Coverage and acquisition dates of the LiDAR data (provided by the City of Cape Town)

The most recent survey, shown in red, was flown in December 2014 and January 2015, and covers the northern margin of False Bay from Fish Hoek to Strand and Gordon's Bay. The data covering Kogel Bay, on the eastern margin of the aerial survey, were acquired in September and October 2013. Note that these dates preceed the field work undertaken in support of the ground based LiDAR study described above by a number of years.

3.4.2 Data Processing

The software used for the processing of the LiDAR data included: ArcMap version 10 by ESRI; ERDAS IMAGINE 2014; and LAStools created by rapidlasso. LAStools is a toolbox which is embedded in other software such as ArcMap and ERDAS.

3.4.2.1 Selection of LAS tiles

A total of 46 tiles (LAS files) of the False Bay region were provided in the City of Cape Town dataset. In order to determine which tiles cover the False Bay coastline and the beaches selected for this study, a 'footprint' shapefile of the datasets was generated using the LAStools toolbox embedded in ArcMap. By overlaying these with a coastline shapefile, the five tiles covering the three study sites could be identified. All other tiles were excluded from further processing. The image below (Figure 3.17) shows the footprints of the LAS tiles and highlights those that are relevant to this study.

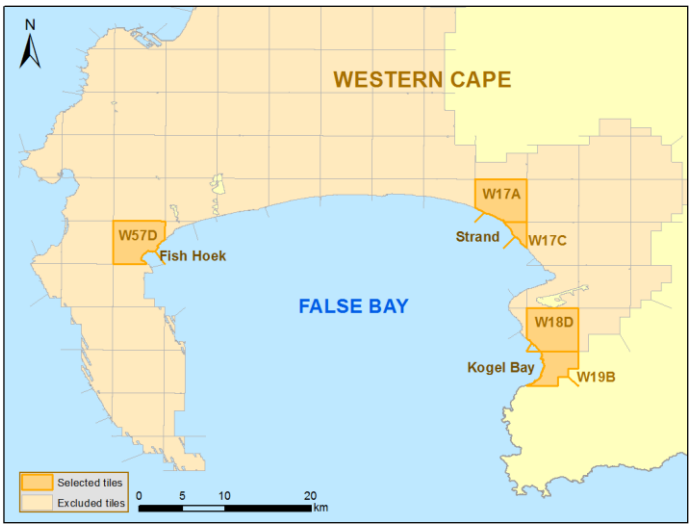

Figure 3.17 Map showing the footprints of the LAS tiles in the City of Cape Town dataset; the tiles covering the study sites are highlighted and labelled

The tile W57D in the map above included the entire Fish Hoek beach. Tiles W17A and W17C covered the beach at Strand while tiles W18D and W19B included the Kogel Bay beach. The total file size of the five selected tiles was 10.1 GB.

3.4.2.2 Derivatives

As discussed in Section 2.2.5, the most common derivatives of LiDAR data are digital elevation models which can be used in a number of applications. Using the ERDAS Imagine software suite, the LiDAR data were converted to a raster format using the LAS to Surface (Rasterizing) function in ERDAS with a horizontal resolution of one meter with the z-value, or elevation, being extracted to form a DSM. Since the areas of interest were beaches, the scanner would only record one return, as there is neither vegetation nor any structures to create multiple returns.

From the DSM, a slope surface was created with each pixel having a value between 0 and 89 representing degrees. The beaches are all relatively flat and the slopes are, for the most part, not expected to exceed 6 or 7 degrees. See example of Fish Hoek below (Figure 3.18).

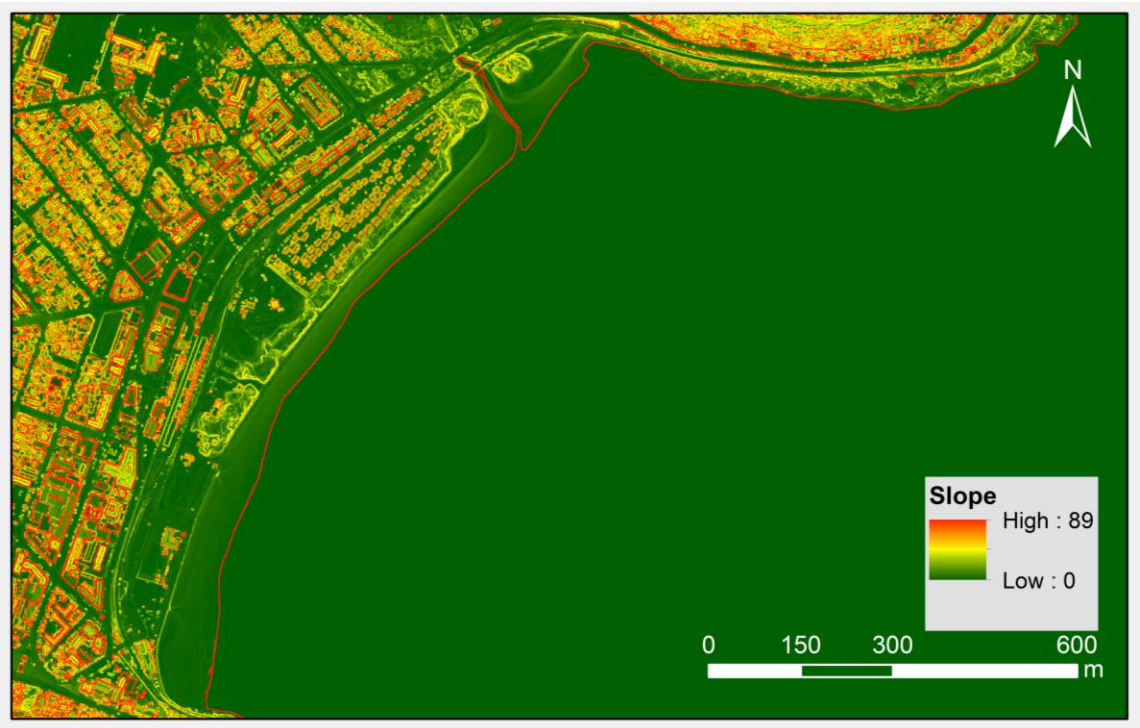

Figure 3.18 LiDAR derived slope surface of Fish Hoek beach, dark green areas are flat and the steeper slopes are yellow to red

The next step was to create an intensity surface, or DIM, by rasterising the point cloud using the 1st return intensity values as the attribute for creating the raster surface. This was also done using the LAS to Surface (Rasterizing) function. The resolution of the output surface was set to 2 m to avoid potential gaps or no data pixels. Recorded intensity values were scaled by the LiDAR sensor to an unsigned 8-bit integer with values ranging from 0 to 255. See the intensity image of Fish Hoek below (Figure 3.19).

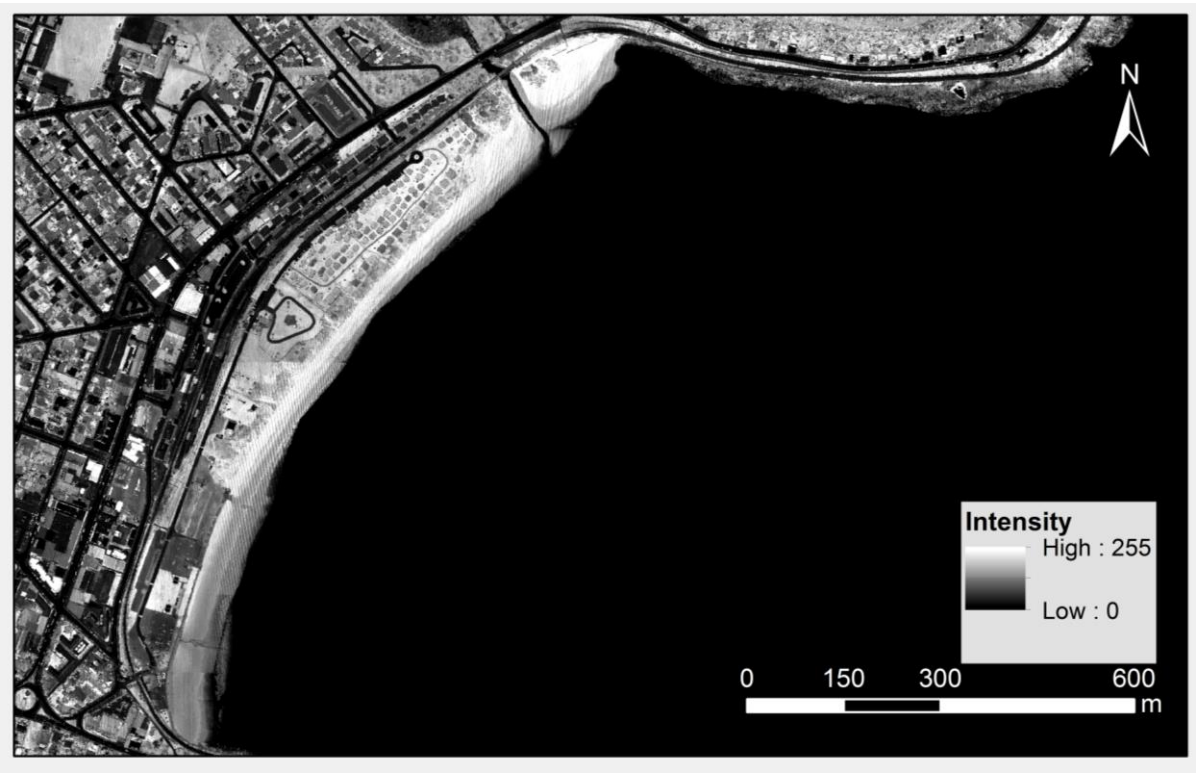

Figure 3.19 LiDAR derived intensity surface of Fish Hoek beach, darker values have lower intensity values

3.4.3 Data analysis

For the analysis of the LiDAR derivatives created in the previous steps, ArcMap version 10 was used as well as Microsoft Excel. By overlaying the DGPS sampled transects at the three beaches with the derivatives from the airborne LiDAR data, both the intensity and slope values could be extracted for all of the sampled points and exported as a table for analysis in Excel.

An additional 100 random points were created at each of the three beaches. The slope and intensity values were extracted for each point location and also exported as a table. For these

points, the correlation of slope and intensity was assessed in Excel as well. Although no reference grain size data were available for these sites at the time of data acquisition, the aim of this step was to confirm whether the relationship between slope (as a function of wave energy) and grain size, as approximated using intensity data, can be established from airborne LiDAR.

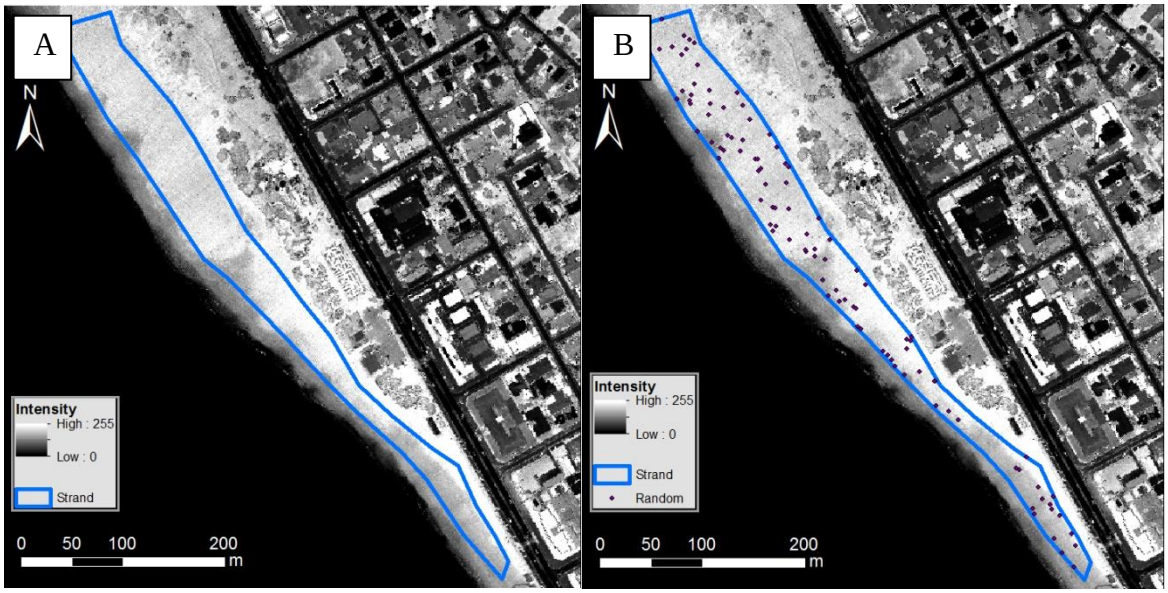

Figure 3.20 The polygon created for Strand beach (A); and the 100 random points within its boundaries (B)

The polygon created for Strand beach is shown outlined in blue in Figure 3.20 above as an example. The polygon was created to exclude the dune and vegetation as well as most of the swash zone which would more likely lead to inaccurate results. In Figure 3.20B, the 100 random points created in the polygon are shown. Both the intensity and slope values were extracted for these points to be analysed in Excel. Similar processes were followed for each of the beaches. These were then analysed in Excel.

CHAPTER 4 RESULTS AND DISCUSSION

This chapter presents the results from the experiments described in the previous section and will discuss them as they relate to the objectives.

4.1 EXPERIMENT 1: TERRESTRIAL LiDAR ANALYSIS

4.1.1 Sieving of sediment samples

Table 4.1 summarises the distribution of the average grain sizes calculated from the sieving results at SU for the three beaches at Strand, Kogel Bay and Fish Hoek. See Appendix 4 for the fully recorded results from the sieving of each individual sample.

The four samples collected from Strand showed that the grain sizes vary in average grain size, between 0.13 mm and 0.22 mm in diameter. The average grain sizes of the nine samples collected at Kogel Bay are generally higher and around 0.35 mm in diameter. The smallest average grain size at Kogel Bay was 0.23 mm which could be as a result of finer wind-blown sand on the beach surface at that location. For Fish Hoek, the average grain size for the samples was very homogeneous and fine at around 0.16 mm which supports the observations of dissipative beaches by Rust (1991).

The values in Table 4.1 were calculated as the percentage that falls into each grain size bracket according to the samples collected, grouped per beach. The values highlighted as bold indicate the two most prevalent grain size fraction per site. For the Kogel Bay beach, there were no measurable weights recorded from the 90 and 63 micron sieves as this beach is very exposed and influenced strongly by wave action as illustrated in literature by authors such as Abuodha (2003). Consequently, none of the finer sand grain fractions are present.

Table 4.1 Grain size distribution for each of the sampled beaches after SU sieving

		Strand	Kogel Bay	Fish Hoek
Sieve size		% of total weight		
1	1.4 mm	0.04	0.29	0.01
2	850 microns	0.25	1.92	0.04
3	710 microns	0.37	2.61	0.07
4	500 microns	1.88	16.23	0.59
5	425 microns	1.92	13.07	0.55
6	355 microns	6.41	**31.96**	2.81
7	300 microns	2.86	8.45	1.41
8	180 microns	**31.88**	**25.43**	**49.48**
9	150 microns	16.99	0.05	**34.68**
10	90 microns	**36.76**	0	10.31
11	63 microns	0.65	0	0.04

The grain size distribution across the three study beaches is perhaps more clearly illustrated in the following graph (Figure 4.1). From the distribution, the single peak for Fish Hoek in the 180 micron bracket closely followed by the 150 micron portion, emphasises the homogeneity of this beach explained by the low levels of wave energy at this site. The samples collected at Strand appear to have 2 peaks in grain size distribution, at 90 and 180 microns. This could be a function of layering caused by increases in wave energy but also the prevalence of wind-blown sand. For Kogel Bay, the amounts of coarser grain sizes clearly dominate. Although there is also a peak in the 180 micron bracket, it is likely that most of this would fall closer to 300 microns but were incorrectly classified due to a lack of sieves in the range between 180 and 300 microns.

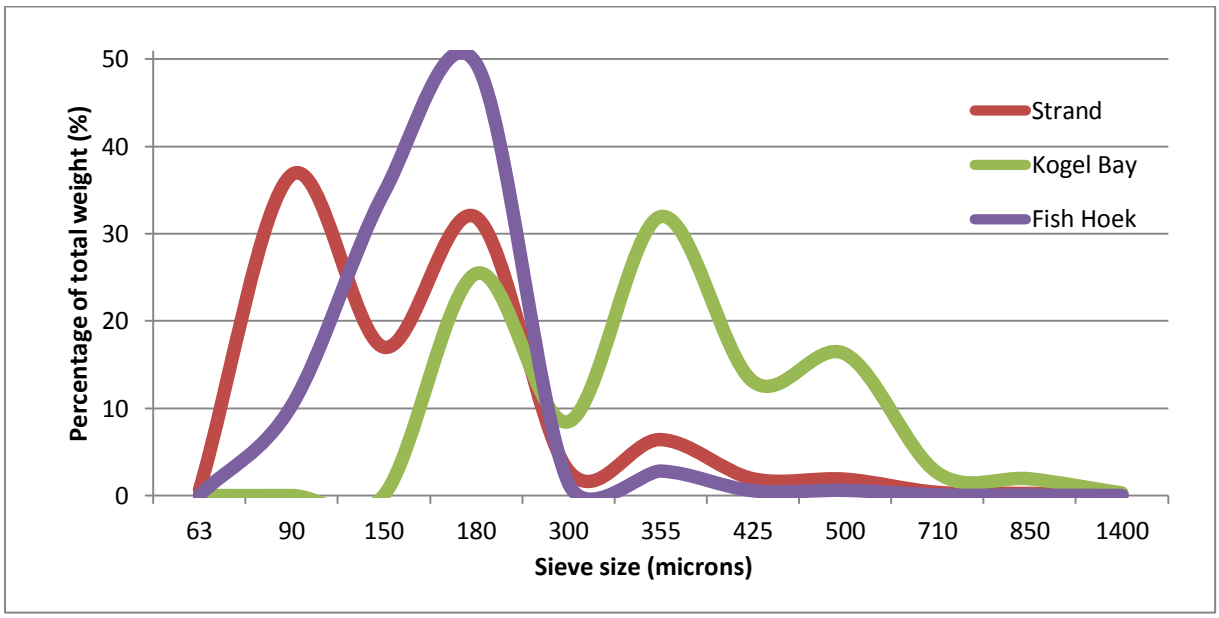

Figure 4.1 Grain size distribution across the sites after SU sieving

4.1.2 LiDAR scanning of sediment samples

The first scanning setup included the grain fractions from all sites after the SU sieving. In Figure 4.3, the intensities of the 1st scanning setup (i.e. after SU sieving) are correlated to the respective grain sizes. There is a trend in the data, with larger grain sizes having a lower intensity. With an R^2 value of 0.611, this relationship is not very significant. The statistical value of the correlation (R^2) is not very strong as a result of the limited number of points. This is restricted by the number of sieve sizes available and the range of sizes present in each sample.These values are averaged from around 1900 pixels for each sample (see Section 3.1.4).

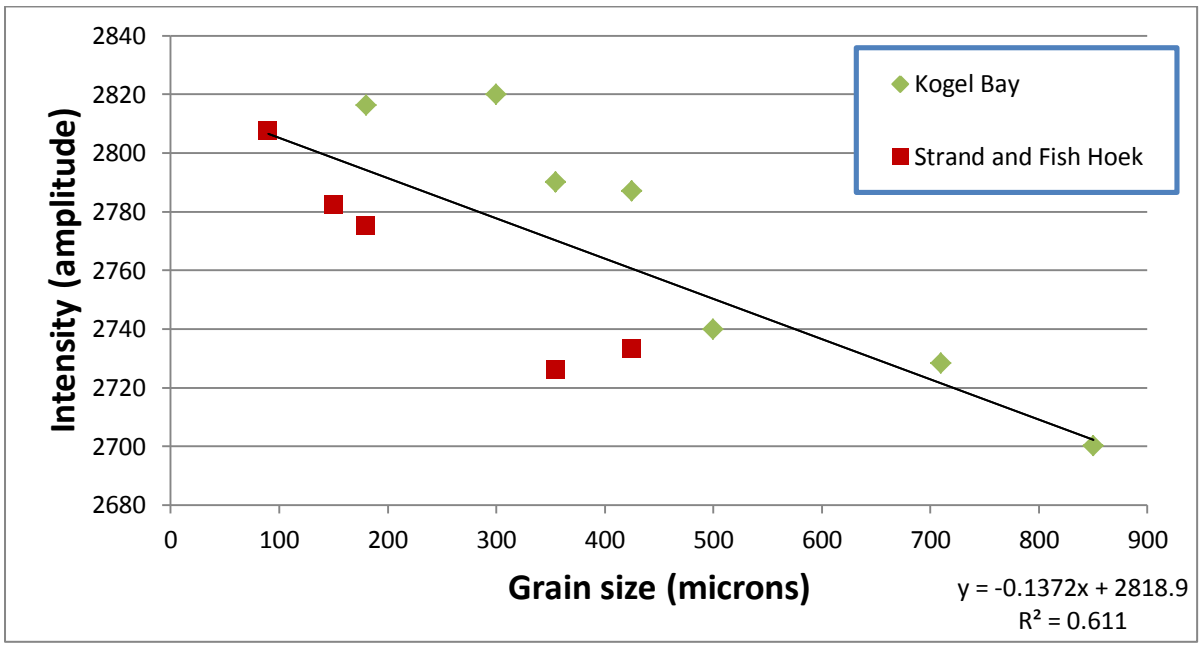

Figure 4.2 Correlation between intensity and grain size for samples from all sites after sieving at SU

After separating the Kogel Bay sand from the other two beaches, the correlation (Figure 4.3) improved, with an R^2 value of 0.9161.

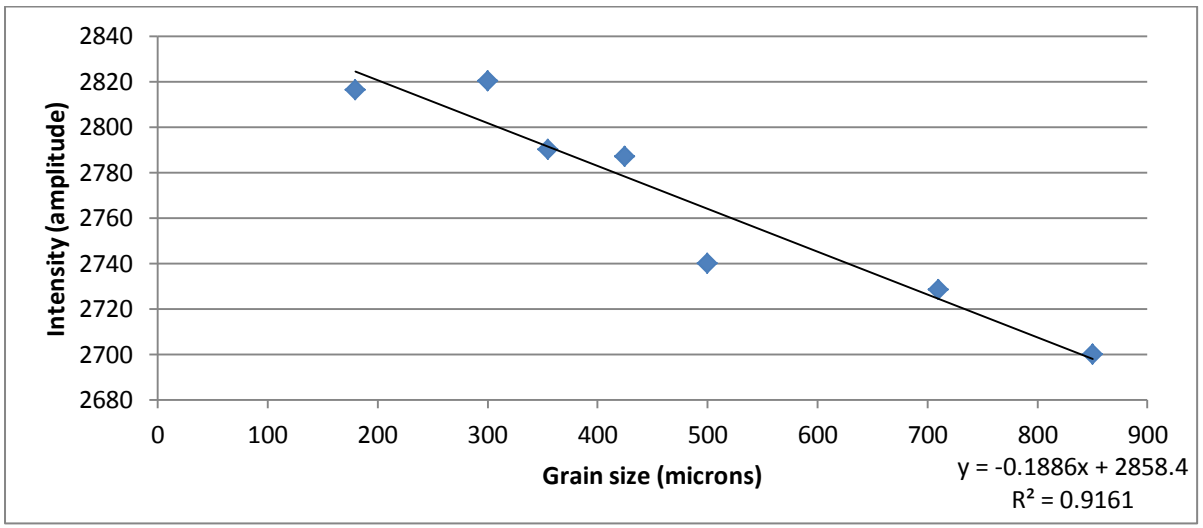

Figure 4.3 Correlation between intensity and grain size for samples from Kogel Bay after sieving at SU

With the beaches at Strand and Fish Hoek the relationship also strengthens with an R^2 value of 0.9249 (see Figure 4.4). The reason for combining the sand from Strand and Fish Hoek was that, in addition to having similar grain size ranges, there was not enough sand for all fractions to form sufficient quantities for scanning.

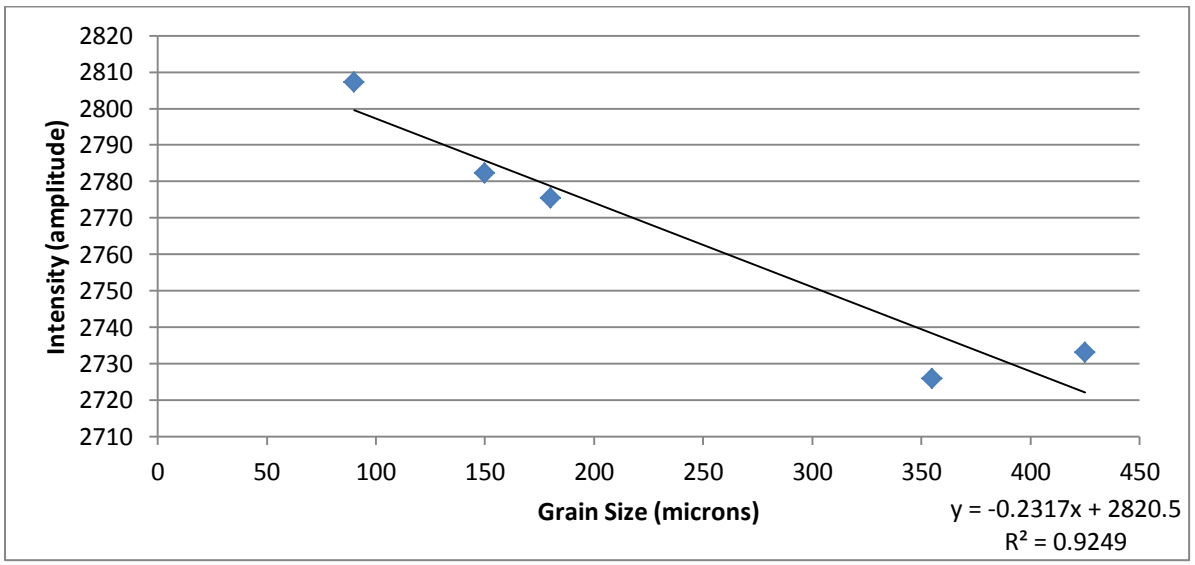

Figure 4.4 Correlation between intensity and grain size for samples from Strand and Fish Hoek after sieving at SU

The strengthening of the correlation between grain size and LiDAR intensity after separating the results from the different beaches suggests that there are additional factors, unrelated to grain size which influence LiDAR intensity supporting the findings of Garestier et al. (2015). From these results, one can assume that sediment composition or colour have an effect on LiDAR intensity.

Given the gap in sieve sizes in the region between 180 and 350 microns at SU, the CSIR facilities were used for further sieving with additional mesh sizes. This was an important step as the variation in grain size on many False Bay beaches are more evident in this range.

After re-sieving the samples at the CSIR, the samples were scanned as per setup number 2 (see Figure 3.12). The new data points between 200 and 300 microns strengthen the correlation. The R^2 value for Kogel Bay (Figure 4.5) increased from 0.9161 to 0.9704.

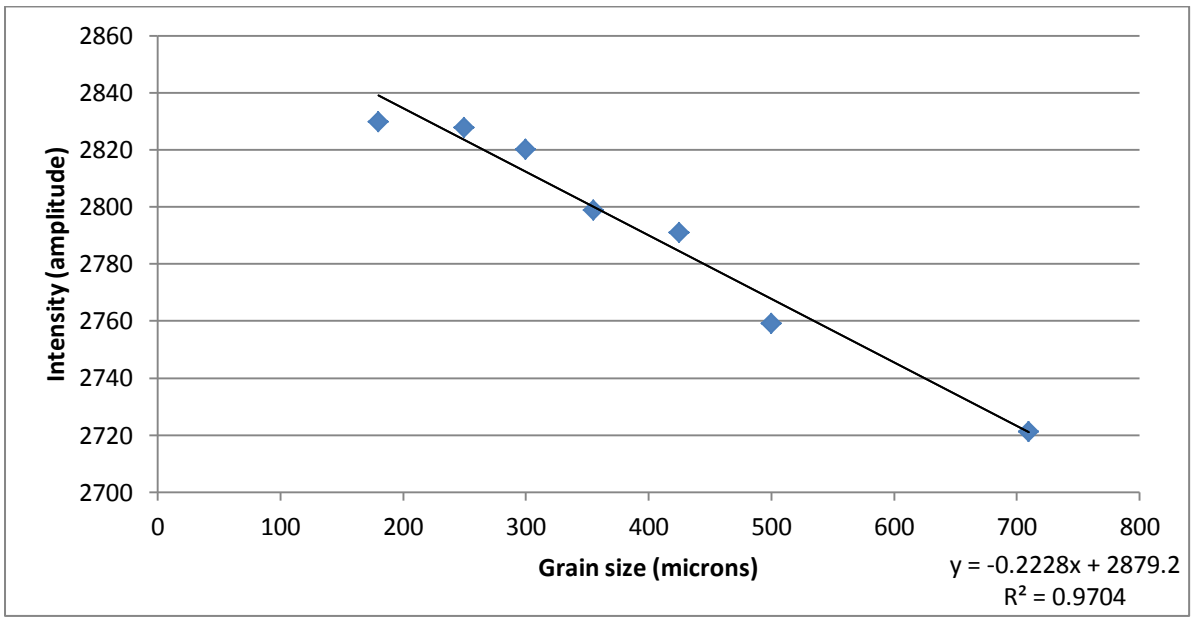

Figure 4.5 Correlation between intensity and grain size of samples from Kogel Bay after sieving at CSIR

For the Strand and Fish Hoek combined samples (Figure 4.6), the R^2 value increased from 0.9249 to 0.9308.

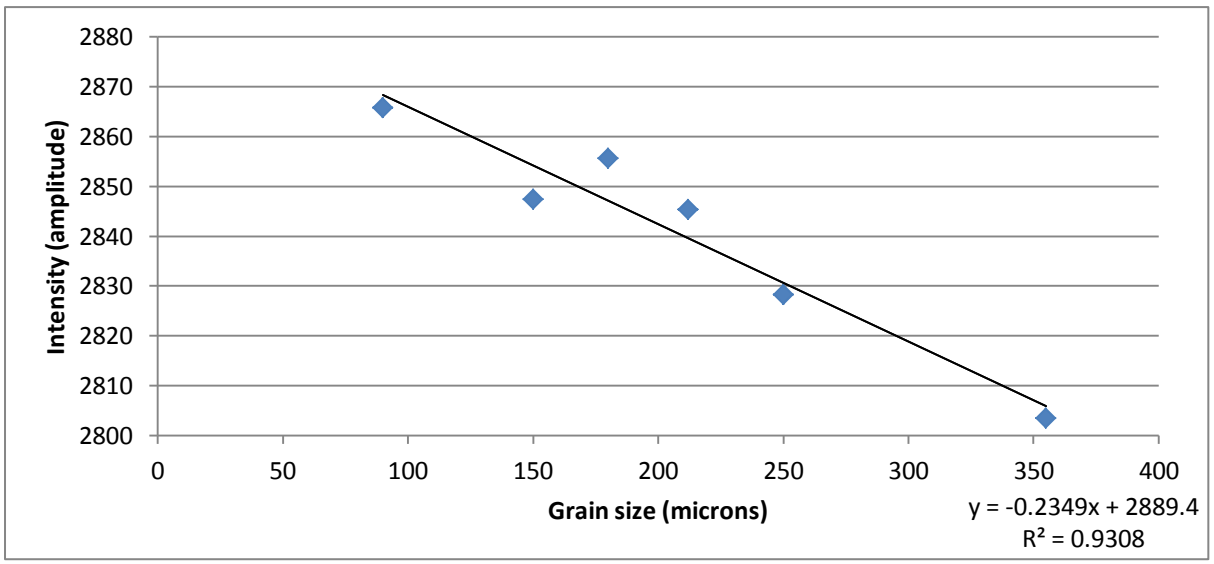

Figure 4.6 Correlation between intensity and grain size for samples from Strand and Fish Hoek after sieving at CSIR

The most significant improvement, however, occurred with the combination of the three beaches with the R^2 value increasing from 0.611 to 0.9706 after the CSIR sieving. This improvement shows that after the SU sieving, the sand was not sorted sufficiently and the

scanned samples were thus not homogeneous. In Figure 4.7 below, the KB samples are represented by the green diamonds where the red squares show the fractions from the other beaches. The larger grain sizes are only seen in the KB samples that were scanned, with the two smallest only represented by ST and FH.

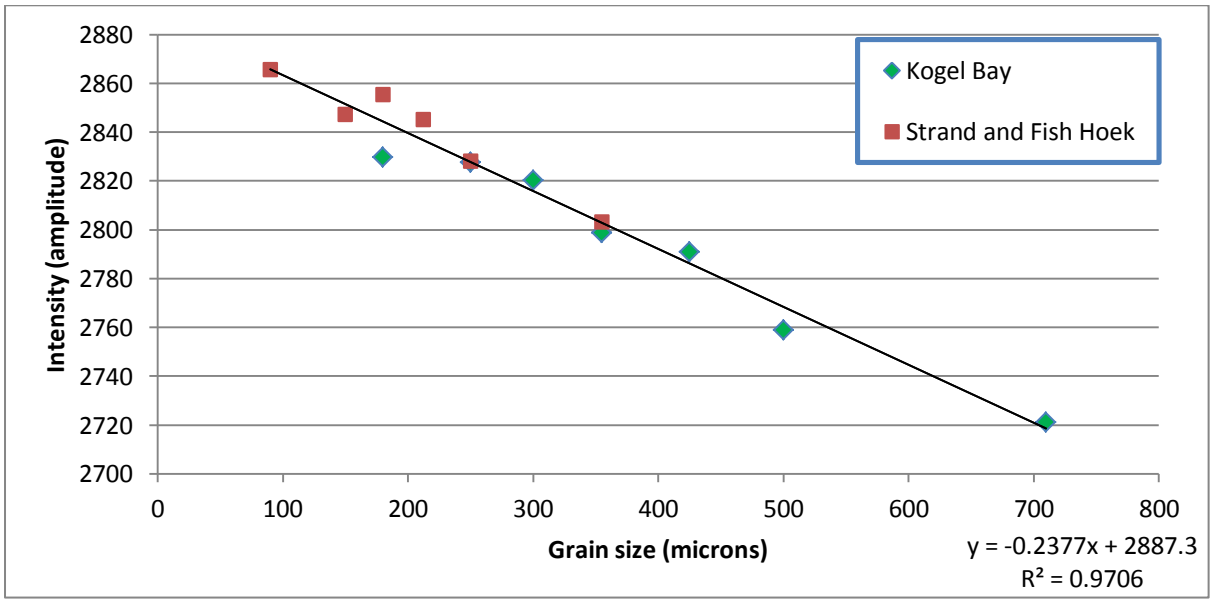

Figure 4.7 Correlation between intensity and grain size for samples from all sites after sieving at CSIR

The strong correlation between grain size and intensity shown in Figure 4.7 contradicts the assumptions made after scanning of the SU sieving results. When analysing the beaches separately, an apparent improvement in correlation seemed to indicate that other factors such as sand colour influenced intensity in addition to grain size as suggested in studies such as Errington & Daku (2017). The correlation in Figure 4.8, however, suggests that sand colour does not have a strong influence on LiDAR intensity and the improvement in the correlation is a result of the additional sorting of grain fractions. Each scanned sample is more homogenous after the sieving at CSIR and the recorded LiDAR intensity can thus be more clearly related to grain size fractions.

4.1.2.1 Results from natural mixed samples

Figure 4.8 shows scanning results from setup number three (Figure 3.13). This setup included only natural samples from the beaches without any sieving.

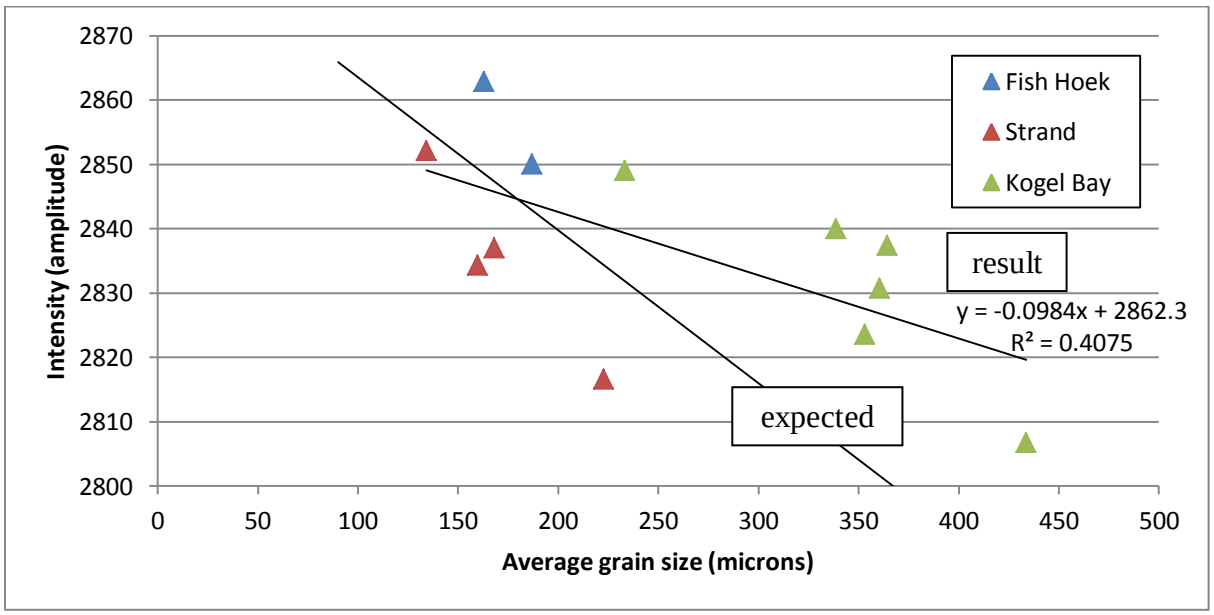

Figure 4.8 Correlation between intensity and average grain size of natural mixed samples from all sites

With the natural samples, the relationship between grain size and LiDAR intensity (R^2 of 0.4075) is clearly not as strong as is the case with the sieved sand as indicated by the second line ('expected') in Figure 4.8 which was calculated previously in Figure 4.7. Each natural sample contains a mixture of different grain sizes and recorded intensity would thus be affected by the range of grain fractions which form the natural sample. Although it is expected that the observed intensity will depend on the dominant or average grain size of sediment on a given beach, on certain beaches for example, the finer sand which is prevalent on the surface causes an increased intensity despite the presence of coarser grain fractions covered by or mixed with finer sand.

There is a slight tendency of the intensity values to decrease as the average grain size of the sample increases but there is not a strong linear relationship as is the case with the homogenous fractions. Another factor which may have had an effect on this relationship is the type of material or sand colour of each sample. Each of the three beaches was comprised of different sediment material as a result of the underlying geology and various sediment sources and the effects of this on LiDAR intensity need to be further investigated.

While grain size has been proven to impact LiDAR intensity, the natural mixed samples are more difficult to characterise only by intensity.

4.2 EXPERIMENT 2: AIRBORNE LiDAR ANALYSIS

This approach assessed whether airborne LiDAR data could be used for large scale grain size estimations. The following sections present the results from the various data analysis of LiDAR derived slope and intensity.

Analyses were done to determine the relationship between grain size, slope and intensity. The following graphs were created by plotting various combinations of the extracted slope and intensity values and measured grain size at the points where all the sand samples were collected and grain sizes extracted for the three beaches.

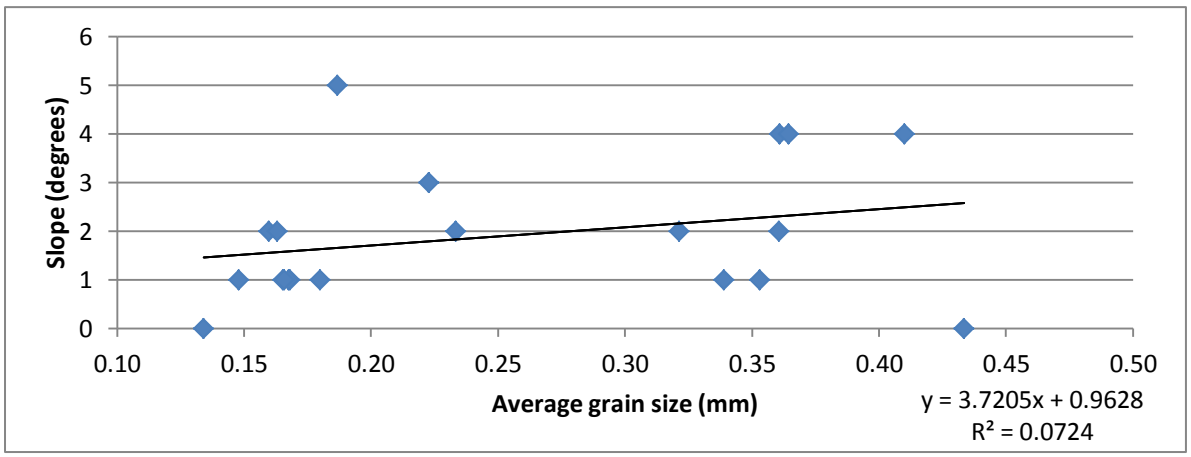

Figure 4.9 LiDAR derived slope plotted against measured grain size after CSIR sieving

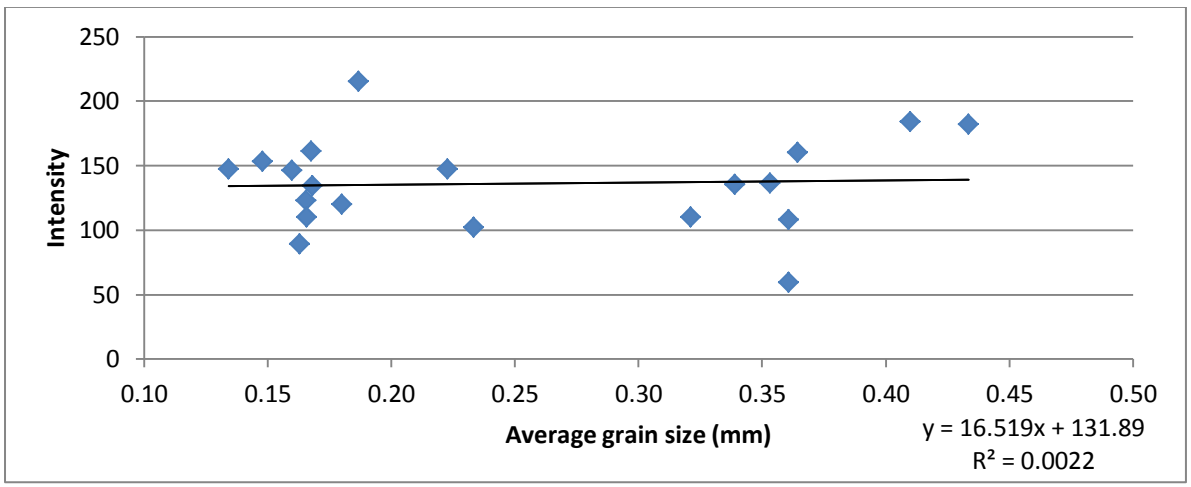

Figure 4.10 LiDAR derived intensity plotted against measured grain size after CSIR sieving

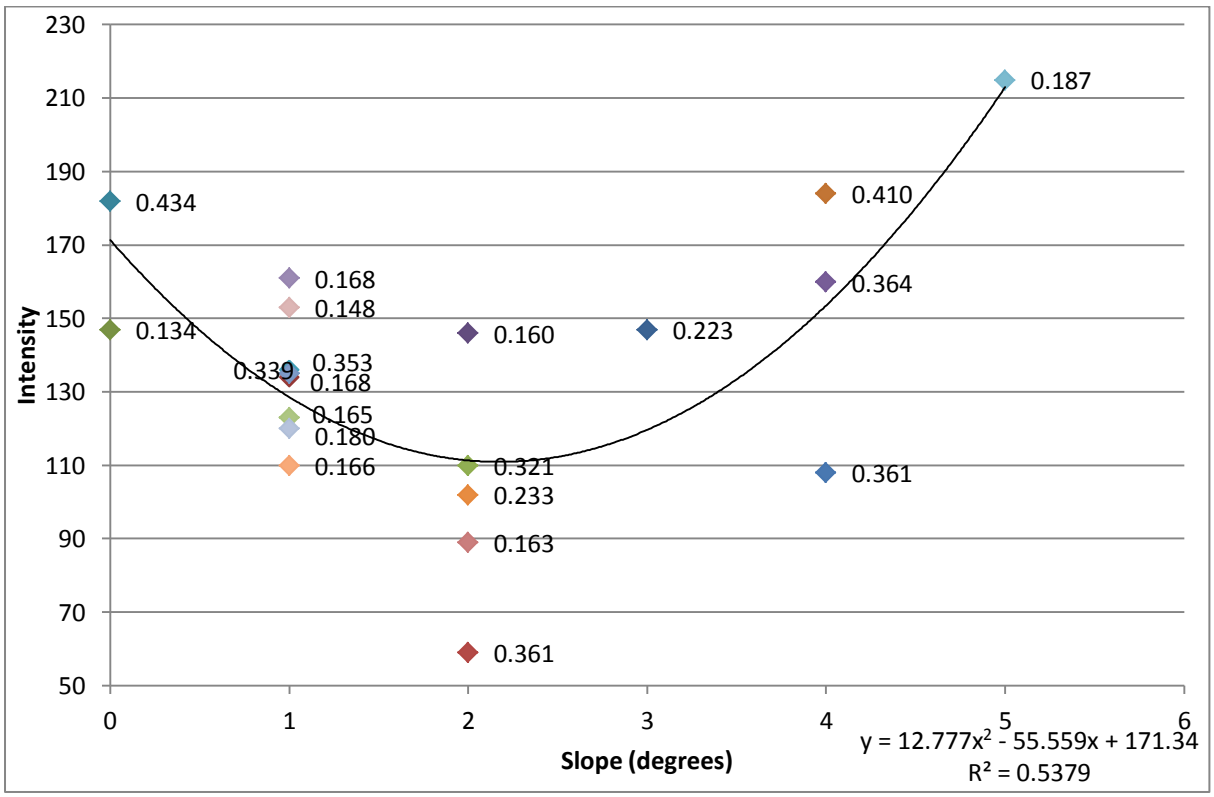

Figure 4.11 LiDAR derived intensity plotted against slope for the sampled sites. Points are labelled with average grain size

In Figure 4.9, the extracted slope is plotted against the average grain size for all the samples. The correlation between the two variables is very low with and R^2 value of 0.07. Similarly, the relationship between LiDAR intensity and measured grain size in Figure 4.10 is very low with an R^2 value of 0.002. The most likely reason for these low correlations is the temporal decorrelation between the airborne LiDAR data and the sample collection being over two years, which is quite significant. Although slope has an established relationship to grain size and the first stream of research in this study has established that LiDAR intensity is also related to grain size, the coastal zone is a particularly dynamic environment. Over a period of two or more years, it is expected that beach morphology has experienced a considerable amount of change as a result of natural and anthropogenic phenomena. Beach slope as well as grain size distribution at specific locations will have been significantly altered by wave action and storms which studies such as those done by Revell, Komar & Sallenger (2002) document.

Unlike the correlations with measured grain size, the relationship between the slope and intensity are not affected by temporal decorrelation as both of these were derived from the same LiDAR dataset. In Figure 4.11, although the relationship is not linear, there is an

apparent trend in the data. The initial dip in intensity as slope increases supports the hypothesis of this study that increasing grain size (represented by decreasing intensity) corresponds to an increase in slope. As the slope continues to increase, however, intensity begins to rise as well. This rising intensity might be explained by the presence of finer wind-blown sand forming steeper slopes or dunes. The assumptions and conclusions drawn from these results cannot be validated, however, as the airborne data were collected at least two years prior to sampling. From the measured grain sizes labelling each point in Figure 4.11, there is a general trend of coarser grain sizes at greater slopes, but there are also a number of outliers. The majority of samples at a slope of 1 degree are less than 0.2 mm in diameter whereas at 4 degrees the average grain size is closer to 0.4 mm in diameter.

In order to further analyse the airborne LiDAR derivatives, 100 random points were created on each of the three sites and the slope and intensity values were extracted from the LiDAR derivatives. The following graphs show the extracted intensity values plotted against the corresponding slope for all of the points at each site (Figures 4.12, 4.13 and 4.14).

Due to the large variation of intensity values for each degree of slope, the values were averaged for each degree of slope to establish the general trend (Figure 4.15).

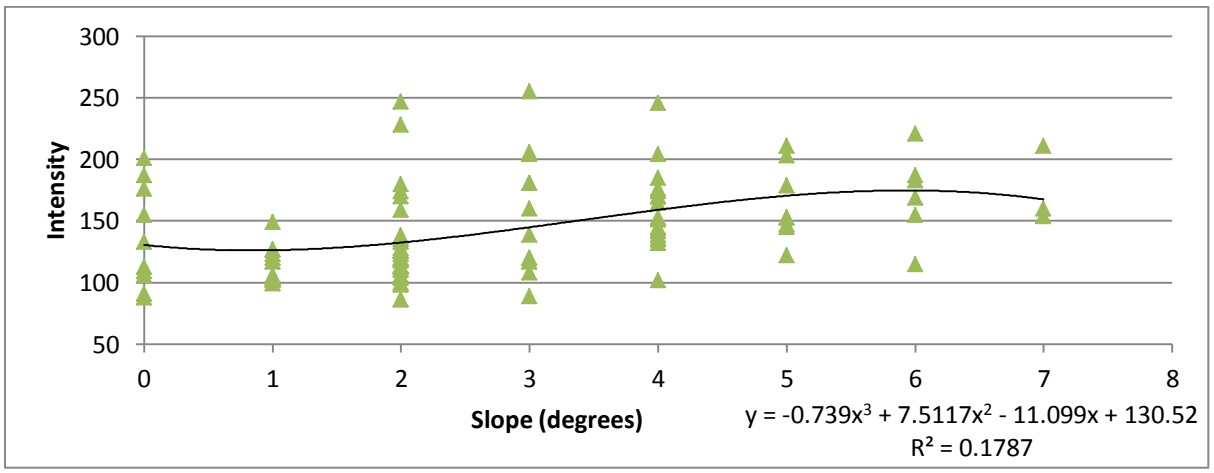

Figure 4.12 Airborne LiDAR derived intensity and slope for Fish Hoek beach

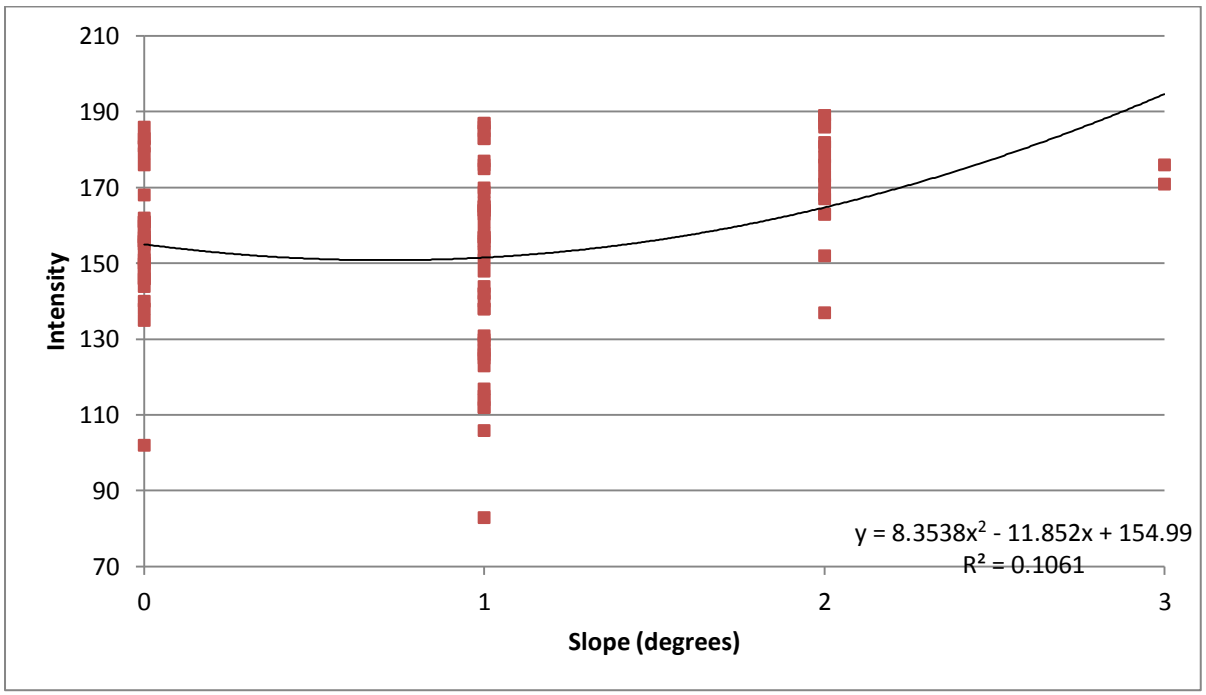

Figure 4.13 Airborne LiDAR derived intensity and slope for Strand beach

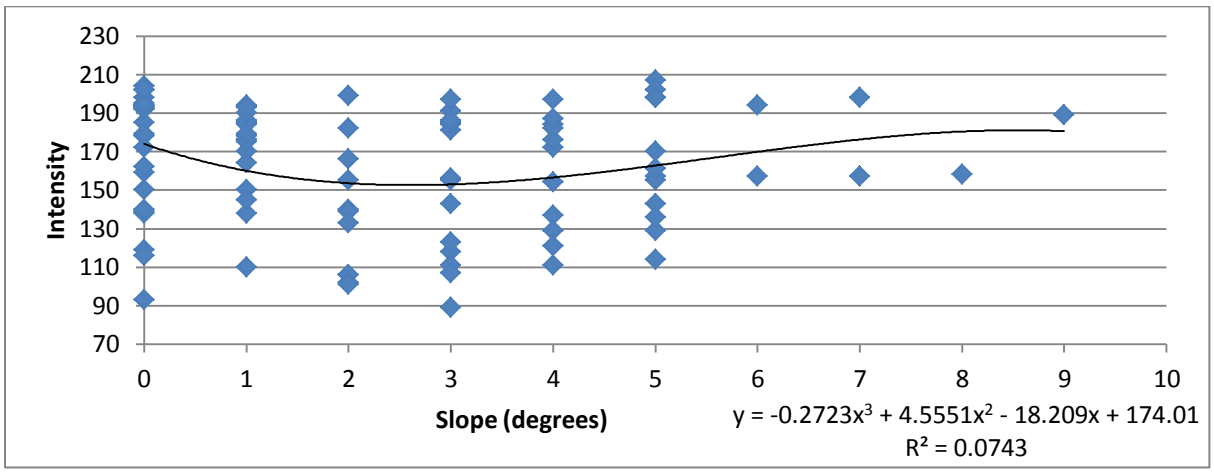

Figure 4.14 Airborne LiDAR derived intensity and slope for Kogel Bay beach

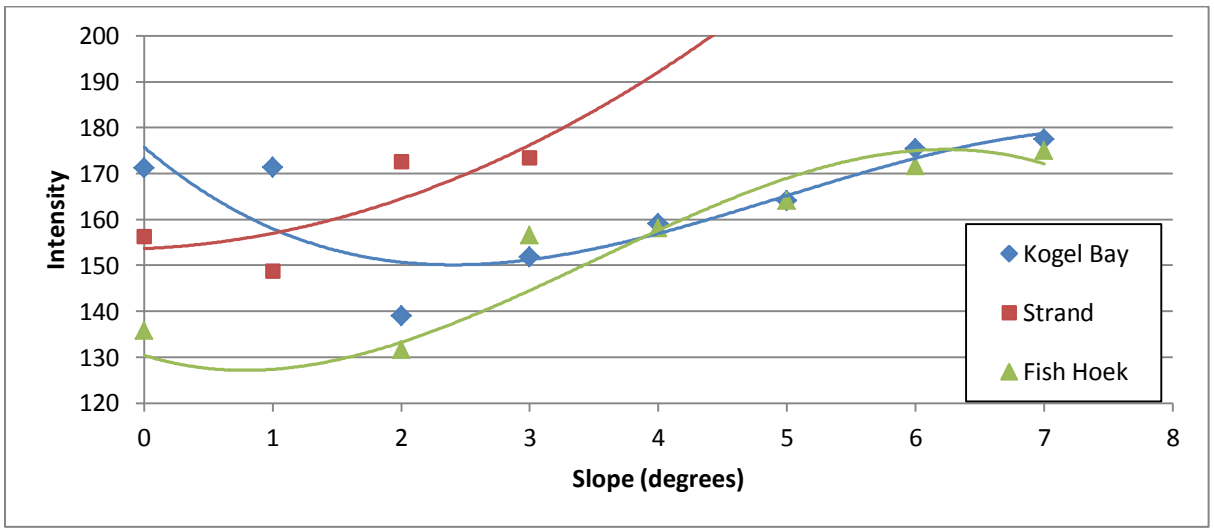

Figure 4.15 Average airborne LiDAR derived intensity values per degree of slope for all beaches

Figures 4.12, 4.13 and 4.14 indicate that there is a high amount of variation in intensity values around the mean, and this causes the low correlations with R^2 values of between 0.07 and 0.18. There are a number of reasons for the variability of intensity values per degree of slope such as the presence of wind-blown sand which needs to be considered but there is also a chance that sections of the beach are wet as a result of tide or swash despite efforts to exclude these areas from analyses.

In all of these correlations there is an evident dip in the intensity values with the first or second degree of slope which is in line with the hypothesis that larger grain sizes (represented by decreasing intensity) corresponds to an increase in slope as illustrated by Wiegl (1984). After this, however, the intensity increases steadily with slope which contradicts the findings so far in this study. It can be assumed that the observed increasing intensity here is not a function of wave action, but can instead be attributed to finer wind-blown sand on the surface of the beach and forming steeper slopes. Another factor influencing intensity is the moisture content of the sand which is discussed by authors such as Burton et al. (2011). The airborne LiDAR system in this study uses infrared laser technology which cannot penetrate water and produces unreliable data when the targets being scanned are not dry. In the swash zone, the recorded LiDAR intensity of the beaches are generally much lower as a result of the wet sand rather than grain size or slope.

Figure 4.15 shows the average intensity values for each degree of slope to more easily identify general trends. While Strand beach did not have much variety in terms of slope, both

Fish Hoek and Kogel Bay display very similar intensity values from 2 through 7 degrees slope. This is a noteworthy observation because whereas Fish Hoek beach is sheltered and flat with very fine sand, Kogel Bay beach is exposed to high levels of wave energy, is steep and has a coarse average grain size. If there is a general relationship between slope and intensity which holds true irrespective of grain size, estimating grain size using LiDAR derivatives will be more difficult.

With this second approach, using the airborne LiDAR data, the correlation between LiDAR intensity and grain size was not as clear as with the lab approach. The primary reason for this is related to the resolution and other characteristics of the airborne LiDAR intensity. The resolution of the airborne data was approximately 3 points per square meter which leaves much room for error when compared to the lab approach which achieved resolutions of around one point per millimetre. Other factors affecting the results are the local conditions at the time of flight for the airborne campaign. Without additional and precise metadata such as acquisition time and date, it is difficult to establish whether the results in this study could have been impacted by the weather and tidal conditions at each of the beaches.

Additional information such as flying altitude and scanning angle of the sensing platform allows for the calculation of scanning geometry and the incidence angle of the laser pulses. Recorded intensity is much less affected by external factors where the incidence angle of scanning is small (Kukko, Kaasalainen & Litkey 2008) but with larger incidence angles, intensity is much lower.

Although the relationship between beach slope and grain size is used mainly for describing wave dominated beaches, wind-blown sand which is prevalent on a given beach will most likely create biases when characterising those beaches from surface observations. One reason that the correlation between grain size and LiDAR intensity was clearer in the results from approach 1 is that the collected samples contained sediment from the upper layer of the beaches and not just the fine sand on the surface.

CHAPTER 5 CONCLUSION

This concluding chapter revisits the objectives, highlighting the significant findings which were achieved with each. Some of the limitations of this study are presented here and recommendations are made to guide similar research in the future.

5.1 REVISITING THE OBJECTIVES

The primary objective was *to use airborne LiDAR data to derive products such as elevation and intensity to describe beaches in terms of slope and grain size*. The steps taken to reach this objective are described with approach two in the previous sections. LiDAR data from an airborne survey by the CoCT was obtained from the CGA for this study, and the dataset included a number of tiles which were provided in LAS format. Five tiles covering the study sites in False Bay coast were identified and processed to create a number of derivatives, such as slope and intensity, for analysis.

The relationship between LiDAR derived slope and intensity revealed a common trend with all three sites. From literature, the expected relationship between slope and grain size is that steeper slopes generally equate to a coarser grain size. If intensity is used as a proxy for grain size, the findings of this study do not correspond with the findings of other research. For all three sites, despite an initial dip in intensity, the recorded LiDAR intensity steadily increases with each degree of slope. There are a number of factors which could have influenced these results. The problem of temporal decorrelation was among the most significant as it was not possible to validate the results of the airborne LiDAR survey using ground observations. Wind blown sand, which is finer, may also contribute to inaccuracies.

The secondary objective was *to conduct laboratory-based research to systematically assess the potential relationship between beach sand grain size and LiDAR intensity*. This was accomplished in the first approach where sand fractions with known grain sizes were scanned using a terrestrial LiDAR scanner and the recorded intensity values analysed. The environmental conditions and incidence angle of the LiDAR scanning were kept constant for the scanning and the correlation between sediment grain size and LiDAR intensity was significant with a correlation coefficient of over 0.9. As grain size increases, the recorded LiDAR intensity decreases in a linear function with the finest sand having the highest

recorded intensity. This could be as a result of coarser sand forming a rougher surface and thus not reflecting as much energy directly to the sensor as opposed to finer grain sizes forming a more uniform and strongly reflecting surface.

The LiDAR intensity measurements of scanned natural mixed samples with the lab approach were also analysed. When compared to the results from the scanning of individual grain sizes, the correlation between grain size and LiDAR intensity is not as strong. A possible explanation for this is the way the sand is packed or arranged; the finer sand in the natural samples fills the gaps between the coarser grains and thus disproportionately changes how energy is reflected. Another factor to consider is the effect that distance to the sensor has even in the lab environment with the sensor mounted on a tripod.

5.2 LIMITATIONS AND RECOMMENDATIONS

A number of limitations were identified with regards to the approach using airborne LiDAR data. The campaign during which the data were captured was flown in 2014. As emphasised in literature, the coastal zone is highly dynamic and is constantly changed by ocean processes and also anthropogenic activities. For research purposes, the airborne data acquisition should therefore ideally coincide with ground validation which was not feasible for this study. The problem of temporal decorrelation needs to be considered when comparing the samples which were collected in 2016 with airborne LiDAR data from two years prior. The exact dates and times of the data collection were also unavailable and this information is important when considering seasonality and tidal conditions which affect the scanning. For further research into the relationship between LiDAR intensity and grain size on beaches, any campaigns should be flown at or as near as possible to the time of the low tide when the beach is driest and most exposed with fieldwork being done concurrently.

Another limitation was the point density of the airborne data. This limitation is largely due to the physical parameters associated with the sensor including flying altitude, incidence angle of the laser pulses, the type and strength of the laser. With the available point density of approximately three points per square meter, the ability to observe very fine details such as texture is therefore limited. Additionally, in order to correct for the various factors affecting the intensity values with airborne LiDAR, all the above-mentioned parameters should be known as well as the atmospheric conditions at the time of data capture. In order to compare

target surfaces, such as beaches, a consistent incidence angle is recommended for LiDAR data acquisition for all scanning. Further investigation needs to be done into determining a method for effectively correcting radiometry of airborne LiDAR intensity particularly where scanning geometry is highly variable.

A recommendation which could lead to improved results for similar studies may be the adoption of a more systematic approach to sampling. When collecting sand samples to be used in characterising certain beaches, it may be beneficial to ensure that samples are collected from the upper, middle and lower sections of the beach along a particular transect. In this study, sample collection was often limited to those sections of the beach which were least saturated and would thus dry quicker in order to proceed with sieving and subsequent LiDAR scanning.

With the laboratory-based approach, any variations observed between different sand types in the captured LiDAR data could be attributed to the composition of the sediment. All other parameters such as atmospheric conditions, laser strength and range, surface slope, etc. are constant or have negligible variations. The range of grain sizes that were scanned in this study were limited; for further research, it is recommended that a more extensive range of grain sizes be collected for scanning. Another avenue to be investigated is into the effect that wet sand will have on the LiDAR scanning.

5.3 FINAL CONCLUSIONS

This study has shown that grain size does have a distinguishable effect on LiDAR intensity in a controlled environment and where there is a high point density, as is the case with close range terrestrial LiDAR systems. The recorded intensity decreases as grain size increases, i.e. finer sand reflects more energy back to the sensor than coarser sand in the lab approach.

Characterising beaches in a natural setting is more difficult as they are not homogenous and contain a range of grain sizes. Although it is possible to see a trend in intensity values for beaches scanned with airborne LiDAR systems, there are numerous external factors such as moisture content, incidence angle, etc., affecting the intensity measurements which are not necessarily related to grain size.

REFERENCES

Abuodha J 2003. Grain size distribution and composition of modern dune and beach sediments, Malindi Bay coast, Kenya. *Journal of African Earth Sciences* 36, 2: 41-54.

Adelana S, Xu Y & Vrbka P 2010. A conceptual model for the development and management of the Cape Flats aquifer, South Africa. *Water SA* 36, 4: 461-474.

Amatya D, Trettin C, Panda S & Ssegane H 2013. Application of LiDAR Data for hydrologic assessments of low-gradient coastal watershed drainage characteristics. *Journal of Geographic Information System* 5, 2: 175-191.

Anandan T 2015. Intelligent Robots: A feast for the senses. [online]. Robotics Online. Available from https://www.robotics.org/content-detail.cfm/Industrial-Robotics-Industry-Insights/Intelligent-Robots-A-Feast-for-the-Senses/content_id/5530 [Accessed 7 April 2016].

Badenhorst P 1988. Nearshore Physical Processes in a Nut Shell. CSIR Report. EMA-T 8803.

Baltsavias E 1999. Airborne laser scanning: Basic relations and formulas. *ISPRS Journal of Photogrammetry and Remote Sensing* 54, 2: 199-214.

Bascom W 1951. The relationship between sand size and beach-face slope. *Transactions, American Geophysical Union* 32, 6: 866.

Bloetscher F & Wood M 2016. Assessing the impacts of sea level rise using existing data. *Journal of Geoscience and Environment Protection* 4, 9: 159-183.

Boak E & Turner I 2005. Shoreline definition and detection: a review. *Journal of Coastal Research* 21, 4: 688-703.

Breuer P, Chmielewski T & Konopka E 2002. Application of GPS technology to measurements of displacements of high-rise structures due to weak winds. *Journal of Wind Engineering and Industrial Aerodynamics* 90: 223-230.

Burton D, Dunlap D, Wood L & Flaig P 2011. Lidar intensity as a remote sensor of rock properties. *Journal of Sedimentary Research* 81, 5: 339-347.

Carrea D, Abellan A, Humair F, Matasci B, Derron M & Jaboyedoff M 2016. ISPRS Journal of Photogrammetry and Remote Sensing Correction of terrestrial LiDAR intensity channel using Oren – Nayar reflectance model : An application to lithological differentiation. *ISPRS Journal of Photogrammetry and Remote Sensing* 113: 17-29.

Carter R 1988. *Coastal environments*. London: Academic Press.

Cartwright A 2008. Coastal vulnerability in the context of climate change: a South African perspective. Cape Town: Centre for Criminology.

Casella E, Rovere A, Pedroncini A, Stark C, Casella M, Ferrari M & Firpo M 2016. Drones as tools for monitoring beach topography changes in the Ligurian sea (NW Mediterranean). *Geo-Marine Letters* 36, 2: 151-163.

Chandler J & Buckley S 2016. Structure from motion (SFM) photogrammetry vs terrestrial laser scanning. In Carpenter, MB & Keane, CM (eds.) *Geoscience handbook 2016*. AGI Data Sheets, 5th ed. Alexandria, VA: American Geosciences Institute.

Chust G, Galparsoro I, Franco J & Uriarte A 2008. Coastal and estuarine habitat mapping, using LIDAR height and intensity and multi-spectral imagery. *Estuarine, Coastal and Shelf Science* 78: 633-643.

Crain C, Halpern B, Beck M & Kappel C 2009. Understanding and managing human threats to the coastal marine environment. *Annals of the New York Academy of Sciences* 1162, 1: 39-62.

D'Alessandro F & Tomasicchio G 2016. Wave-dune interaction and beach resilience in large-scale physical model tests. *Coastal Engineering* 116: 15-25.

Davidson-Arnott R 2010. *Introduction to coastal processes and geomorphology*. Cambridge: Cambridge University Press.

Davidson-Arnott R 2016. *Climate change impacts on the Great Lakes*. Ausable Bayfield Conservation Authority.

Davis R 1994. *The Evolving Coast*. New York: Scientific American Library.

De Moraes M, Tommaselli A, Santos L, Rubio M, Carvalho G & Garcia T 2016. Monitoring bank erosion in hydroelectric reservoirs with mobile laser scanning. *IEEE Journal of Selected Topics in Applied Earth Observation and Remote Sensing* 1: 1-9.

De Schipper M, De Vries S, Ruessink G, De Zeeuw R, Rutten J, Van Gelder-Maas C & Stive M 2016. Initial spreading of a mega feeder nourishment: Observations of the Sand Engine pilot project. *Coastal Engineering* 111: 23-38.

Department of Environmental Affairs 2014. National coastal access strategy for South Africa 2014. Strategy 2 to the implementation of the ICM Act, March 2014. Cape Town: Department of Environmental Affairs.

Department of Environmental Affairs 2015. State of the oceans and coasts around South Africa 2014. Cape Town: Department of Environmental Affairs.

Ding Q, Chen W, King B, Liu Y & Liu G 2013. Combination of overlap-driven adjustment and Phong model for LiDAR intensity correction. *ISPRS Journal of Photogrammetry and Remote Sensing* 75: 40-47.

Doig A & Ware J 2016. Act Now or Pay Later: Protecting a billion people in climate-threatened coastal cities. [online]. Reliefweb. Available from http://www.christianaid.org.uk/Images/act-now-pay-later-climate-report-may-2016.pdf [Accessed 22 June 2016].

Donoghue D, Watt P, Cox N & Wilson J 2007. Remote sensing of species mixtures in conifer plantations using LiDAR height and intensity data. *Remote Sensing of Environment* 110: 509-522.

Duxbury J & Dickinson S 2007. Principles for sustainable governance of the coastal zone: In the context of coastal disasters. *Ecological Economics* 63, 2: 319-330.

Eitel J, Hö B, Vierling LA, Abellán A, Asner G, Deems J, Glennie C, Joerg P, Lewinter A, Magney T, Mandlburger G, Morton D, Müller J & Vierling K 2016. Remote sensing of environment beyond 3-D : The new spectrum of lidar applications for earth and ecological sciences. *Remote Sensing of Environment* 186: 372-392.

Errington A & Daku B 2017. Temperature compensation for radiometric correction of terrestrial LiDAR intensity data. *Remote Sensing* 9, 4: 356.

Fang Y, Yin J & Wu B 2016. Flooding risk assessment of coastal tourist attractions affected by sea level rise and storm surge: a case study in Zhejiang Province, China. *Natural Hazards* 84, 1: 611-624.

Flood M 2001. LiDAR activities and research priorities in the commercial sector. *International Archives of Photogrammetry, Remote Sensing and Spatial Information Sciences* 34, 3: 22-24.

Fourie J, Ansorge I, Backeberg B, Cawthra H, MacHutchon M & Van Zyl F 2015. The influence of wave action on coastal erosion along Monwabisi. *South African Journal of Geomatics* 4, 2: 96-109.

Froese C & Mei S 2008. *Mapping and monitoring coal mine subsidence using LiDAR and InSAR*. Procedings of the 61st Canadian Geotechnical Conference held 21-24 September 2008, Edmonton, Canada.

Gardner J 1977. *Physical geography*. New York: Harper's College Press.

Gares P, Wang Y & White S 2006. Using LIDAR to monitor a beach nourishment project at Wrightsville Beach, North Carolina, USA. *Journal of Coastal Research* 22, 5: 1206-1219.

Garestier F, Bretel P, Monfort O, Levoy F & Poullain E 2015. Anisotropic surface detection over coastal environment using near-IR LiDAR Intensity maps. *IEEE Journal of Selected Topics In Applied Earth Observations And Remote Sensing* 8, 2: 727-739.

Gesch D 2009. Analysis of Lidar elevation data for improved identification and delineation of lands vulnerable to sea-level rise. *Journal of Coastal Research* 53: 49-58.

Göhring D, Wang M, Schnürmacher M & Ganjineh T 2011. *Radar/LiDAR sensor fusion for car-following on highways*. Proceedings of the 5th International Conference on Automation, Robotics and Applications (ICARA) held 6-8 December 2011, Wellington, Nieu Zealand.

Guenther G, Cunningham A, Larocque P & Reid D 2000. Meeting the accuracy challenge in airborne Lidar Bathymetry. *EARSeL eProceedings* 1, 1: 1-27.

Harrap R & Lato M 2010. An overview of LiDAR: Collection to Application. *NGI publication* 2: 1-9.

Harris L, Nel R, Holness S & Schoeman D 2015. Quantifying cumulative threats to sandy beach ecosystems: A tool to guide ecosystem-based management beyond coastal reserves. *Ocean and Coastal Management* 110: 12-24.

Höfle B & Pfeifer N 2007. Correction of laser scanning intensity data: Data and model-driven approaches. *ISPRS Journal of Photogrammetry and Remote Sensing* 62, 6: 415-433.

Inman ADL & Nordstrom CE 1971. On the Tectonic and Morphologic Classification of Coasts. *Journal of Geology* 79, 1: 1-21.

IPCC 2013. The Physical Science Basis. Contribution of Working Group I to the Fifth Assessment Report of the Intergovernmental Panel on Climate Change. In Stocker T, Qin D, Plattner G, Tignor M, Allen S, Boschung J, Nauels A, Xia Y, Bex V & Midgley P (eds). Cambridge/New York: Cambridge University Press.

Irish J & Lillycrop W 1999. Scanning laser mapping of the coastal zone: the SHOALS system. *Journal of Photogrammetry and Remote Sensing* 54, 2: 123-129.

Jackson L, Lipschitz S, Van der Merwe H & Zietsman L 1984. *Coastal sensitivity atlas of Southern Africa 1984*. Pretoria: Department of Transport.

Kaasalainen S, Hyyppä H, Kukko A, Litkey P, Ahokas E, Hyyppä J, Lehner H, Jaakkola A, Suomalainen J, Akujärvi A, Kaasalainen M & Pyysalo U 2009. Radiometric calibration of LiDAR Intensity with commercially available reference targets. *IEEE Transactions on Geoscience and Remote Sensing* 47, 2: 588-598.

Kashani A, Olsen M, Parrish C & Wilson N 2015. A review of LiDAR radiometric processing: from ad hoc intensity correction to rigorous radiometric calibration. *Sensors* 15: 28099-28128.

Kemp J & Burns J 2016. *Agricultural monitoring using pursuit monostatic TanDEM-X coherence in the Western Cape, South Africa*. Proceedings of EUSAR 2016: 11th European Conference on Synthetic Aperture Radar (EUSAR) conference held 6-9 June 2016. Berlin, Germany.

Kisters A 2016. What lies beneath Table Mountain or all models are wrong, but some are useful. Inaugural lecture: Stellenbosch University.

Klaar M, Kidd C, Malone E, Bartlett R, Pinay G, Chapin F & Milner A 2015. Vegetation succession in deglaciated landscapes: Implications for sediment and landscape stability. *Earth Surface Processes and Landforms* 40, 8: 1088-1100.

Komar P 2010. Shoreline evolution and management of Hawke's Bay, New Zealand: tectonics, coastal processes, and human impacts. *Journal of Coastal Research* 261: 143-156.

Krabill W, Wright C, Swuft R, Frederick E, Manizade S, Yungel J, Martin C, Sonntag J, Duffy M, Hulslander W & Brock J 2000. Airborne laser mapping of Assateague National seashore beach. *Photogrammetric Engineering & Remote Sensing* 66, 1: 65-71.

Kron W 2013. Coasts: the high-risk areas of the world. *Natural Hazards* 66: 1363-1382.

Krooks A, Kaasalainen S, Hakala T & Nevalainen O 2013. Correction of intensity incidence angle effect in terrestrial laser scanning. *ISPRS Annals of the Photogrammetry, Remote Sensing and Spatial Information Sciences* 2: 145-150.

Kukko A, Kaasalainen S & Litkey P 2008. Effect of incidence angle on laser scanner intensity and surface data. *Applied Optics* 47, 7: 986-992.

Lück-Vogel M, Mbolambi C, Rautenbach K, Adams J & Van Niekerk L 2016. South African Journal of Botany Vegetation mapping in the St Lucia estuary using very high-

resolution multispectral imagery and LiDAR. *South African Journal of Botany* 107: 188-199.

Ma R 2005. DEM generation and building detection from LiDAR Data. *Photogrammetric Engineering and Remote Sensing* 71, 7: 847-854.

Mallet C & Bretar F 2009. Full-waveform topographic lidar: State-of-the-art. *ISPRS Journal of Photogrammetry and Remote Sensing* 64, 1: 1-16.

Mbolambi C 2016. Assessment of coastal vegetation degradation using remote sensing in False Bay, South Africa. Master's Thesis. Stellenbosch: Stellenbosch University, Department of Geography and Environmental Studies.

McGranahan G, Balk D & Anderson B 2007. The rising tide: assessing the risks of climate change and human settlements in low elevation coastal zones. *Environment & Urbanization* 19, 1: 17-37.

McLachlan A & Dorvlo A 2005. Global patterns in sandy beach macrobenthic communities. *Journal of Coastal Research* 21, 4: 674-687.

McLean R & Kirk R 1969. Relationships between grain size, size-sorting, and foreshore slope on mixed sand - shingle beaches. *New Zealand Journal of Geology and Geophysics* 12, 1: 138-155.

Metcalf-Lindenburger D 2016. A comparison of landslide inventories along the shoreline of Steamboat Island Peninsula, Thurston County, WA: office based protocol vs. field based protocol. Master's Thesis, University of Washington, Department of Earth and Space Science.

Mitasova H, Overton M, Recalde J, Bernstein D & Freeman C 2009. Raster-based analysis of coastal terrain dynamics from multitemporal LiDAR data. *Journal of Coastal Research* 25, 2: 507-514.

Moore L, Ruggiero P & List J 2006. Comparing mean high water and high water line shorelines: should proxy-datum offsets be incorporated into shoreline change analysis? *Journal of Coastal Research* 22, 4: 894-905.

Mpe T 2015. Assessment of mining impacts on the west coast of Western Cape using LiDAR data. Honour's Thesis. Stellenbosch: Stellenbosch University, Department of Geography and Environmental Studies.

Obu J, Lantuita H, Grosse G, Günther F, Sachs T, Helm V & Fritz M 2016. *Geomorphology* 293, 15: 331-346.

O'Keeffe N, Delgado-fernandez I, Jackson D, Aplin P & Marston C 2016. Meso-scale aeolian transport of beach sediment via dune blowout pathways within a linear foredune. *Geophysical Research Abstracts* 18: 14081.

Operation Phakisa, Department of Environmental Affairs, 2014. Unlocking the economic potential of South Africa's oceans. Marine Protection Services and Governance Executive Summary.

Ozcoasts 2015. OzCoasts Conceptual model: Sediment transport in wave-dominated estuaries. [online]. Ozcoasts.gov.au. Available from http://www.ozcoasts.gov.au/conceptual_mods/geomorphic/wde/wde_sed_trans.jsp [Accessed 1 September 2017].

Palaseanu-Lovejoy M, Danielson J, Thatcher C, Foxgrover A, Barnard P, Brock J & Young A 2016. Automatic delineation of seacliff limits using LiDAR-derived high-resolution DEMs in Southern California. *Journal of Coastal Research* 76, 1: 162-173.

Palaseanu-Lovejoy M, Nayegandhi A, Brock J, Woodman R & Wright C 2009. Evaluation of airborne lidar data to predict vegetation presence/absence. *Journal of Coastal Research* 53: 83-97.

Patrizio P, Aucelli C, Di Paola G, Incontri P, Rizzo A, Vilardo G, Benassai G, Buonocore B, Pappone G, Patrizio P & Aucelli C 2016. Coastal inundation risk assessment due to subsidence and sea level rise in a Mediterranean alluvial plain (Volturno coastal plain – southern Italy). *Estuarine, Coastal and Shelf Science* 198B: 597-609.

Pe'eri S & Long B 2011. LiDAR technology applied in coastal studies and management. *Journal of Coastal Research* 1: 1-5.

Poelhekke L, Jäger W, Van Dongeren A, Plomaritis T, Mccall R & Ferreira Ó 2016. Predicting coastal hazards for sandy coasts with a Bayesian Network. *Coastal Engineering* 118: 21-34.

Prasad D & Kumar N 2014. Coastal erosion studies – A review. *International Journal of Geosciences* 5: 341-345.

Reis A & Gama C 2010. Sand size versus beachface slope – An explanation based on the Constructal Law. *Geomorphology* 114, 3: 276-283.

Revell D, Komar P & Sallenger A 2002. An application of LiDAR to analyses of El Niño erosion in the Netarts littoral cell, Oregon. *Journal of Coastal Research* 18, 4: 792-801.

Richter A, Faust D & Mass HG 2011. Dune cliff erosion and beach width change at the northern and sourthern spits of Sylt detected with multi-temporal LiDAR. *Catena* 103: 103-111.

Rumson A, Hallett S & Brewer T 2017. Coastal risk adaptation: the potential role of accessible geospatial Big Data. *Marine Policy* 83: 100-110.

Rust I 1991. Environmental geology of the coastal zone: a South African perspective. *South African Journal of Marine Science* 10, 1: 397-405.

SAnews 2015. SA News [online]. SAnews.gov.za Durban. Available from http://www.sanews.gov.za/south-africa/sas-ocean-economy-expected-contribute-r20bn-gdp [Accessed 5 August 2017].

Saadat P, Safari S, Ramezani O & Solivan R 2016. What factors effects on a touristic destination? *Journal of Business and Management Sciences* 4, 3: 68-75.

Sallenger A, Krabill W, Swift RN, Brock J, List J, Hansen M, Holman R, Manizade S, Sontag J, Meredith A, Morgan K, Yunkel J, Frederick E & Stockdon H 2003. Evaluation of airborne topographic lidar for quantifying beach changes. *Journal of Coastal Research* 19, 1: 125-133.

Samsung-Lim C, Thatcher J, Brock D, Kimbrow J, Danielson & Reynolds B 2013. Accuracy assessment of a mobile terrestrial lidar survey at Padre Island National Seashore. *International Journal of Remote Sensing* 34, 18: 23-53.

Sanders B 2007. Evaluation of on-line DEMs for flood inundation modeling. *Advances in Water Resources* 30, 8: 1831-1843.

Saye S, Van der Wal D, Pye K & Blott S 2005. Beach-dune morphological relationships and erosion/accretion: An investigation at five sites in England and Wales using LiDAR data. *Geomorphology* 72, 1: 128-155.

Saylam K, Hupp J & Averett A 2017. *Quantifying the bathymetry of the lower Colorado River basin, Arizona, with airborne LiDAR*. Procedings of American Society of Photogrammetry and Remote Sensing (ASPRS) conference held 11-17 March 2017. Baltimore, Maryland, USA.

Schubert J, Gallien T, Majd M & Sanders B 2015. Terrestrial laser scanning of anthropogenic beach berm erosion and overtopping. *Journal of Coastal Research* 31, 1: 47-60.

Schwarz B 2010. Mapping the world in 3D. *Nature Photonics* 4: 429-430.

Sharma A, Rout C & Garg V 2010. The emerging role of LiDAR remote sensing for hydrological application: opportunities and constrants. *Environmental Monitoring and Assessment* 173, 1: 789-801.

Sheeja P & Gokul A 2016. Application of digital shoreline analysis system in coastal erosion assessment. *International Journal of Engineering Science and Computing* 6, 6: 7876-7883.

Short A 1987. A note on the controls of beach type and change, with S.E. Australian examples. *Journal of Coastal Research* 3, 3: 387-395.

Short A 2006. Australian beach systems—nature and distribution. *Journal of Coastal Research* 221, 1: 11-27.

Smeeckaert J, Mallet C, David N, Chehata N & Ferraz A 2013. Large-scale classification of water areas using airborne topographic LiDAR data. *Remote Sensing of Environment* 138: 134-148.

Soltau C 2009. The cross-shore distribution of grain size in the longshore transport zone. Master's Thesis. Stellenbosch: Stellenbosch University, Department of Engineering.

Song J, Han S, Yu K & Kim Y-I 2002. Assessing the possibility of land-cover classification using LiDAR intensity data. *International Archives of Photogrammetry, Remote Sensing and Spatial Information Sciences* 34, 3: 259-262.

Stockdon H, Doran K & Sallenger A 2009. Extraction of LiDAR-based dune-crest elevations for use in examining the vulnerability of beaches to inundation during hurricanes. *Journal of Coastal Research* 53: 59-65.

Theron A & Schoonees J 2007. Sand transport at and shoreline response to a breakwater attached to a large tidal pool at Monwabisi, Cape Town. *Journal of the South African Institution of Civil Engineers* 49, 2: 2-9.

Theron A, Rossouw M, Barwell L, Maherry A, Diedericks G & de Wet P 2010. *Quantification of risks to coastal areas and development : wave run-up and erosion.* Procedings of the Science Real and Relevant conference held 30 August–01 September 2010. CSIR International Convention Centre, Pretoria.

Tõnisson H, Vilumaa K, Kont A, Sugita S, Rosentau A & Muru M 2016. Past storminess recorded in the internal architecture of coastal formations of Estonia in the NE Baltic Sea region. *Geophysical Research Abstracts* 18: 9925.

Tuell G, Barbor K & Wozencraft J 2010. Overview of the coastal zone mapping and imaging lidar (CZMIL): a new multisensor airborne mapping system for the U.S. Army Corps of Engineers. Proceedings of SPIE conference held 12 May 2010. Orlando, Florida.

Vain A, Kaasalainen S, Pyysalo U, Krooks A & Litkey P 2009. Use of naturally available reference targets to calibrate airborne laser scanning intensity data. *Sensors* 9, 4: 2780-2796.

Viles H 2016. Technology and geomorphology: Are improvements in data collection techniques transforming geomorphic science? *Geomorphology* 270: 121-133.

Wang C & Philpot W 2007. Using airborne bathymetric lidar to detect bottom type variation in shallow waters. *Remote Sensing of Environment* 106, 1: 123-135.

Wang C & Glenn N 2009. Integrating liand elevation data for terrain characterization in a forested area. *IEEE Geoscience and Remote Sensing Letters* 6, 3: 463-466.

Webster T, Mcguigan K, Crowell N, Collins K & Macdonald C 2016. Optimization of data collection and refinement of post-processing techniques for maritime Canada's first shallow water topographic-bathymetric LiDAR survey. (Special Issue) *Journal of Coastal Research* 76, 1: 31-43.

Wenger S 2016. Evaluation of SFM against traditional stereophotogrammetry and LiDAR techniques for DSM creation in various land cover areas. Master's Thesis. Stellenbosch: Stellenbosch University, Department of Geography and Environmental Studies.

Wiegel R 1964. *Oceanographical Engineering*, Englewood Cliffs, New Jersey: Prentice Hall.

Woodroffe C 2003. *Coasts: form, process and evolution*. Cambridge: Cambridge University Press.

WWF-SA 2016. *Oceans facts and futures: Valuing South Africa's ocean economy*. WWF-SA, Cape Town, South Africa.

Xhardé R, Long B & Forbes D 2006. *Accuracy and limitations of airborne LiDAR surveys in coastal environments.* Proceedings of the International Geoscience and Remote Sensing Symposium (IGARSS): 2412-2415.

Yan W & Shaker A 2014. Radiometric correction and normalization of airborne LiDAR intensity data for improving land-cover classification. *IEEE Transactions on Geoscience and Remote Sensing* 52, 12: 7658-7673.

Yan W, Shaker A & El-Ashmawy N 2015. Urban land cover classification using airborne LiDAR data: A review. *Remote Sensing of Environment* 158: 295-310.

Yates M, Guza R, O'Reilly W & Seymour R 2009. Overview of seasonal sand level changes on southern California beaches. *Shore and Beach* 77, 1: 39-46.

APPENDICES

APPENDIX 1 Specifications for the TrimbleR4GNSS DGPS.

DATASHEET

TRIMBLE R4 GNSS SYSTEM

KEY FEATURES

Trimble R-Track satellite tracking technology

Includes Trimble Maxwell 6 chip with 220 channels

Scalable from postprocessing to VRS to multi-constellation RTK configurations

Cable-free for convenience

Accurate, reliable and rugged system

Trimble Slate controller

DEPENDABLE WHEN EVERY POINT COUNTS

Designed for surveyors looking for easy-to-use GNSS technology, the Trimble® R4 GNSS System performs under even the most rigorous conditions. GNSS support upgrade options, integrated Trimble R-Track™ satellite tracking technology, and a straightforward system design result in a system that is flexible, reliable, and rugged.

A COMPLETE GNSS SYSTEM

Lightweight, convenient and cable-free, the Trimble R4 GNSS system with Trimble Access™ field software provides the ease of use of an integrated receiver and everything you need to perform a basic survey campaign.

The dual-frequency antenna enhances tracking capacity and delivers sub-millimeter phase center stability for precise results in demanding conditions. Internally powered with removable batteries, this system provides a full working day of uninterrupted field operation.

ADVANCED TRIMBLE R-TRACK TECHNOLOGY

The Trimble R4, powered with a Trimble Maxwell™ 6 chip with 220 channels, delivers the accuracy and reliability required for precision surveying with superior tracking and RTK performance. With GPS L2C and the Japanese QZSS support included, you can track more satellites and measure more successfully in challenging environments. L2C provides more than just additional signals – the advanced signal structure provides better strength for more reliable satellite tracking.

Trimble R-Track satellite tracking technology delivers reliable, precise positioning performance. Trimble R-Track with Signal Prediction™ compensates for intermittent or marginal RTK correction signals, enabling extended precision operation after an RTK signal is interrupted.

The CMRx communications protocol provides correction compression for optimized bandwidth and full utilization all of the satellites in view, giving you reliable positioning performance.

CHOOSE THE LEVEL OF GNSS SUPPORT YOU REQUIRE TODAY

Choose the level of GNSS support you require today with the flexible upgrade options available on the Trimble R4. Founded on proven GNSS technology, the Trimble R4 comes standard with GPS L1, L2, L2C and QZSS. Beyond this standard GNSS support, the Trimble R4 offers upgrades to GLONASS, Galileo, and BeiDou (COMPASS)—just choose what you need.

FUNCTIONS AS A VRS ROVER, RTK ROVER, OR FIELD BASE STATION

Use as a lightweight rover for static surveying or RTK. The Trimble R4 is also completely compatible with Trimble VRS™ solutions, creating a VRS rover for use inside real-time networks. With a built-in 450 MHz receive-only radio or a fully integrated GSM/GPRS radio, this system can be adapted to meet a variety of needs. As a base station, the Trimble R4 with the integrated UHF transmit option is rugged, weather-resistant and compatible with a range of radio solutions.

A DEDICATED, RELIABLE GNSS FIELD SOLUTION

Pair the Trimble R4 with Trimble Access and the Trimble Slate Controller[1] for a dedicated GNSS solution that is effective for both real time and postprocessed GNSS surveys.

Powerful, connected, and compact, the Trimble Slate Controller combines the convenience and ease-of-use of a smartphone with the durability for which Trimble is known. Its slim, ergonomic design is easy to grasp and its screen provides superior sunlight readability enabling all-day use by hard-working survey professionals.

Trimble Access field software provides specialized and customized workflows to make surveying tasks quicker and easier while enabling teams to communicate vital information between field and office in real-time.

Survey companies can also implement their unique workflows by taking advantage of the customization capabilities available in the Trimble Access Software Development Kit (SDK).

Need to get data back to the office immediately? Benefit from real-time data sharing via Trimble Access Services, now available with any valid Trimble Access maintenance agreement.

Back in the office, users can seamlessly process data with Trimble Business Center office software.

The Trimble R4 GNSS system – ready and reliable for your everyday surveying needs.

1 The Trimble R4 can be used with a Trimble TSC3, Trimble CU, or Trimble Tablet Rugged PC with the purchase of an advanced data collector option.

Trimble

TRIMBLE R4 GNSS SYSTEM

DATASHEET

PERFORMANCE SPECIFICATIONS

Measurements

- Advanced Trimble Maxwell 6 Custom Survey GNSS chip with 220 channels
- Trimble R-Track technology
- High precision multiple correlator for GNSS pseudorange measurements
- Unfiltered, unsmoothed pseudorange measurements data for low noise, low multipath error, low time domain correlation and high dynamic response
- Very low noise GNSS carrier phase measurements with <1 mm precision in a 1 Hz bandwidth
- Signal-to-Noise ratios reported in dB-Hz
- Proven Trimble low elevation tracking technology
- Satellite signals tracked simultaneously:
  - GPS: L1C/A, L1C, L2C, L2E
  - GLONASS[1]: L1C/A, L1P, L2C/A, L2P, L3
  - SBAS: L1C/A
  - Galileo[1]: E1, E5A, E5B
  - BeiDou[1] (COMPASS): B1, B2
- SBAS: QZSS, WAAS, EGNOS, GAGAN
- Positioning rates: 1 Hz, 2 Hz, 5 Hz, and 10 Hz

POSITIONING PERFORMANCE[2]

Code differential GNSS positioning

Horizontal	0.25 m + 1 ppm RMS
Vertical	0.50 m + 1 ppm RMS
SBAS differential positioning accuracy[3]	typically <5 m 3DRMS

STATIC GNSS SURVEYING

High-precision static

Horizontal	3 mm + 0.1 ppm RMS
Vertical	3.5 mm + 0.4 ppm RMS

Static and FastStatic

Horizontal	3 mm + 0.5 ppm RMS
Vertical	5 mm + 0.5 ppm RMS

POSTPROCESSED KINEMATIC (PPK) GNSS SURVEYING

Horizontal	8 mm + 1 ppm RMS
Vertical	15 mm + 1 ppm RMS

REAL TIME KINEMATIC SURVEYING[4]

Single Baseline <30 km

Horizontal	8 mm + 1 ppm RMS
Vertical	15 mm + 1 ppm RMS

NETWORK RTK

Horizontal	8 mm + 0.5 ppm RMS
Vertical	15 mm + 0.5 ppm RMS
Initialization time[5]	typically <8 seconds
Initialization reliability[5]	typically >99.9%

1 Optional upgrade.
2 Precision and reliability may be subject to anomalies due to multipath, obstructions, satellite geometry, and atmospheric conditions. The specifications stated recommend the use of stable mounts in an open sky view, EMI and multipath clean environment, optimal GNSS constellation configurations, along with the use of survey practices that are generally accepted for performing the highest-order surveys for the applicable application including occupation times appropriate for baseline length. Baselines longer than 30 km require precise ephemeris and occupations up to 24 hours may be required to achieve the high precision static specification.
3 Depends on SBAS system performance.
4 Network RTK PPM values are referenced to the closest physical reference station.
5 May be affected by atmospheric conditions, signal multipath, obstructions and satellite geometry. Initialization reliability is continuously monitored to ensure highest quality.
6 Receiver will operate normally to –40 °C, internal batteries are rated to –20 °C, optional internal GSM modem operates to -30 °C.
7 Tracking GPS, GLONASS and SBAS satellites. Optional upgrade required for GLONASS.
8 Varies with temperature and wireless data rate. When using a receiver and internal radio in the transmit mode, it is recommended that an external 6 Ah or higher battery is used.
9 Varies with terrain and operating conditions.
10 Bluetooth type approvals are country specific.

PN 022543-490E (04/13)

HARDWARE

Physical

Dimensions (W×H)	19 cm × 10.2 cm (7.5 in x 4.0 in), including connectors
Weight	1.52 kg (3.35 lb) with internal battery, internal radio with UHF antenna 3.04 kg (6.70 lb) items above plus range pole, controller, and bracket
Temperature[6]	
Operating	–40 °C to +65 °C (–40 °F to +149 °F)
Storage	–40 °C to +75 °C (–40 °F to +167 °F)
Humidity	100%, condensing
Water/dustproof	IP67 dustproof, protected from temporary immersion to depth of 1 m (3.28 ft)
Shock and vibration	Tested and meets the following environmental standards:
Shock	Non-operating: Designed to survive a 2 m (6.6 ft) pole drop onto concrete. Operating: to 40 G, 10 msec, sawtooth
Vibration	MIL-STD-810F, FIG.514.5C-1

Electrical

- Power 11 V DC to 28 V DC external power input with over-voltage protection on Port 1 (7-pin Lemo)
- Rechargeable, removable 7.4 V, 2.6 Ah Lithium-Ion battery. Power consumption[7] is 3.2 W in RTK rover mode with internal radio and Bluetooth in use.
- Operating times on internal battery[8]:
  - 450 MHz receive only option: 5.0 hours
  - 450 MHz receive/transmit option (0.5 W): 2.5 hours
  - Cellular receive option: 4.7 hours

Communications and Data Storage

- Serial: 3-wire serial (7-pin Lemo) on Port 1; full RS-232 serial on Port 2 (Dsub 9 pin)
- Radio modem: fully Integrated, fully sealed internal 450 MHz receiver/transmitter option:
  - Transmit power: 0.5 W
  - Range[9]: 3–5 km typical / 10 km optimal
- Cellular: fully integrated, sealed internal GSM/GPRS option
- Bluetooth: fully integrated, sealed 2.4 GHz communications port (Bluetooth®)[10]
- External communication devices for corrections supported on Serial and Bluetooth ports
- Data storage: 11 MB internal memory, 188.6 hours of raw observables (approx. 1.4 MB/day), based on recording every 15 seconds from an average of 14 satellites

Data formats

- CMR: CMR+, CMRx input and outputs
- RTCM: RTCM 2.1, RTCM 2.3, RTCM 3.0, RTCM 3.1 input and outputs
- Other outputs: 23 NMEA outputs, GSOF, RT17 and RT27 outputs, supports BINEX and smoothed carrier

Supported Trimble Controllers

- Trimble Slate Controller
- Optional[1]: Trimble TSC3 controller, Trimble CU controller, Trimble Tablet Rugged PC

Certifications

FCC Part 15 (Class B device), 22, 24, 90; CE Mark; C-Tick; 850/1900 MHz; Class 10 GSM/GPRS module; Bluetooth EPL

Specifications subject to change without notice.

CE C Bluetooth®

TRIMBLE AUTHORIZED DISTRIBUTION PARTNER

NORTH AMERICA
Trimble Navigation Limited
10368 Westmoor Dr
Westminster CO 80021
USA

EUROPE
Trimble Germany GmbH
Am Prime Parc 11
65479 Raunheim
GERMANY

ASIA-PACIFIC
Trimble Navigation
Singapore Pty Limited
80 Marine Parade Road
#22-06, Parkway Parade
Singapore 449269
SINGAPORE

Trimble.

APPENDIX 2 Correspondence relating to permit required for sampling.

Re: Permit required for sampling beach sand in False Bay?

Melanie Luck-Vogel <MLuckVogel@csir.co.za>

Thu 14/04/2016 15:15

To: gregg.oelofse@capetown.gov.za <gregg.oelofse@capetown.gov.za>; Howard.Gold@capetown.gov.za <Howard.Gold@capetown.gov.za>; darryl.colenbrander@gmail.com <darryl.colenbrander@gmail.com>;

Cc: Burns, JJ, Mnr <17197902@sun.ac.za> <17197902@sun.ac.za>;

Thank you for the feedback, Gregg.

Best regards
Melanie
>>> Gregg Oelofse <Gregg.Oelofse@capetown.gov.za> 14/04/2016 12:00 >>>
Hi, sounds great. No permit needed. I will inform relevant city staff. Best. Gregg

Sent from my iPhone

On 14 Apr 2016, at 10:43 AM, Melanie Luck-Vogel <MLuckVogel@csir.co.za> wrote:

> Dear Gregg,
>
> I'm a senior researcher at the Coastal Systems Research Group at the CSIR in Stellenbosch. One of my students would like to do a lab analysis (to inform airborne LiDAR data acquisitions) on how different slopes and grain sizes of beach sand do feature in the LiDAR data. The hypothesis to proof is that beach grain size can determined using airborne LiDAr data. If this turns out to be the case, this would be very interesting input for all kind of ecosystems and vulnerability assessments.
>
> For that purpose we would like to sample some beach sand in False Bay. We think of about 15 samples, of about 2kg sand each.
>
> I'm trying to find out if I would need a Permit for that sampling from anybody.
> DEA and WC DEADP would not require a Permit from their side, see below.
>
> Please could you advise if there would be a Permit required from CoCT?
>
> Kind regards

Dr Melanie Lück-Vogel

Senior Researcher Remote Sensing
Coastal Systems Research Group
Natural Resources and the Environment
CSIR

P.O. Box 320, Stellenbosch, 7599
11 Jan Cilliers Street, Stellenbosch, 7600
South Africa

+27 21 888 2412 (Office)
+27 21 888 2693 (Fax)
mluckvogel@csir.co.za (email)

http://www.csir.co.za

>>> "Fhumulani Angwenyi" <FAngwenyi@environment.gov.za> 08/04/2016 15:46 >>>
Dear Melanie

The collection of about 15-20 samples bags(2Kg) of beach sand will not trigger EIA listed activities.A total of 20 bags each weighing about 2Kg when combined is still way less than $5m^3$ which is the trigger for EIA .20 bags each weighing 2kg will make about $1m^3$ which is less than $5m^3$.

The Western Cape Provincial Environmental Affairs will have to confirm that as the Competent Authority.They have a enquiry template which the applicant can complete before they confirm officially .

Regards
Fhumulani
>>> "Lauren Williams" <LWilliams@environment.gov.za> 07/04/2016 15:14 >>>
Dear Melanie

That sounds like it's below the EIA thresholds, but I've included my colleague Fhumulani who is responsible for EIAs. She will be able to provide guidance.

Kind regards,

Lauren Williams Pr.Sci.Nat. | GISc Tg (SA)

GISc Professional
Department of Environmental Affairs
Branch: Oceans and Coasts
CD: Integrated Coastal Management

A: 2 East Pier Building, V&A Waterfront
T: 021 819 2492
E: LWilliams@environment.gov.za
W: www.environment.gov.za
GPS: -33.901286 S; 18.425517 E

"Knowing where things are, and why, is essential to rational decision making" - Jack Dangermond (ESRI)

<ATT00001>

>>> "Melanie Luck-Vogel" <MLuckVogel@csir.co.za> 4/7/2016 11:01 AM >>>
Dear Alan and Lauren,

one of my MSc students, Mr James Burns, wants to analyse how beach grain size and beach slope influence the intensity in a LiDAR image.

The general idea is that if grain size could reliably determined from airborne LiDAR data, this would be of great value as input for any kind of coastal vulnerability assessment.

We will be using the existing CoCT LiDAR data for False Bay as a starting point, but due to the high temporal variability of the beach it will be challenging to validate the results.

We therefore also want to establish the relationship between LiDAR - grain size - slope in a lab approach, using CSIR's portable Laser scanner. For that purpose we would like to collect samples of sand from selected sites in False Bay. We will then sieve them to determine their actual grain size composition and then scan and analyse the probes in the lab.

We are aiming for about 15-20 samples of about 2kg each.

My question now is, if we would need a Permit from DEA or anybody else to do so?

If yes, please could you point me towards the respective contact person?

Many thanks and best regards

Melanie

APPENDIX 3 Correspondence relating to access to Kogel Bay resort for sampling.

FW: Kogel Bay beach fieldwork

Ian Combrink <Ian.Combrink@capetown.gov.za>

Mon 30/05/2016 20:33

To: Burns, JJ, Mnr <17197902@sun.ac.za> <17197902@sun.ac.za>;

Cc: Christopher Gerard Brooks <ChristopherGerard.Brooks@capetown.gov.za>; Teresa James <TeresaJames@capetown.gov.za>; Genevieve Adams <Genevieve.Adams@capetown.gov.za>; Kamiela Evans <Kamiela.Evans@capetown.gov.za>;

Importance: High

Dear James

I have no problem with this. Please liaise with Chris Brooks, who is my manager for the Kogel Bay Resort. You can contact him on 084 413 4093.All the best with your research and please share your results once you have completed your research.

Kind regards
Ian Combrink
Head: Sport, Recreation and Amenities
Area: 3.5

Harmony Park Administrative Office
Flow Street, Gordon's Bay

Tel: 021-444 0525
Cell: 084 922 9227
E-mail: ian.combrink@capetown.gov.za

CITY OF CAPE TOWN
ISIXEKO SASEKAPA
STAD KAAPSTAD

Making progress possible. Together.

From: Kamiela Evans
Sent: 30 May 2016 12:15 PM
To: Ian Combrink
Cc: Genevieve Adams; Teresa James
Subject: FW: Kogel Bay beach fieldwork
Importance: High

Good Day,

Please see subjoined email below for your urgent attention / response

---

From: Burns, JJ, Mnr <17197902@sun.ac.za> [mailto:17197902@sun.ac.za]
Sent: Monday, May 30, 2016 11:54 AM

To: Genevieve Adams; Kamiela Evans
Subject: Kogel Bay beach fieldwork

Good morning Ms Adams and Ms Evans,

I am currently registered as a masters student with the department of Geography and Environmental Studies at the University of Stellenbosch. As part of my masters research, I am investigating various beach characteristics and how they relate to sand grain size particularly. False Bay has a number of different beach types and I am currently in the process of collecting sand samples from some of these to analyse in the lab.

The reason for emailing concerns the Kogel Bay beach. A colleague and I are planning to do the sampling early next week, most likely Monday or Tuesday morning (at low tide). We will be using valuable equipment as part of the sampling and I would therefore like to ask if it would be possible to make use of the Kogel Bay campsite parking (through the gates) for added security, and to access the beach from there.

Thank you in advance for your assistance, it is much appreciated.

Kind regards,
James

James J Burns
Geo-informatics
Stellenbosch University

APPENDIX 4 Comprehensive results from the sand sieving at Stellenbosch University.

SAMPLE	STRAND				KOGEL BAY								FISH HOEK			
	ST15	ST17	ST25	ST28	KB14	KB16	KB19	KB42	KB45	KB47	KB70	KB72	KB74	FH9	FH11	FH25	FH28
TOTAL WIEGHT (g)	**261.10**	**259.68**	**260.72**	**263.38**	**265.23**	**275.41**	**254.75**	**257.86**	**257.64**	**279.65**	**266.52**	**261.28**	**262.09**	**257.40**	**267.79**	**265.97**	**258.15**
SIEVE SIZE																	
1 1.4 mm	0.04	0.11	0.26	0.00	0.92	1.78	1.80	0.97	0.46	0.39	0.05	0.00	0.41	0.06	0.00	0.03	0.00
2 850 microns	1.10	0.85	0.51	0.11	14.97	6.85	8.35	5.52	2.06	3.73	0.97	0.03	2.28	0.19	0.08	0.14	0.04
3 710 microns	2.55	0.78	0.30	0.19	16.68	10.98	8.96	7.47	2.78	7.30	2.62	0.17	3.98	0.16	0.07	0.48	0.07
4 500 microns	15.04	2.93	0.71	0.94	77.68	68.95	39.77	41.20	20.87	54.68	37.38	3.69	34.86	0.91	1.00	3.20	1.11
5 425 microns	13.95	4.00	0.60	1.56	43.60	53.07	29.98	29.59	25.78	41.02	42.92	7.20	32.07	0.88	0.59	1.77	2.48
6 355 microns	35.32	15.51	2.47	13.72	61.92	80.35	73.51	87.20	100.07	88.35	107.14	54.70	93.37	4.09	2.57	6.75	16.01
7 300 microns	13.18	6.12	1.84	8.73	18.35	18.59	16.70	23.88	27.12	20.25	27.40	24.43	20.72	2.43	1.51	3.06	7.79
8 180 microns	85.28	94.26	61.40	92.49	23.79	31.56	67.56	57.51	73.58	59.90	45.54	162.16	72.56	117.49	144.26	92.12	164.56
9 150 microns	27.46	43.90	47.98	58.35			0.38		0.70					94.35	92.05	126.65	50.37
10 90 microns	65.33	89.85	142.78	86.51										36.45	25.50	31.21	14.90
11 63 microns	1.59	1.78	2.31	1.17										0.20	0.08	0.07	0.08
total measured	**260.84**	**260.09**	**261.16**	**263.77**	**257.91**	**272.13**	**247.01**	**253.34**	**253.42**	**275.62**	**264.02**	**252.38**	**260.25**	**257.21**	**267.71**	**265.48**	**257.41**
total loss	**0.26**	**-0.41**	**-0.44**	**-0.39**	**7.32**	**3.28**	**7.74**	**4.52**	**4.22**	**4.03**	**2.50**	**8.90**	**1.84**	**0.19**	**-0.08**	**0.49**	**0.74**
% loss	**0.10**	**-0.16**	**-0.17**	**-0.15**	**2.76**	**1.19**	**3.04**	**1.75**	**1.64**	**1.44**	**0.94**	**3.41**	**0.70**	**0.07**	**0.03**	**0.18**	**0.29**

Note: the plastic cup weighed 32.75 g (scale was set to 0g with cup)

APPENDIX 5 Image of the RIEGL VZ-400 LiDAR scanner.